Experimental Investigation of Reflection of Airborne Noise at Duct Terminations

A Thesis
Presented to
The Academic Faculty

By
Alexander Michaud

In Partial Fulfillment
Of the Requirements for the Degree
Master of Science in Mechanical Engineering

Georgia Institute of Technology
August 2007

Experimental Investigation of Reflection of Airborne Noise at Duct Terminations

Approved by:

Dr. Kenneth A. Cunefare
School of Mechanical Engineering
Georgia Institute of Technology

Dr. Yves Berthelot
School of Mechanical Engineering
Georgia Institute of Technology

Dr. F. Levent Degertekin
School of Mechanical Engineering
Georgia Institute of Technology

Date Approved: April 9, 2007

ACKNOWLEDGEMENTS

I would like to acknowledge those who helped in the preparation of this thesis. First, thank you Dr. Cunefare for introducing me to the exciting area of acoustics, teaching me the importance of skepticism, and patiently leading me through the perils of experimental research. Thank you to Dr. Berthelot and Dr. Degertekin for agreeing to be on my thesis reading committee. And thank you to ASHRAE Technical Committee 2.6 for their financial support and procedural guidance.

Thank you to the helpful and hardworking staff in the Mechanical Engineering academic office, especially Glenda, Norma, and Theresa. Thank you to Linda for bending over backwards. Thank you to Jeff for the unending and unwarranted help, useful advice, duct moving expertise, and constant good nature. Thank you to Anne-Marie for showing patience and giving guidance whenever I had concerns and questions. And thank you to Mom and Dad for your love and moral support when research left me less than motivated and crunch time reared its ugly head.

TABLE OF CONTENTS

LIST OF TABLES

LIST OF FIGURES

CHAPTER 1

INTRODUCTION

Heating, Ventilating, and Air Conditioning (HVAC) systems utilize ducts to transport temperature controlled air to and from occupied spaces. HVAC system noise is a common problem between 25 and 500 Hz. Duct noise caused primarily by fans and turbulent in-duct airflow is a common byproduct and often exits at duct terminations. An open duct termination represents an acoustic boundary and causes noise to either reflect back into the duct or exit the duct. The amount of noise that is reflected back into a duct is referred to as the end reflection loss (ERL). The objective of this thesis was to experimentally determine the ERL of a variety of rectangular duct configurations. This research focused on determining the impact that termination variations have on ERL and how experimental results correspond with analytic predictions and current ERL values in the American Society of Heating, Refrigerating, and Air-Conditioning Engineers (ASHRAE) Handbook [1]. ERL has not been experimentally quantified for rectangular ducts using a variety of duct configurations with real world application. In addition, ERL behavior below 63 Hz on a variety of duct configurations has not been experimentally investigated and compared to analytic predictions. Finally, there is no experimental data using rectangular ducts to quantify their agreement with circular duct ERL behavior.

The remainder of this chapter provides basic background information on HVAC duct systems, fundamental information on the determination of ERL, prior research in the determination of ERL, current ERL values listed in the ASHRAE Handbook, the effects of measurement bandwidth and averaging techniques used to report ERL, and the motivation for this research. Chapter two contains a detailed description of the

experimental apparatus including the physical setup, duct construction, microphone configuration, duct configurations and labeling, and signal generation and data acquisition systems. Chapter three presents the experimental procedure used to obtain accurate ERL results, the measurement method, frequency considerations, and the error analysis used during experimentation and in reporting results. Chapter four presents the experimental results organized according to the various applicable termination parameters. Finally, chapter five discusses the significance of these experimental findings and possible future research avenues to better understand ERL.

1.1 Basic HVAC Background

A basic HVAC duct setup is depicted in Figure 1 with arrows representing air flow and noise propagation. Duct noise is transmitted along a duct system and eventually escapes into occupied spaces at duct terminations. Flex duct, a flexible fiberglass duct supported by a thin metal skeleton with an outer and inner lining, is often used to connect rigid ductwork with diffusers. Air is transported to the air handler via return ductwork, though noise is also transmitted through the return ductwork and escapes into the occupied space. Equation (1.1) relates HVAC duct noise to ERL as

$$L_{W,room} = L_{W,duct} - \mathrm{ERL}, \tag{1.1}$$

where $L_{W,room}$ = sound power level from the duct,
$L_{W,duct}$ = sound power level in the duct, and
ERL = sound power reflected by the termination impedance.

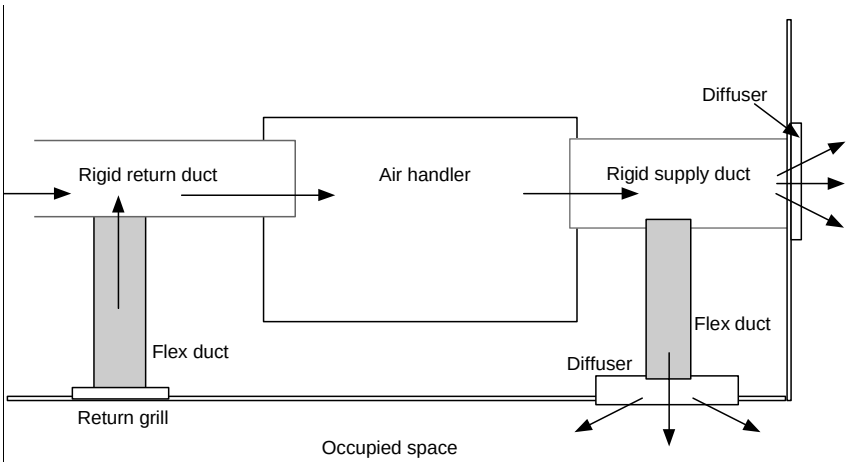

Figure 1. Simple HVAC Setup

1.2 End Reflection Loss: A Detailed Explanation

Methods elaborated by Kinsler and Frey [2] and Blackstock [3] will be used to derive ERL in terms of plane wave incidence on an impedance interface, the reflection coefficient as a function of impedance, and ERL defined as a function of the reflection coefficient. These derivations allow for the analytic determination of ERL for circular and rectangular ducts with baffled and free space termination conditions.

The general solution for one dimensional plane wave propagation is [2]

$$p = Ae^{j(\omega t - kx)} + Be^{j(\omega t + kx)}, \tag{1.2}$$

where A and B = complex pressure amplitudes,
ω = angular frequencies in radians per second,
$j = \sqrt{-1}$
k = wave number,
t = time in seconds, and
x = direction of propagation.

Acoustic impedance represents a medium's complex resistance to energy transfer. Specific acoustic impedance is "the ratio of acoustic pressure in a medium to the associated particle speed" and is expressed as [2]

$$z = \frac{p}{u}, \tag{1.3}$$

where u = particle speed. For plane waves, Equation (1.3) is also equal to the characteristic impedance of the medium, which is defined as

$$z = \pm \rho_0 c, \tag{1.4}$$

where ρ_0 = volume density and c = speed of sound. It is apparent that different media have specific acoustic impedances.

Figure 2 depicts a wave normally incident on the boundary between two media. The acoustic pressure and particle velocity normal to the boundary between the two media are assumed equivalent. The boundary condition for incident, reflected, and transmitted pressure is

$$p_i + p_r = p_t. \tag{1.5}$$

The incident, reflected, and transmitted plane waves are:

$$p_i = P_i e^{j(\omega t - k_1 x)}, \tag{1.6}$$

$$p_r = P_r e^{j(\omega t + k_1 x)}, \tag{1.7}$$

$$p_t = P_t e^{j(\omega t - k_2 x)}, \tag{1.8}$$

where P_i = incident pressure amplitude,
P_r = reflected pressure amplitude, and
P_t = transmitted pressure amplitude.

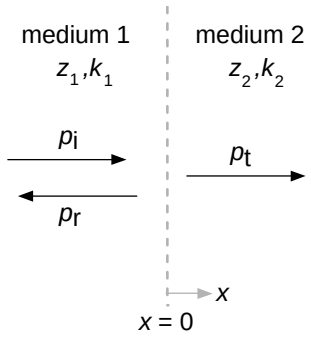

Figure 2. Normal Incidence Boundary Behavior Between Two Media

Reflected sound power represents the sound energy reflected by the duct termination impedance. This termination impedance is a ratio of acoustic pressure to particle velocity. As seen in Figure 2, an impedance change acts like a physical reflective boundary; some sound energy passes through while some energy is reflected back. The reflection coefficient is a ratio of reflected to incident sound pressure amplitudes and is defined as

$$R = \frac{P_r}{P_i}. \tag{1.9}$$

At a boundary (e.g. an open rigid duct termination), the reflection coefficient can be expressed in terms of the two different medium impedances as

$$R = \frac{z_2 - z_1}{z_2 + z_1} = \frac{1 - z_1 / z_2}{1 + z_1 / z_2}. \tag{1.10}$$

The transmission coefficient is a ratio of transmitted to incident sound pressure amplitudes and is defined as

$$T = \frac{P_t}{P_i}, \tag{1.11}$$

and in terms of two different medium impedances is

$$T = \frac{2z_2}{z_2 + z_1} = \frac{2}{1 + z_1 / z_2}. \tag{1.12}$$

1.2.1. Duct Terminations and ERL

End reflection loss for a duct is now explained in terms of the reflection and transmission coefficients at the duct termination. Within a duct with a reflecting termination, the total pressure is the sum of the incident and reflected waves

$$p = Ae^{j[\omega t - kx]} + Be^{j[\omega t + kx]}.$$

The termination impedance for a duct is equal to the radiation impedance, and may be related to the incident and reflected wave amplitudes by

$$Z_m = Z_r = \rho_0 c S \frac{A + B}{A - B}. \tag{1.13}$$

Solving Equation (1.13) for R yields [2]

$$R = \frac{B}{A} = \frac{Z_m / (\rho_0 c S) - 1}{Z_m / (\rho_0 c S) + 1}. \tag{1.14}$$

The power transmission coefficient is determined from the reflection coefficient as

$$T_\pi = 1 - |B / A|^2 = 1 - |R|^2. \tag{1.15}$$

Finally, end reflection loss is

$$ERL = -10 \log\left(1 - |R|^2\right) = -10 \log\left(T_\pi\right), \tag{1.16}$$

$$ERL = -10\log\left(1-\left|\frac{Z_m/(\rho_0 cS)-1}{Z_m/(\rho_0 cS)+1}\right|^2\right). \tag{1.17}$$

The logarithmic relationship between the reflection coefficient and ERL expressed in Equation (1.16) is depicted in Figure 3. The top plot shows ERL values for reflection coefficients between 0 and 1. The bottom plot shows ERL values for reflection coefficients between 0.99 and 1. A reflection coefficient of 0.9 results in an ERL of 7.2 dB while a reflection coefficient of 0.99 results in an ERL of 17 dB.

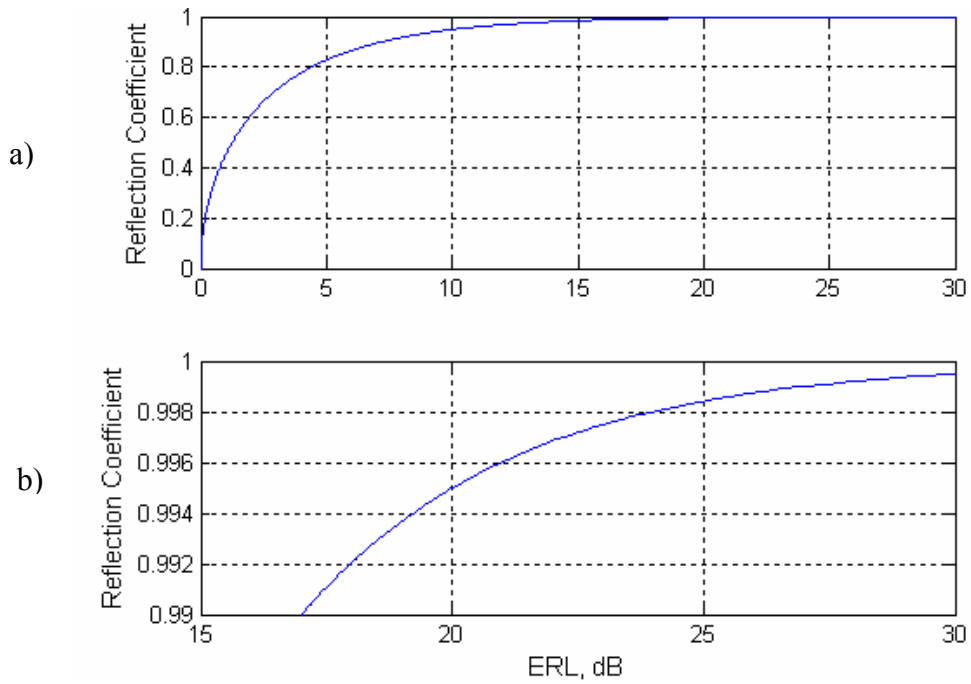

Figure 3. ERL and Reflection Coefficient Relationship for a) *R* from 0-1 and b) *R* from 0.99-1

1.2.2. ERL for Circular Ducts

The analytic determination of ERL for ducts terminating in a rigid baffle and in free space is found in several sources [2-5]. ERL for circular ducts terminating in a rigid baffle (flanged) requires the termination impedance to equal the radiation impedance into the space above the baffle. Radiation impedance is expressed with respect to duct diameter, D, for $kD << 2$ as [2]

$$\frac{Z_m}{\rho_0 c S} = \frac{1}{8}(kD)^2 + j\frac{4}{3\pi}kD. \tag{1.18}$$

ERL is obtained from inserting Equation (1.18) into Equation (1.17). It should be noted that this thesis presents Equations (1.18), (1.19), and (1.20) in terms of duct diameter, D, but they are originally expressed in terms of duct radius, a.

For open ducts terminating in free space, Levine and Schwinger determined the reflection coefficients for $kD < 2$ and $kD > 2$ as [6]:

$$|R| = \exp\left[\frac{-(kD)^2}{8}\right]\left[1+\frac{(kD)^4}{96}\left(\log\left(\frac{2}{\gamma kD}\right)+\frac{19}{12}\right)\right] \text{ for } kD < 2\,, \tag{1.19}$$

$$|R| = \sqrt{\left(\frac{1}{2}\pi kD\right)}\exp\left(-\frac{1}{2}kD\right)\left[1+\frac{3}{8}\frac{1}{(kD)^2}\right] \text{ for } kD > 2, \tag{1.20}$$

where γ = ratio of specific heats and ERL is found using Equation (1.16).

The analytic ERL for flush and free space circular duct terminations that was determined in previous equations is depicted in Figure 4.

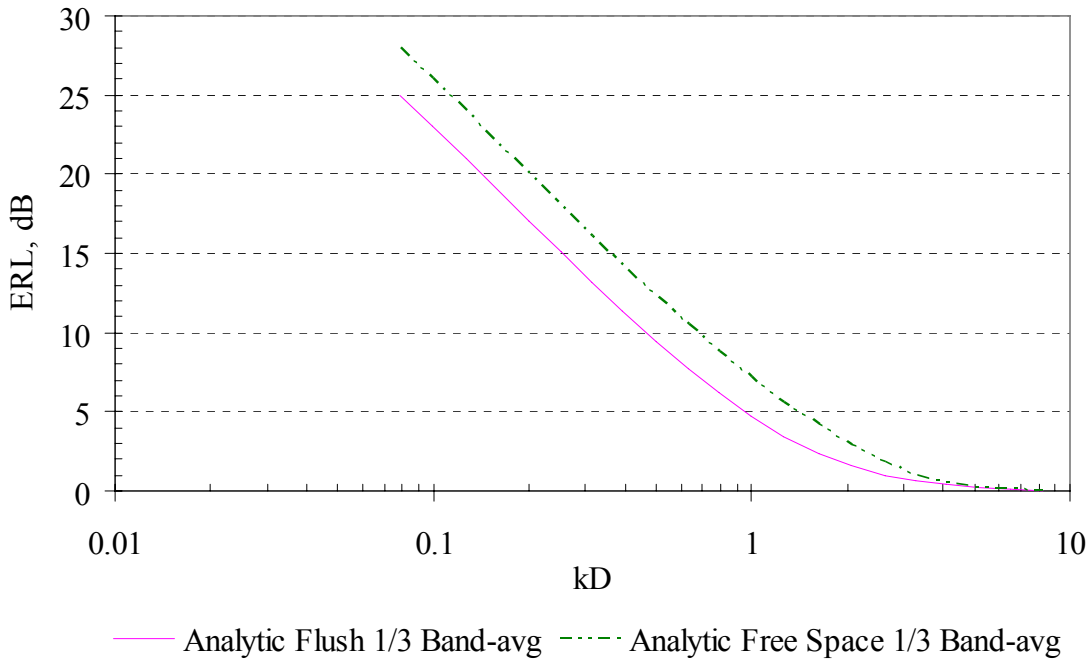

Figure 4. Analytic Circular ERL for Flush and Free Space Duct Terminations

1.2.3. Rectangular Duct ERL

Analytical ERL for rectangular ducts is found by Pierce et al. through the determination of the radiation impedance as[7]:

$$\frac{Z_m}{\rho_0 c S} = \frac{k}{2i\pi S}\iiiint \frac{e^{ikR}}{R}\,dx'\,dy'\,dx\,dy = \frac{1}{i\pi}\begin{pmatrix} ka\left[2X\left(ka,0,0,a/b\right)-\left(a/b\right)Z\left(ka,0,0,a/b\right)\right] \\ +kb\left[2X\left(kb,0,0,b/a\right)-\left(b/a\right)Z\left(kb,0,0,b/a\right)\right]\end{pmatrix}, \tag{1.21}$$

$$X\left(ka,0,0,a/b\right) = \int_0^{\tan^{-1}(b/a)} T_1\left(ika\sec\phi\right)\sec\phi\, d\phi, \tag{1.22}$$

$$Z\left(ka,0,0,a/b\right) = \int_0^{\tan^{-1}(b/a)} T_2\left(ika\sec\phi\right)\tan\phi\sec\phi\, d\phi, \tag{1.23}$$

$$T_1\left(D\right) = \frac{1}{2D^2}\left[e^{2D}-2D-1\right], \tag{1.24}$$

$$T_2(D) = \frac{1}{D^3}\left[De^{2D} - e^{2D} + D + 1\right]. \tag{1.25}$$

where $D = ika\sec\phi$. ERL is obtained from inserting Equation (1.21) into Equation (1.17).

ERL for an open duct is dependant on duct size, as demonstrated in Figure 5 and evident in the impedance equations. Figure 5 indicates that at a fixed frequency, a 6X6 duct has a higher ERL than a 18X54 duct. Comparison of identical configurations for different duct sizes is achieved by using non-dimensional ERL and is depicted in Figure 6. This size comparison is accomplished by plotting ERL with respect to *kD*, where *D* equals the circular or effective duct diameter and is discussed following Figure 6.

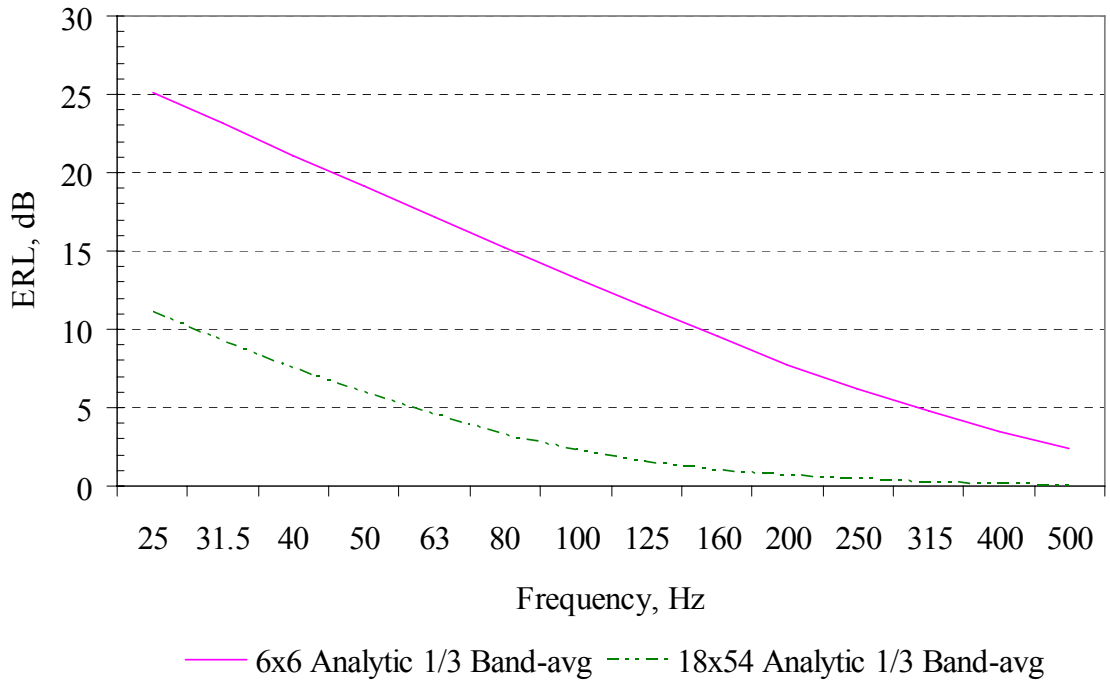

Figure 5. 6X6 and 18X54 Analytic ERL vs. Frequency for Flush Termination Condition

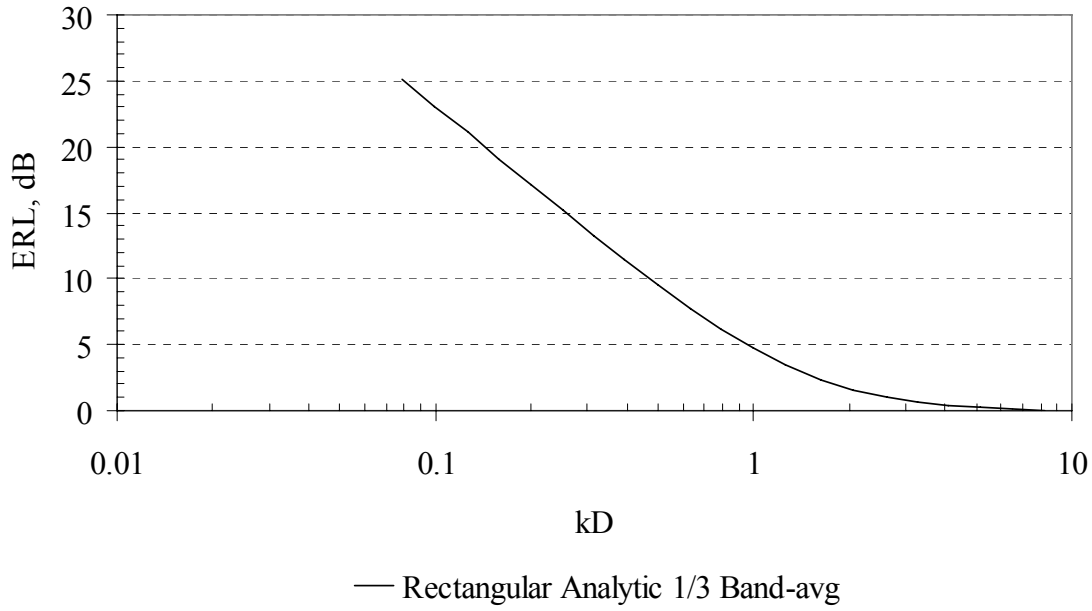

Figure 6. Analytic Rectangular Duct ERL vs. *kD* for Flush Termination Condition

The ASHRAE Handbook states that comparison of rectangular and circular duct ERL is possible by using an equivalent circular duct with the same flow area [1]. The effective circular diameter, *D*, is

$$D = \sqrt{\frac{4r_1 r_2}{\pi}}, \tag{1.26}$$

where r_1 = duct height and r_2 = duct width.

That rectangular and circular ducts with the same flow area implied by Equation (1.26) are equivalent with respect to ERL is evident in Figure 7, where, for a circular duct of 6.77 inches and for a square duct of the same effective diameter, the analytic ERL from Equation (1.18) for circular ducts and Equation (1.21) for rectangular ducts have both been plotted versus *kD*; the individual ERL lines can not be discriminated as they fall on top of each other.

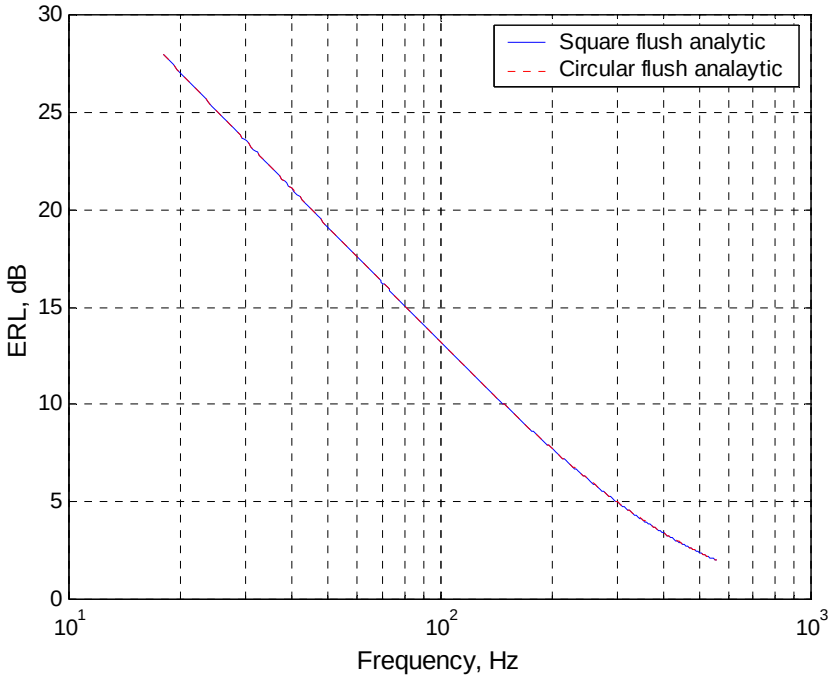

Figure 7. Analytic Circular and Rectangular Duct ERL for D_{eff} = 6.77 in.

1.3 Prior Research

ERL may be predicted analytically for configurations as discussed in the previous section, and may be measured experimentally. Most estimates or calculations of ERL consider the radiation impedance of a baffled piston. A common method for experimentally determining ERL is the "two-microphone" method.

Analytic predictions of ERL for circular ducts of infinite length were considered by Davies and Coelho to determine the reflection coefficient at waveguide terminations [8]. Norris and Sheng analytically determined ERL for an open flanged pipe [9] while Selamet, Ji, and Kach employed the boundary element method to determine ERL for various duct termination distances above a baffle [10]. In these works, only circular

ducts of infinite length were considered with no experimental validation supporting the analytic and numerical findings.

Experimental consideration of ERL using the two-microphone impedance method of Chung and Blaser [11, 12] is another means to determine the complex reflection coefficient at a duct termination. The basic setup for application of the method is shown in Figure 8. This technique allows for the determination of the reflection coefficient for arbitrary media and its modification allows for the determination of ERL. A prelude to the Chung and Blaser work, Seybert and Ross developed an experimental two-microphone method using the cross-spectral density function for determining acoustic properties in 1977 [13]. Chung and Blaser used a more efficient transfer function method that allows the determination of all normal incidence acoustic properties both theoretically [11] and experimentally [12]. The Chung and Blaser method is also able to determine the transmission loss whereas the Seybert and Ross method required a third microphone. The Chung and Blaser transfer function method is the primary technique used today for determining an impedance change directly. The method assumes no mean flow, plane wave propagation, and negligible tube wall losses.

Possible error influences and frequency range issues should be considered when using the two-microphone method. Bodén and Åbom addressed possible error influences in the two-microphone method including microphone spacing, microphone distance from the termination, and duct length influence on random error [14]. Accurate determination of ERL at low frequencies depends on microphone spacing and the analysis system. The error sources considered by Bodén and Åbom are generally greater at lower frequencies, with bandwidth of acquisition and phase matching being two critical aspects. That low

frequency limitations exist in the application of the method may be seen in the work of Katz [15], and of Jones and Stiede [16]. In both of these works, the authors did not perform measurements in the range of interest to the work documented in this thesis, below 100 Hz, with Katz reporting results from 1 kHz and above, and Stiede and Jones reporting results above 300 Hz.

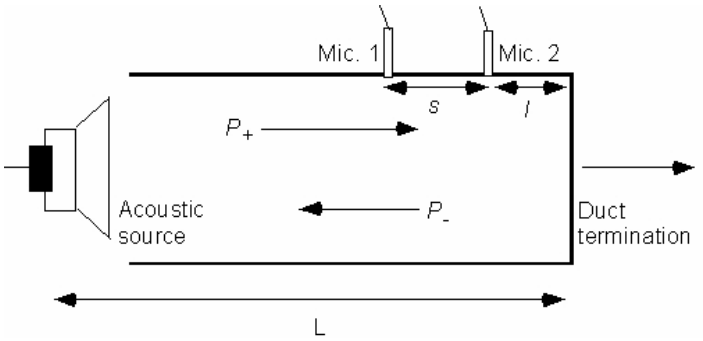

Figure 8. Basic Two-microphone Method Setup

With reference to the notation and configuration depicted in Figure 8, the determination of ERL theoretically [11] and experimentally [12, 17] using the two-microphone method requires the determination of the measured transfer function between microphones 1 and 2

$$H_{12} = \frac{P_2}{P_1} = \frac{\left[P_{2i} + P_{2r}\right]}{\left[P_{1i} + P_{2i}\right]}, \tag{1.27}$$

where P_n = pressure at microphone n,
P_{ni} = pressure due to incident waves at microphone n, and
P_{nr} = pressure due to reflected waves at microphone n.

The complex reflection coefficient at microphone 1 is

$$R_1 = \frac{\left[H_{12} - e^{-jks}\right]}{\left[e^{jks} - H_{12}\right]}, \tag{1.28}$$

and the reflection coefficient at the termination is

$$R = R_1 e^{j2k(l+s)}. \tag{1.29}$$

Finally, ERL is determined using Equation (1.29) as

$$ERL = -10\log\left(1 - |R|^2\right) = -10\log\left(1 - \left|\frac{\left[H_{12} - e^{-jks}\right]}{\left[e^{jks} - H_{12}\right]}\right|^2\right). \tag{1.30}$$

1.4 A Note on Narrow Band vs. Broadband Measurement of ERL

The measurement bandwidth and type of noise used both affect experimental ERL results. Narrow bandwidth measurements will typically agree more closely with a continuous result than broadband measurements. Noise is typically produced as either white or pink noise. White noise contains equal power at each frequency. Assuming white noise excitation, then the power incident on the duct termination is

$$W_{BI} = \Delta f \times W_i. \tag{1.31}$$

The reflected power is

$$W_{BI} = \sum_i R^2(f) W_i, \tag{1.32}$$

and the transmitted power is

$$W_{BT} = W_{BI} - W_{BR} = \Delta f \times W_i - \sum_i R^2 W_i, \tag{1.33}$$

where W_{BI} = total incident power in band Δf,
W_{BR} = total reflected power,

W_{BT} = total transmitted power, and
Δf = bandwidth of the measurement.

Measured ERL is then

$$ERL = -10\log\left(1 - \frac{\sum R^2}{\Delta f}\right). \tag{1.34}$$

Consider pink noise excitation with incident power

$$W_{BI} = W_0 \sum_i \frac{f_0}{f_i}. \tag{1.35}$$

Reflected power is

$$W_{BR} = \sum_i R^2 \frac{f_0}{f_i} W_0, \tag{1.36}$$

such that the transmitted power is

$$W_{BT} = W_{BI} - W_{BR} = W_0 f_0 \sum \frac{1}{f_i} - W_0 f_0 \sum \frac{R_i^2}{f_i}, \tag{1.37}$$

where W_0 = some reference power. ERL is then

$$ERL = -10\log\left(1 - \frac{\sum R_i^2 / f_i}{\sum 1/f_i}\right). \tag{1.38}$$

Figures 9-12 depict the impact of band averaging on ERL. Figure 9 depicts excellent agreement between the analytic ERL for continuous and one-third octave band values for the flush termination condition using white noise averaging. The octave band values indicate greater deviation from the continuous values than the one-third octave band values. ERL averaging discrepancies at 125 Hz are depicted in Figure 10 between continuous analytic, one-third octave band, and octave band ERL using white noise averaging. Figure 10 demonstrates the improved description of ERL behavior that comes

from using a narrow band (one-third octave) instead of broadband (octave) measurement. Figure 11 depicts the sound source and averaging techniques for octave bands described in Equations (1.34) and (1.38) along with the ASHRAE Table values for the flush termination condition at 125 Hz. The ASHRAE Table 23 value is higher than the analytic prediction for the flush termination condition at 125 Hz. Figure 12 depicts the sound source and averaging techniques for octave bands described in Equations (1.34) and (1.38) along with the ASHRAE Table 22 values for the free space termination condition at 125 Hz. The ASHRAE Table value is lower than the analytic prediction for the free space termination condition at 125 Hz. These results indicate that narrow bandwidth measurements will agree more closely with the continuous result than will broadband measurements. Also, the choice of signal type for broadband measurements will affect the result.

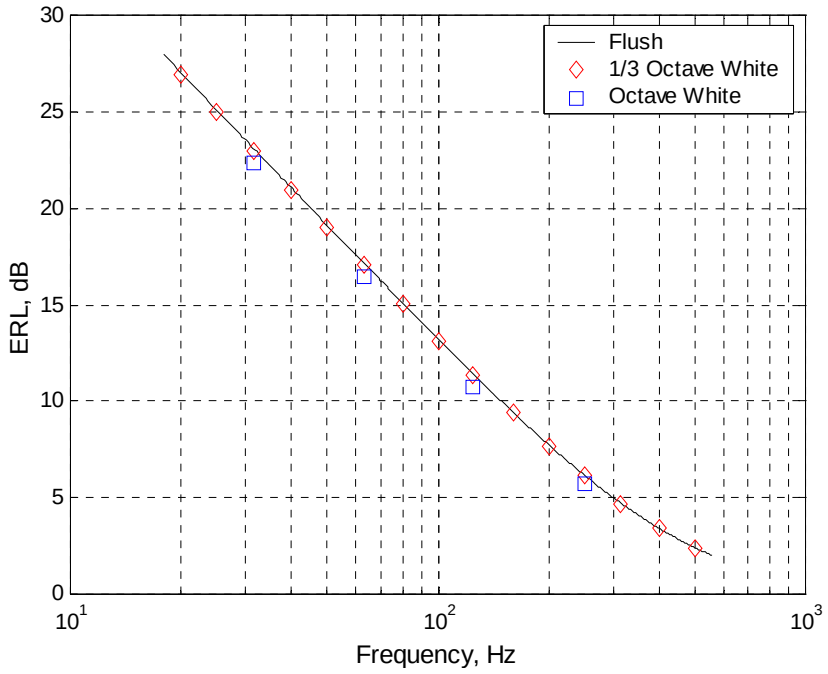

Figure 9. 6X6 Analytic ERL – Continuous, Octave, and One-third Octave Bands

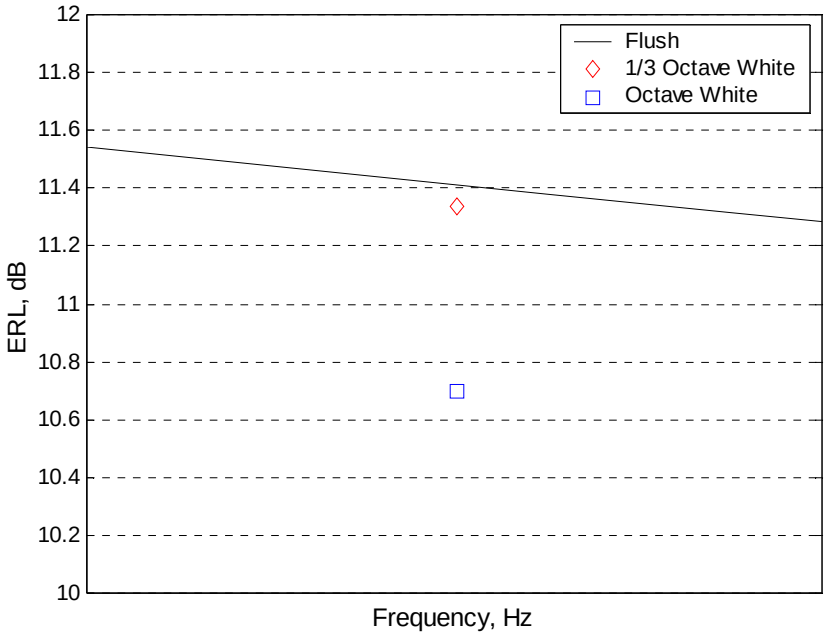

Figure 10. 6X6 Analytic ERL at 125 Hz – Continuous, Octave, and One-third Octave Bands

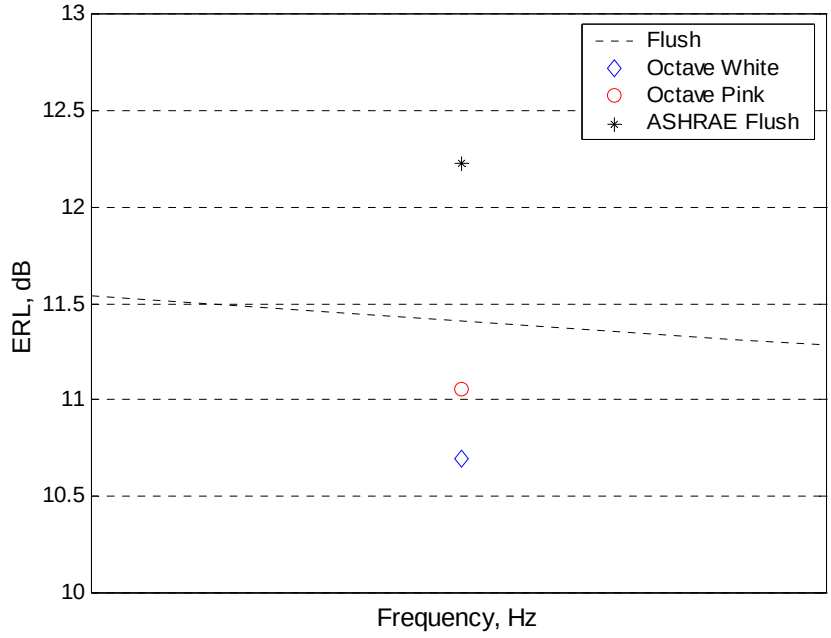

Figure 11. Comparison of Flush 6X6 ERL Values Obtained by Octave Band Averaging and to ASHRAE Table 23 values at 125 Hz

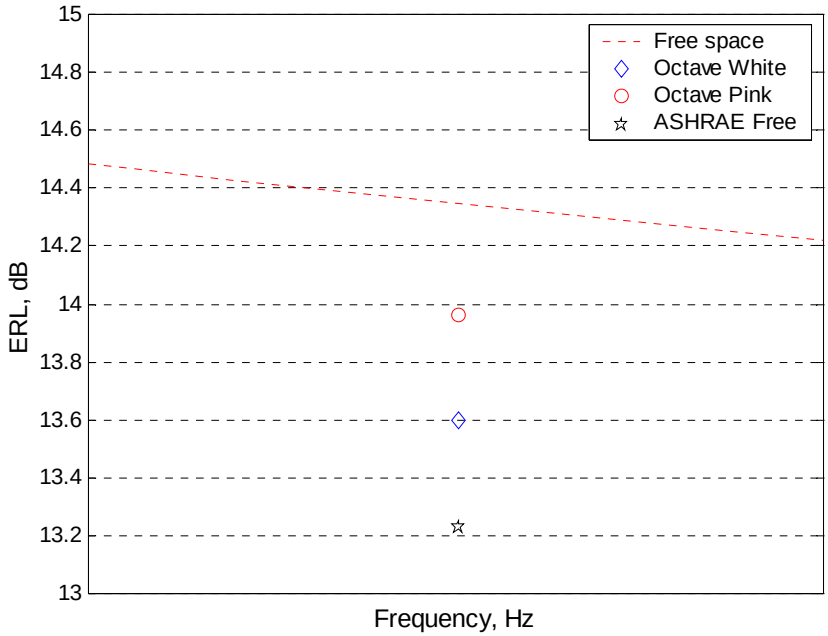

Figure 12. Comparison of Free Space 6X6 ERL Values Obtained by Octave Band Averaging and to ASHRAE Table 23 values at 125 Hz

1.5 ASHRAE Handbook ERL Values

The duct termination conditions considered by the ASHRAE Handbook are shown in Figure 13. Builders must often meet HVAC noise requirements and rely on the ASHRAE Handbook for determining ERL values. The ASHRAE Handbook only considers rigid open ducts terminating flush in an infinite baffle or in free space. One of the goals of this thesis was to determine the validity of the listed ASHRAE Handbook ERL Table, which are shown in Tables 1 and 2 [1].

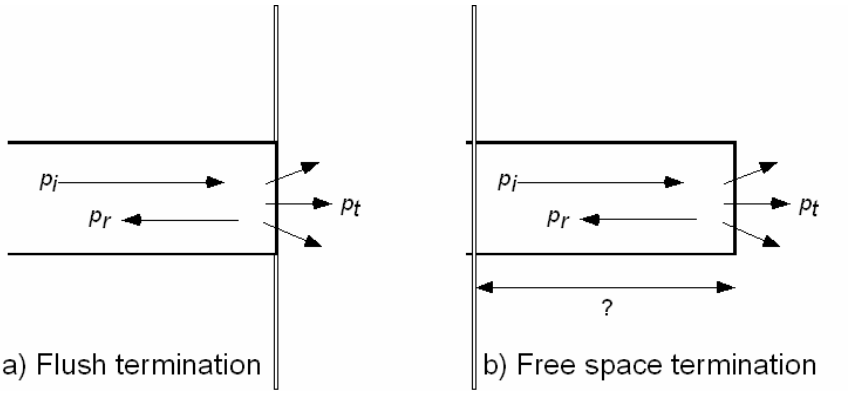

Figure 13. a) ASHRAE Table 23 Flush Termination Configuration and b) ASHRAE Table 22 Free Space Termination Configuration

Table 1. ASHRAE Table 22 for ERL of Duct Terminated in Free Space [1]

Duct Diameter	End Reflection Loss, dB Octave Band Center Frequency, Hz					
(in.)	**63**	**125**	**250**	**500**	**1000**	**2000**
6	20	14	9	5	2	1
8	18	12	7	3	1	0
10	16	11	6	2	1	0
12	14	9	5	2	1	0
16	12	7	3	1	0	0
20	10	6	2	1	0	0
24	9	5	2	1	0	0
28	8	4	1	0	0	0
32	7	3	1	0	0	0
36	6	3	1	0	0	0
48	5	2	1	0	0	0
72	3	1	0	0	0	0

Table 2. ASHRAE Table 23 for ERL of Rigid Duct Terminated Flush with Baffle [1]

Duct Diameter	End Reflection Loss, dB Octave Band Center Frequency, Hz				
(in)	**63**	**125**	**250**	**500**	**1000**
6	18	13	8	4	1
8	16	11	6	2	1
10	14	9	5	2	1
12	13	8	4	1	0
16	10	6	2	1	0
20	9	5	2	1	0
24	8	4	1	0	0
28	7	3	1	0	0
32	6	2	1	0	0
36	5	2	1	0	0
48	4	1	0	0	0
72	2	1	0	0	0

The method used to determine the published ERL values listed in the ASHRAE Handbook is not clearly defined or substantiated. The ASHRAE Handbook cites the 1981 Perdue University report *Investigation of End Reflection Coefficient Accuracy Problems with AMCA Standard 300-67* [18] and AMCA Standard 300 as sources for the listed ERL Table values. The Perdue report did not determine *R* values high enough to produce accurate low frequency ERL results (< 63 Hz), but agreed well with analytic predictions above 125 Hz. One problem with the ASHRAE Handbook ERL values is that they only extend down to 63 Hz. The ASHRAE Handbook never defines the acoustic free space condition and assumes "diffusers that terminate in a suspended lay-in acoustic ceiling can be treated as terminating in free space" [1]. This configuration is analogues to many drop ceiling applications, yet there is a large degree of configuration variability in practice that is not addressed by the configurations implied for use of the ASHRAE Tables. The ASHRAE ERL table values also only take into account hard termination baffles, even though many real world applications use soft termination baffles (e.g. ceiling tiles). As a result, any possible influence from baffle hardness is not considered when using the ASHRAE Table values. Another limitation of ASHRAE ERL Tables 22-23 is the inability to account for termination variation effects. The impact from diffusers with or without flex duct is not addressed. One of the goals of this thesis was to determine the validity of the ASHRAE Handbook ERL Table values. This was achieved by experimentally determining ERL for ASHRAE Handbook duct configurations and comparing the results to the corresponding ASHRAE values and analytic predictions.

Experimental ERL values for the flush termination condition shown in Figure 8a are compared to ASHRAE Table 23 values and the corresponding analytic prediction. The free space experimental determination of ERL first requires the determination of a termination distance above the baffle that acoustically represents "free space." As mentioned earlier, it is unknown if the ASHRAE ERL Table 22 values accurately represent free space ERL and requires experimental validation and comparison to the analytic prediction. Experimentally verifying ERL for open rigid ducts will also help determine the acoustic impact from diffuser, grill, and flex duct usage.

Figure 14 shows the differences between analytic and ASHRAE ERL Table values for flush and free space rigid open duct configurations. The ASHRAE ERL Tables list ERL in octave bands. ASHRAE ERL Table values for the flush termination condition are consistently higher than the corresponding analytic predictions. ASHRAE ERL Table values for the free space termination condition are consistently lower than the corresponding analytic predictions.

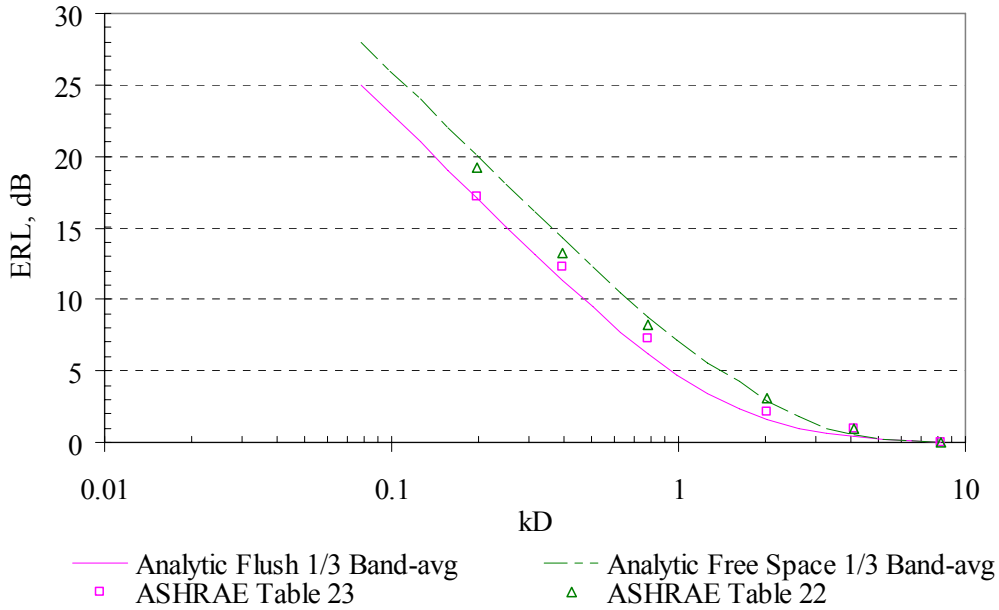

Figure 14. Analytic and ASHRAE ERL Comparison

1.6 Motivation

Motivation for this research comes from the limited experimental determination of ERL for duct geometries and terminations often found in HVAC practice as well as the desirability of determining ERL at lower frequencies than is currently available. Current building specifications using the ASHRAE Handbook are based on information that is over 30 years old and has not been experimentally validated. Two major caveats in the understanding of ERL are low frequency behavior (<100 Hz) and possible termination variation effects. In order to provide useful information for the HVAC industry, the ERL for ducts of comparable geometry and varying termination conditions must be understood and experimentally verified against analytic predictions. This thesis specifically investigated the impact of rectangular duct size, termination baffle hardness, termination distances at and above the termination baffle, and termination variation on ERL. These configuration conditions are discussed in more detail in the following chapter.

CHAPTER 2

EXPERIMENTAL SETUP

This chapter presents hardware and software setups used to experimentally determine ERL for a variety of duct sizes and termination variation conditions. The experimental setup used is a modified version of the test rig discussed in ASTM Standard E1050 [17]. The ASTM Standard E1050 *Standard Test Method for Impedance and Absorption of Acoustical Materials Using A Tube, Two Microphones and A Digital Frequency Analysis System* employs the two-microphone method of Chung and Blaser and provides the basic methodology implemented in this thesis for determining ERL [17]. This section provides an overview of the physical setup, duct construction, microphone configuration, duct configurations and labeling, and the signal generation and data acquisition system.

2.1 Physical Setup

The basic test duct elements depicted in Figure 15 comprise a sound source, test duct, termination baffle, and microphone pair. The test duct starts in the reverberation chamber and terminates in the hemi-anechoic chamber. A sound generation system drives an acoustic signal into the duct inlet at the reverberation chamber end. The sound generation system depicted in Figure 16 comprises a signal generator, equalizer, amplifier, and speaker. The signal generator sends a step-sine signal to the parametric equalizer. The parametric equalizer sends the modified step-sine signal to an amplifier. The amplifier sends the modified signal to a Sonicraft SC-1250 12” subwoofer, which

produces the acoustic signal at the duct inlet. The subwoofer is housed in a sealed MDF speaker box. The speaker box feeds into the rectangular duct with no direct coupling, which decreases vibration transmission between the sound source and duct. Fiberglass insulation near the sound source reduces standing wave influences on ERL measurements. The duct passes through a 5-inch thick chamber wall separating the two chambers, which prevents unwanted reverberation chamber noise from entering the hemi-anechoic chamber. The duct terminates in the hemi-anechoic chamber at or above the termination baffle. Sound measurements are obtained using two Brüel & Kjær (B&K) phase matched microphones (PMMs). More detailed hardware information is listed in Appendix B.

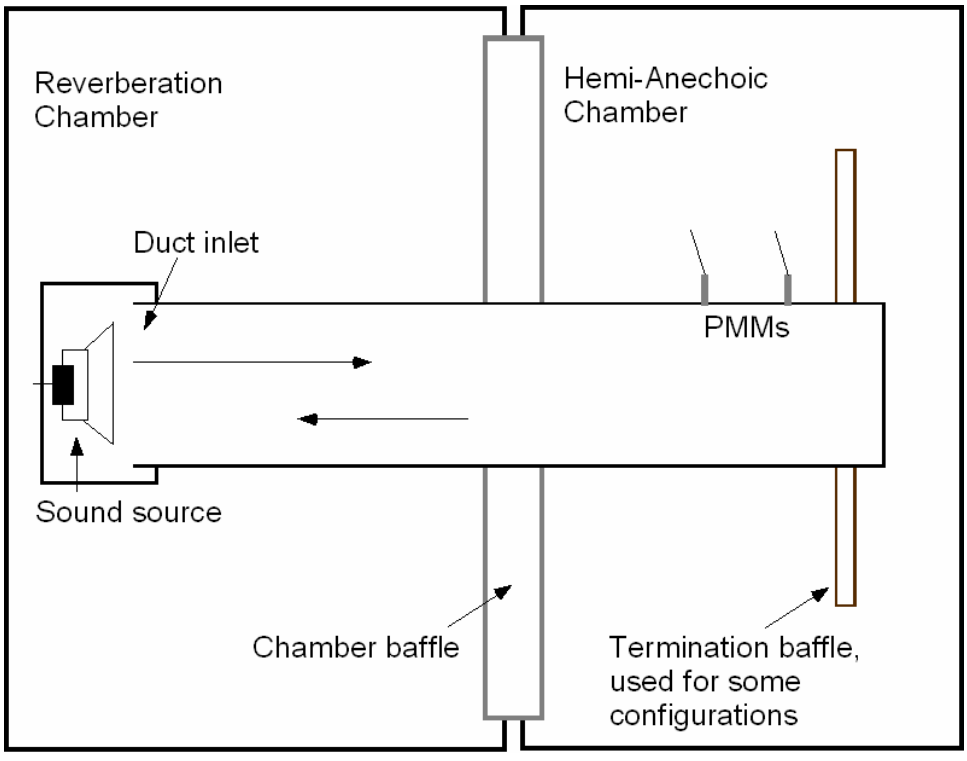

Figure 15. Test Duct Setup

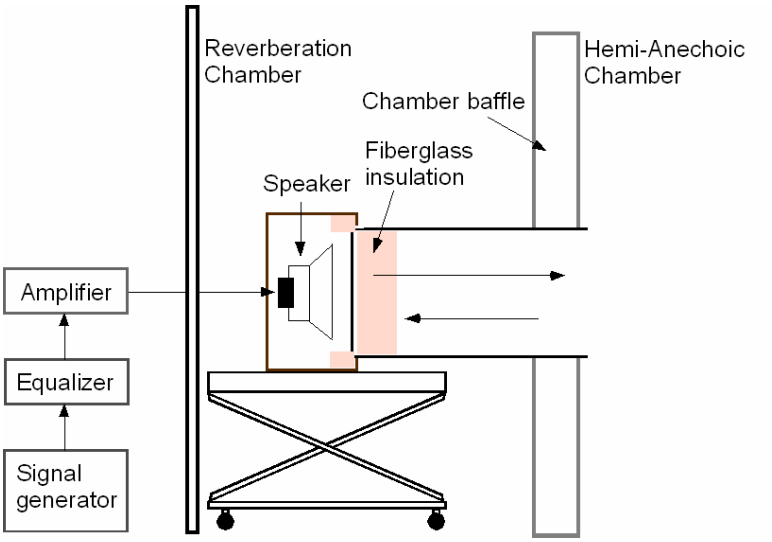

Figure 16. Sound Generation System

2.2 Duct Construction

Figure 17 illustrates the test duct, which is constructed from three duct sections joined together. The two upstream duct sections were constructed out of drywall and metal duct, MDF, or duct board. Real-world applications often use "rigid duct", which is made out of thin metal. For this thesis, metal duct vibrated a great deal at low frequencies, contaminating measurements. To alleviate this problem, two layers of ¾"-thick drywall were rigidly attached to the metal duct. This mass and stiffening increase reduced duct vibration in the frequency range of interest. The drywall and metal duct has an extremely low absorption coefficient, allowing for minimal sound loss between the sound source and microphones. Low absorption is extremely important in achieving a high signal-to-noise ratio (SNR). Duct board is made of lightweight compressed fiberglass with a foil coating. It has a low absorption coefficient in the lower frequencies

and is easy to fabricate because of its precut construction. MDF duct is easier to fabricate than metal and drywall duct and provides minimal vibration and sound transmission.

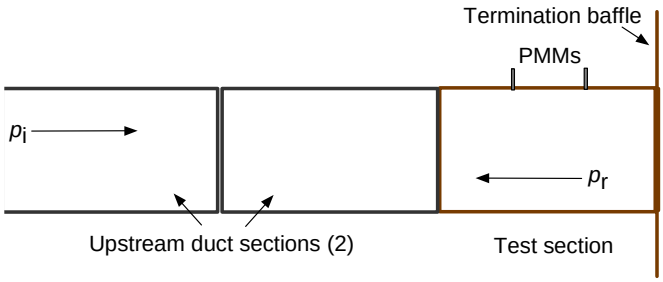

Figure 17. Basic Test Duct Configuration

Acoustic measurements are collected in the final section of the test duct. The final duct section is referred to as the test section. It is constructed out of two layers of ¾"-thick MDF and houses the PMMs. Termination variations are implemented on the test section and all test section ducts are two feet in length.

2.3 Microphone Configuration

The microphone setup is shown in Figure 18. The microphone housing consists of a hollow polycarbonate cylinder, which slides into a rubber-sleeved hole drilled through the MDF test section wall. The polycarbonate housing uses two plastic screws to hold the PMM in place and allows for quick removal and adjustment when needed (e.g. when the PMMs are calibrated they must be removed from the polycarbonate housing). A rubber o-ring seal separates the microphone diaphragm grill from the polycarbonate housing. The o-ring provides an air-tight seal between the inside and outside of the duct.

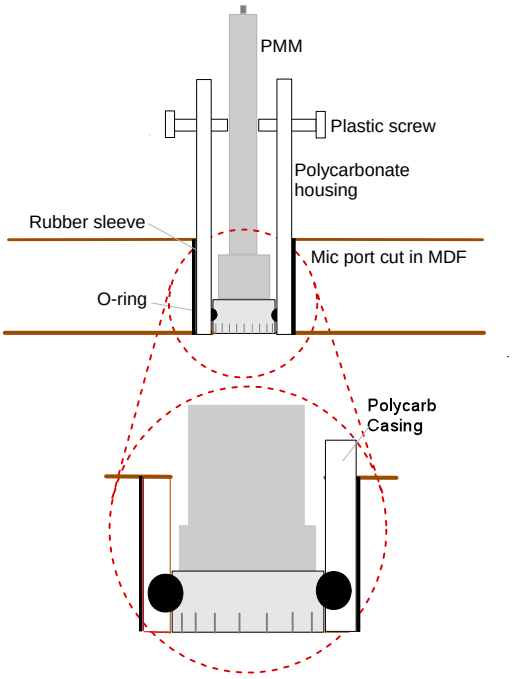

Figure 18. Phase Matched Microphone (PMM) Setup

2.4 Duct Configurations and Labeling

Duct configurations were divided into four major groups: duct size, termination distance above the baffle, termination baffle hardness, and diffuser and/or flex duct presence at the duct termination. These four conditions were analyzed independent of each other, allowing the impact on ERL of each to be quantified. For all ERL plots shown in the results chapter and Appendix C, a simple identification technique is employed to concisely describe the setup. The identification is a label structured as:

$$r_1 \times r_2 \text{ HARDNESS-DISTANCE-TERMINATION,} \tag{2.1}$$

where r_1 = rectangular duct width in inches,
r_2 = rectangular duct height in inches,
HARDNESS = "Hard" or "Soft" termination baffle,
DISTANCE = "Flush", "0.5D", "1D", "2D", "5D", "Flex", or "Free", and
TERMINATION = "Open" or diffuser type (i.e. "ML-39", "TDC", etc).

An open 6X6 rectangular duct terminating flush with a rigid baffle would be referred to as "6X6 Hard-Flush-Open." A 6X10 rectangular duct terminating 1D above a soft termination baffle with a Titus ML-39 Single-slot diffuser would be referred to as "6X10 Soft-1D-ML39." This duct description method makes it much easier to refer back and forth between setups without needing a lengthy description. The term "VARIOUS" is also used to take the place of "HARDNESS", "DISTANCE", and "TERMINATION" when multiple setups within that parameter are being compared.

The first duct configuration condition considered here was duct size. Table 3 lists the seven different rectangular duct sizes that were tested. Duct sizes are given in inches and are referred to as "small" (6X6, 6X10, and 6X18) and "large" (6X36, 18X18, 18X30, and 18X54).

Table 3. Duct Sizes Tested

Dimensions (in.)	Effective Diameter (in^2)
6x6	6.77
6x10	8.74
6x18	11.73
6x36	16.58
18x18	20.31
18x30	26.22
18x54	35.18

Figure 19 illustrates the second configuration condition; termination distance above the termination baffle. Five termination distances were tested; Flush, 0.5*D*, 1*D*, 2*D*, and 5*D*. *D* is the effective diameter and was previously discussed. Analytic predictions only exist for a flush baffle and free space termination. Duct termination distances that were tested with respect to duct size are listed in Table 4. Larger duct size

ERL was investigated using only Hard-Flush-Open terminations, while the smaller duct sizes were used for additional measurements with the duct terminating above the baffle.

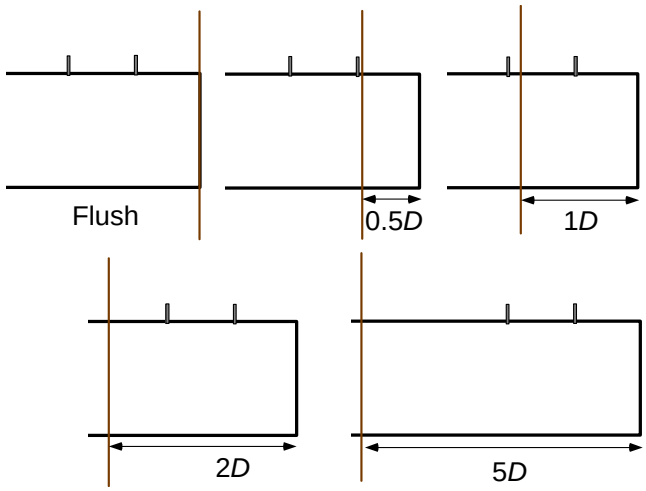

Figure 19. Duct Termination Distance Conditions

Table 4. Termination Distances Tested and Corresponding Duct Sizes

Duct Size	Termination Distances
6x6	Flush, 0.5D, 1D, 2D, 5D
6x10	Flush, 0.5D, 1D
6x18	Flush, 0.5D, 1D
18x18	Flush
18x30	Flush
18x54	Flush

The third duct configuration condition was termination baffle hardness. A termination baffle made of plywood with or without USG R76775 Luna *ClimaPlus* ceiling tiles attached using thin wood strips was used. The plywood termination baffle was presumed to represent an acoustically hard surface and is depicted in Figure 20. The ceiling tile termination baffle was presumed to represent an acoustically soft surface and is depicted in Figure 21. The acoustically soft termination condition is important since

many HVAC applications involve drop ceilings, which are considered acoustically soft by the ASHRAE Handbook.

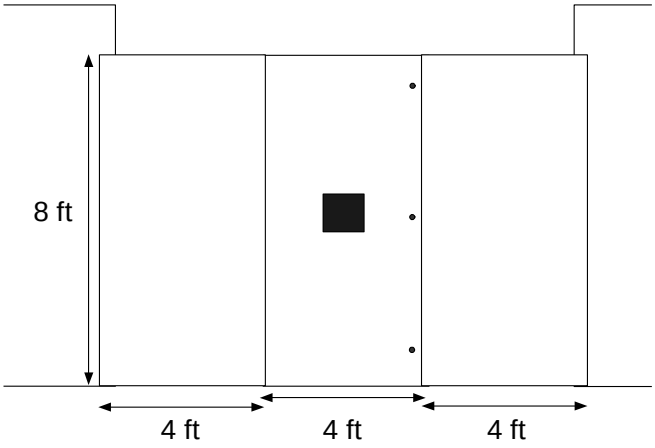

Figure 20. Acoustically Hard Termination Baffle – Plywood Layout

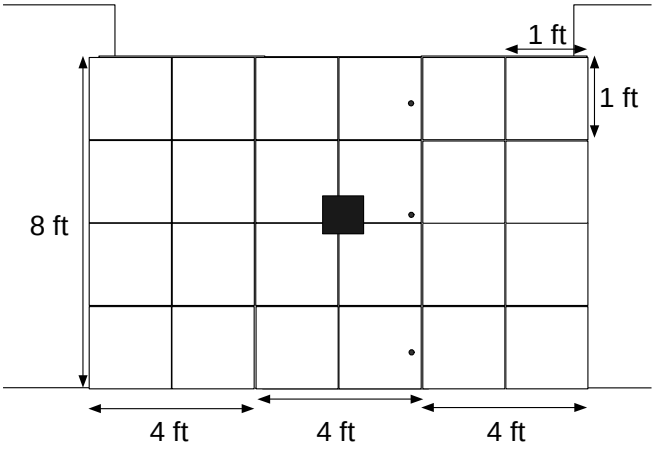

Figure 21. Acoustically Soft Termination Baffle – Ceiling Tile Layout

Frequency is important in determining how large a baffle must be in order to appear acoustically infinite. The frequency at which a baffle appears acoustically infinite can be approximated as

$$\frac{\lambda}{d} > 1, \tag{2.2}$$

where λ = wavelength and d = distance from the duct center to the nearest baffle corner.

Equation (2.2) results in a frequency of approximately 160 Hz for the termination baffle. The termination baffle cannot be assumed acoustically infinite below this frequency.

The fourth duct configuration condition involved diffuser and flex duct termination variations. As discussed in chapter 1, many HVAC applications utilize a diffuser to improve air dispersion, so several were tested to assess their impact on ERL. Also as was discussed in chapter 1, flex duct is often used to connect rigid duct with a diffuser. This flex configuration was tested to determine ERL effects with and without a diffuser. A total of eight termination variations were tested using a combination of diffusers and flex duct. Table 5 lists all the termination variations tested (recall that "Small" refers to the 6X6, 6X10, and 6X18 duct sizes).

Table 5. Termination Types Tested with Corresponding Duct Sizes and Flex Duct Usage

Termination Type	Flex Duct	Duct Sizes	TERMINATION
Single-slot diffuser	No	6x10	ML39
Open	Yes	Small	Open
Rigid (2-layers MDF)	Yes	Small	Rigid
Single-slot diffuser	Yes	6x10	ML39
Square-face diffuser	Yes	6x6 & 6x10	TDC
Plenum	Yes	6x10	Plenum
Plenum with single-slot diffuser	Yes	6x10	Plenum + ML39

The first diffuser configuration discussed is depicted in Figure 22 and comprises a single slot diffuser rigidly mounted to a rigid duct termination. The specific slot diffuser that was tested is a Titus ML-39 Single-slot diffuser. This setup was only used with the

6X10 duct, as it became apparent that the ML-39 diffuser was not being used as originally intended and lacked application relevance. Normally, the slot diffuser is inserted into a plenum, which is fed via flex duct from the rigid duct (i.e. main line). In this setup, the termination is essentially a rigid termination. Figure 23 shows a Titus ML-39 slot diffuser. Air flows through the one inch slots, *s*. Figure 23 shows a slot diffuser with two slots; the actual test setup had one slot. Figure 24 illustrates the side view setup for the Titus ML-39 Single-slot diffuser with the rigid MDF test section and termination baffle. For this test, the ML-39 diffuser was positioned in the center of a ¾"-thick piece of MDF that was rigidly attached to the MDF test section duct termination.

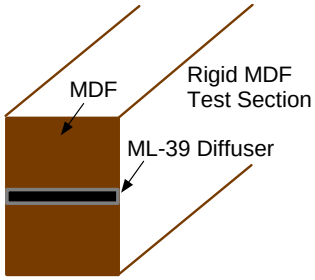

Figure 22. Titus ML-39 Diffuser and MDF Termination Configuration

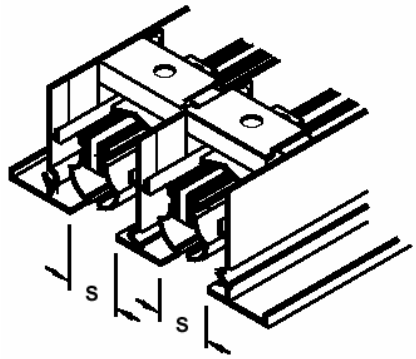

Figure 23. Detailed View Titus ML-39 Slot Diffuser (2 slots)

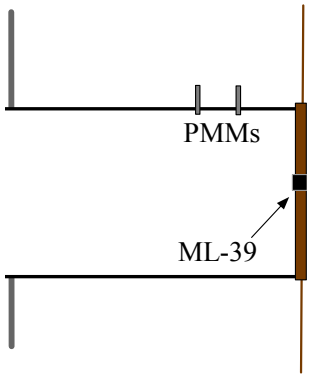

Figure 24. Basic Side View Titus ML-39 Single-slot Diffuser Setup

Figure 25 illustrates the basic setup employed when flex duct was tested. Flex duct was used between the rigid MDF test section and the baffle at a length of 2*D*, which is twice as long as the corresponding rigid duct's effective diameter. Only the small duct sizes were tested using flex duct. The 2*D* length of flex duct resulted in lengths of 13.54, 17.48, and 23.46 inches for the 6X6, 6X10, and 6X18 ducts, respectively.

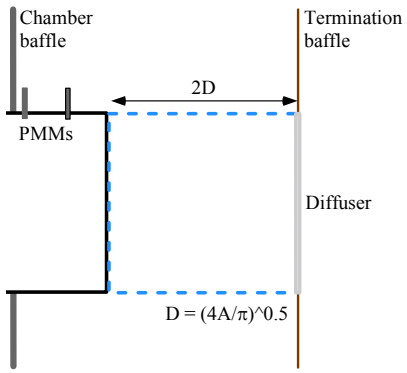

Figure 25. Basic Side View of Generic Flex Duct Setup

Flex duct testing involved six different termination configurations, listed earlier in Table 5. Figure 26 shows the 2*D* length flex duct and Titus ML-39 diffuser setup. The

same Titus ML-39 Single-slot diffuser was used for the flex duct testing and the rigid duct testing. An open flex duct termination means there was no diffuser or rigid termination. A rigid termination consisted of a 1.5”-thick MDF wall at the flex duct termination. These two configurations, open and rigid, represent the two extremes of flex duct termination variation. Flex duct using three diffuser setups was also tested, but not for all rectangular duct sizes. The three diffuser setups used with flex duct were a Titus ML-39 diffuser, Plenum with and without ML-39 diffuser, and TDC diffuser.

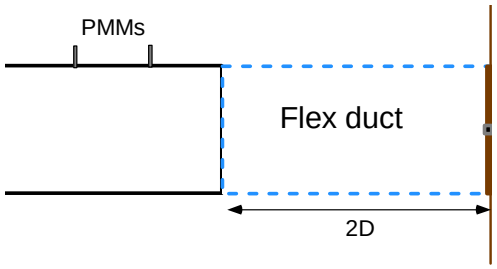

Figure 26. Side View Titus ML-39 Diffuser with 2*D* Flex Duct Setup

Figure 27 shows a simple flex duct and plenum setup while Figure 28 shows the actual plenum used in testing; specifically a Titus TBD-30 adjustable plenum slot diffuser [19]. Slot diffusers are typically used in conjunction with a plenum. A plenum is a fiberglass-lined metal box that joins and accommodates possible duct size change changes between a feed line and diffuser to improve air flow across the entire slot diffuser. Plenums are needed in the case of a slot diffuser because normally slot diffusers have extreme aspect ratios that require a way to evenly distribute airflow across the entire element. Testing was performed with and without the ML-39 slot diffuser in place on the plenum.

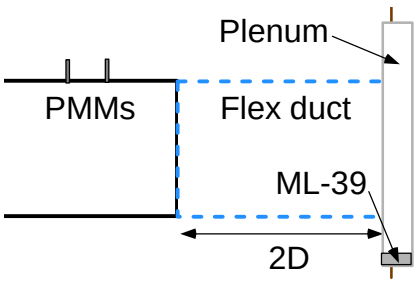

Figure 27. Side View Titus Plenum with 2*D* Flex Duct Setup

Figure 28. Titus Plenum and ML-39 Slot Diffuser [19]

Another common square diffuser used in drop ceilings applications is the Titus TDC diffuser. Flex duct leads from the main line (i.e. rigid duct) to a square diffuser. Figure 29 shows the general flex duct and TDC diffuser setup. Figure 30 shows the front view of the TDC diffuser and Figure 31 shows a more detailed cross section of the TDC diffuser. This diffuser has a circular inlet to square outlet transition; the round flex duct hooks up directly to the back of the square-faced diffuser. Airflow is uniformly dispersed to the occupied space via an array of metal fins in the TDC diffuser.

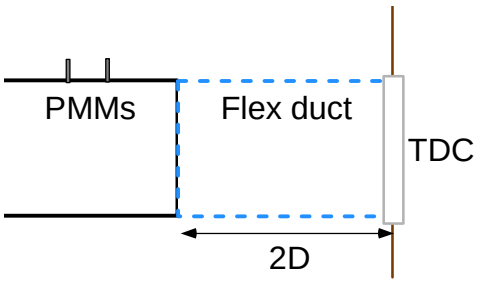

Figure 29. Side View Titus TDC Diffuser with 2D Flex Duct Setup

Figure 30. Front View Titus TDC Diffuser [19]

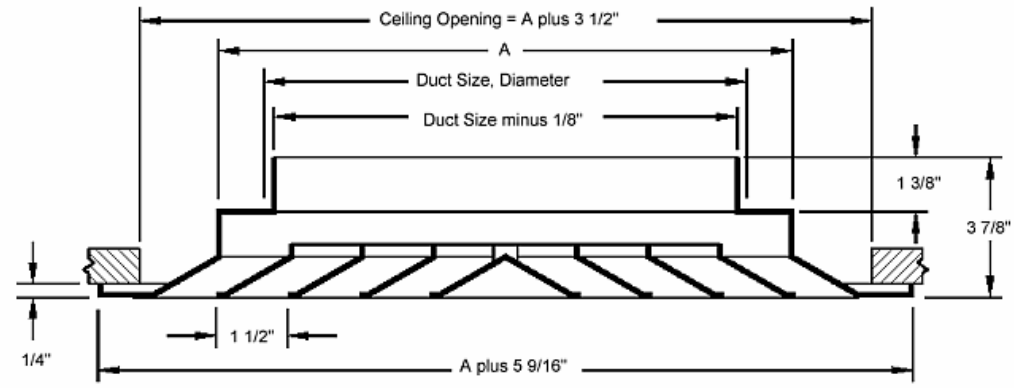

Figure 31. Detailed Side View Titus TDC Diffuser [19]

2.3 Signal Generation and Data Acquisition System

Figure 32 illustrates the different components that make up the signal generation and data acquisition system. Signal generation consisted of four key components, which included a function generator, parametric equalizer, amplifier, and subwoofer. A function generator sent a signal to a parametric equalizer and amplifier. This signal powered a subwoofer that produced the acoustic signal at the test duct inlet. A step-sine technique was employed using a SigLab system that measured the frequency response function of a dynamic system. In this case, the transfer function between the two B&K PMMs was measured and recorded. The signal produced by the SigLab function generator was equalized using an ASHLEY digital parametric equalizer. The signal was amplified using a Pyramid 200 Watt P.A. amplifier and sent to the subwoofer. The SigLab provided an input to the subwoofer between 18 and 560 Hz with a 2 Hz tracking filter bandwidth.

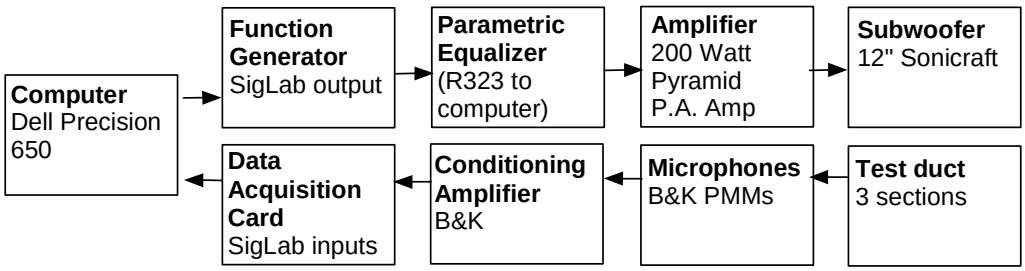

Figure 32. Schematic Representation of Signal Generation and Data Acquisition System

CHAPTER 3

EXPERIMENTAL PROCEDURE

This chapter presents the experimental procedure used to determine ERL for the seven rectangular duct sizes and various termination conditions mentioned previously. The basic test procedure for determining ERL consisted of controlling a basic input (sound generation) and recording a basic output (transfer function between the two PMMs). The basic test setup procedure, measurement method, frequency considerations, and post processing (error analysis) are discussed in the following sections.

3.1 Basic Test Procedure

The test duct and termination setups were constructed according to the configuration matrix in Appendix A and described previously. Termination variations for a specific duct size were performed before proceeding to another test duct size. Microphone phase calibration was performed in the hemi-anechoic chamber once the test setup was in place. Microphone calibration was performed using a Larson Davis Residual Intensity Calibrator 291 (CAL291), which applies the same acoustic pressure to both microphones. The calibration transfer function used to correct phase mismatch between the microphones is

$$h_c = \frac{C_2 P_O}{C_1 P_O} = \frac{C_2}{C_1}, \tag{3.1}$$

where h_c = calibration transfer function,
C_1 and C_2 = unknown frequency-dependent complex calibrations for each microphone, and
P_O = acoustic pressure applied by the CAL291.

The transfer function measured between the PMMs in the test duct is

$$h_{12} = \frac{C_2 P_2}{C_1 P_1}, \tag{3.2}$$

where P_1 and P_2 = acoustic pressure measured at microphone 1 and 2, respectively.

Utilizing the calibration transfer function allows for the accurate determination of the transfer function of the two microphones in the duct as

$$h_{12}^* = \frac{C_2 P_2}{C_1 P_1} \times \frac{C_1}{C_2} = \frac{P_2}{P_1} = \frac{h_{12}}{h_c}. \tag{3.3}$$

The PMMs were placed in the test duct and the signal generation system sent a step-sine signal into the duct inlet. The PMMs collected pressure values and the SigLab system collected a complex transfer function between the two microphones. Post processing led to the determination of ERL.

3.2 Measurement Method

Four main components within the SigLab system allow for measurement control; the number of frequency steps, number of measurements averaged at each step, the frequency range, and the tracking bandwidth allow for improved precision at the expense of a longer acquisition time. The SigLab system allows for a maximum of 100 frequency steps over a range of interest. A maximum of 20 measurements can be averaged at each frequency step. Random error decreases as the number of measurements at each step increases. Decreasing the frequency bandwidth improves precision and a smaller

frequency range results in smaller step intervals. A narrow tracking bandwidth improves SNR [20].

Because of limitations in the data acquisition and control system, measurements over the frequency range of interest were broken into two smaller ranges, the "low frequency" range from 25-100 Hz and the "high frequency" range from 100-500 Hz. The entire frequency range of interest was 25-500 Hz. Each set of frequency data consisted of averaged measurements at 100 frequency steps, with each step being the result of averaging 20 measurements. Each data set was averaged with at least three other data sets to reduce random error.

Table 6 lists the number of frequency steps per one-third octave for the high frequency data set when 100 steps are used. Only the 100-500 Hz ERL data was used from the high frequency data.

Table 6. High Frequency ERL Data in One-third Octave Bands

1/3 Octave Bands (Hz)	**No. of Steps**
100	8
125	6
160	7
200	7
250	6
315	7
400	7
500	7

Table 7 lists the number of frequency steps per one-third octave band for the low frequency data set when 100 steps are used. The low frequency data set increased both the number of steps in each one-third octave band and thereby the precision. Low frequency and high frequency data were combined to produce the final results. The low

and high frequency data were collected during the same testing time period to minimize any change that might occur in the apparatus or surrounding environment. The low and high frequency data also had individual phase calibration files acquired during the same measurement period.

Table 7. Low Frequency ERL Data in One-third Octave Bands

1/3 Octave Bands (Hz)	**No. of Steps**
25	13
31.5	13
40	13
50	12
63	13
80	13
100	12

3.3 Frequency Considerations

Frequency considerations impact measured ERL accuracy when using the two-microphone method. ASTM E1050 defines the working frequency range as [17]

$$f_l < f < f_u, \tag{3.4}$$

where f = operating frequency, Hz,
f_l = lower working frequency of the tube, Hz, and
f_u = upper working frequency of the tube, Hz.

The cutoff frequency for plane wave propagation is defined as

$$f_u < \frac{Kc}{d} \quad \text{or} \quad d < \frac{Kc}{f_u}, \tag{3.5}$$

where f_u = upper frequency limit, Hz,

c = speed of sound in the tube, m/s,
d = largest section dimension of the tube, m, and
K = 0.5 (for rectangular ducts).

Equation (3.5) results in the duct cutoff frequencies listed in Table 8 for rectangular ducts assuming c = 343 m/s. The larger ducts have cutoff frequencies that fall within the frequency test range. At these higher frequencies, cross-modes can occur.

Table 8. Upper Frequency Limits for Rectangular Duct Sizes

Duct Size (in.)	**Cutoff Frequency** (Hz)	**Cutoff** kD
6x6	1125	3.54
6x10	675	2.74
6x18	375	2.05
6x36	188	1.45
18x18	375	3.54
18x36	225	2.74
18x54	125	2.05

3.4 Error Analysis

Determining and minimizing random and experimental error was paramount in obtaining precise and accurate ERL results. Generally, random error is improved by increasing the sample size to obtain a mean value negligibly influenced by random measurements. Random error illustrates measurement precision, and by decreasing this uncertainty the results hold more statistical significance. The downside of increasing sample size is the corresponding increase in data acquisition time. Systematic error cannot be corrected simply by increasing the sample size, since it reflects a consistent and repeatable bias or offset. Systematic error is a reflection of accuracy, which in this case usually dealt with analytic and experimental ERL agreement. Systematic error was

minimized through the use of microphone phase calibration and consistent measurement and setup configurations.

Bodén and Åbom [14] examine many of the error issues in the two-microphone method. Several ways to minimize bias error include "keeping the overall duct length (L) small, in practice (say) $L \approx$ 5-10 duct diameters; the source end of the duct should be as nonreflective as possible; and microphone 1 should be placed as close as possible to the duct end" [14]. Many publications on the two-microphone method also discuss the importance of microphone separation and distance to the termination, microphone calibration, frequency resolution requirements for highly reflective terminations, and maintaining a minimum SNR of 10 dB in order to minimize measurement errors [14, 15, 17].

Confidence limits for the mean were used to determine how the mean varies between samples and indicate the degree of uncertainty in the true mean estimate. As this confidence limit decreases, the precision of the estimate increases [21]. The percent change in ERL values were calculated when the mean values had a statistically significant difference, as indicated from a *t*-test. A *t*-test determines if the mean value of two groups is statistically different from each other and is calculated using the mean, variance and number of samples for each group. The difference in means is scaled by the standard error of the difference. The scale factor is computed by taking variance of each group and dividing it by the number of samples in that group, adding these two quantities and taking the square root. The *t* value is defined as

$$t = \frac{\overline{X}_T - \overline{X}_c}{\sqrt{\frac{\text{var}_\text{T}}{N_\text{T}} - \frac{\text{var}_\text{c}}{N_\text{c}}}}, \tag{3.6}$$

where $\overline{X}$ = sample average,
var = variance, and
N = sample size.

This t-value is used with a table of t-distribution percentiles to test if the ratio is large enough to say the difference between the groups is not likely to have been a random finding. ERL results contained confidence limits for the mean defined as

$$\overline{Y} \pm \frac{t_{(\alpha/2, N-1)} s}{\sqrt{N}}, \tag{3.7}$$

where $\overline{Y}$ = sample mean,
s = sample standard deviation,
N = sample size,
α = desired significance level, and
$t_{(\alpha/2, \text{N-1})}$ = upper t-distribution critical value with $N - 1$ degrees of freedom.

CHAPTER 4

RESULTS

Experimental ERL results are presented according to duct size using a flush rigid open termination, duct termination distance above the termination baffle, termination baffle hardness, rigid duct with slot diffuser termination, and termination variations utilizing flex duct. Appendix A contains the duct configuration matrix, which describes all the performed duct tests. Appendix C contains the individual duct configuration plots of ERL with respect to *kD*.

4.1 Duct Size Using a Flush Rigid Open Termination

The analytic predictions for ERL are directly related to duct size and this behavior is shown using one-third octave band ERL values in Figure 33 for the Hard-Flush-Open configuration. ERL at a fixed frequency decreases as duct size increases. This behavior was observed in the experimental results from all seven rectangular duct sizes tested. Non-dimensional analytic ERL behavior is depicted in Figure 34 for all seven rectangular duct sizes tested. Figure 35 depicts the experimental results for the seven duct sizes tested using the Hard-Flush-Open configuration. Comparison of Figures 34 and 35 depict overall experimental agreement with the analytic predictions for the Hard-Flush-Open condition. Experimental ERL clarity is improved in Figure 35 by not using error bars.

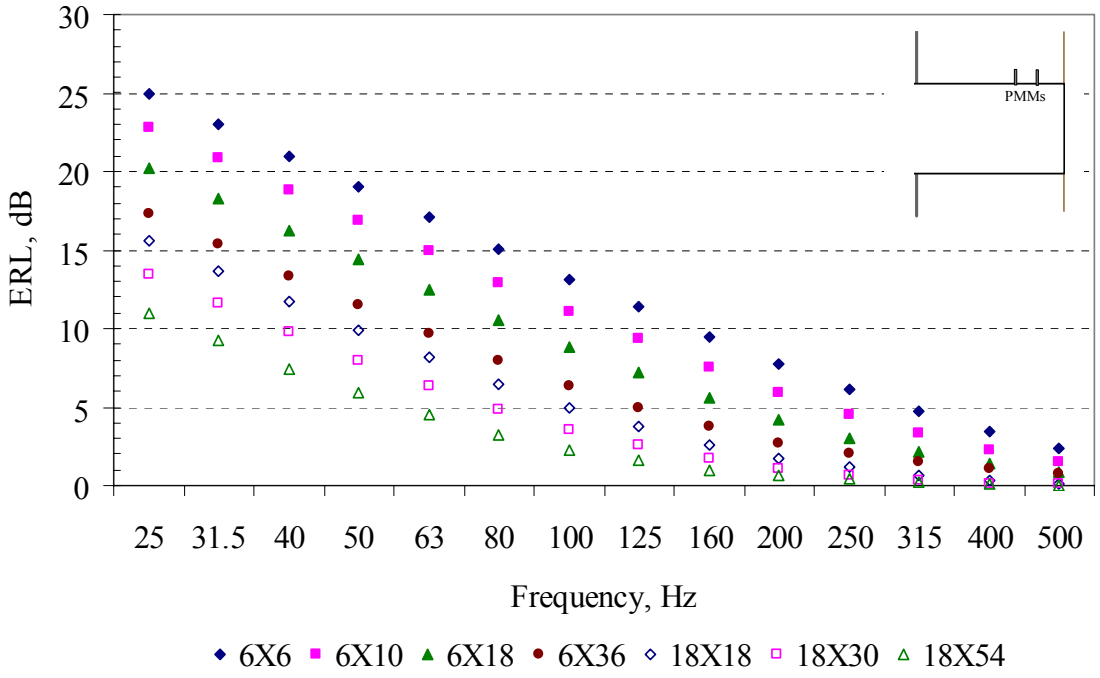

Figure 33. Analytic Hard-Flush-Open ERL for Seven Duct Sizes in One-third Octave Bands vs. Frequency

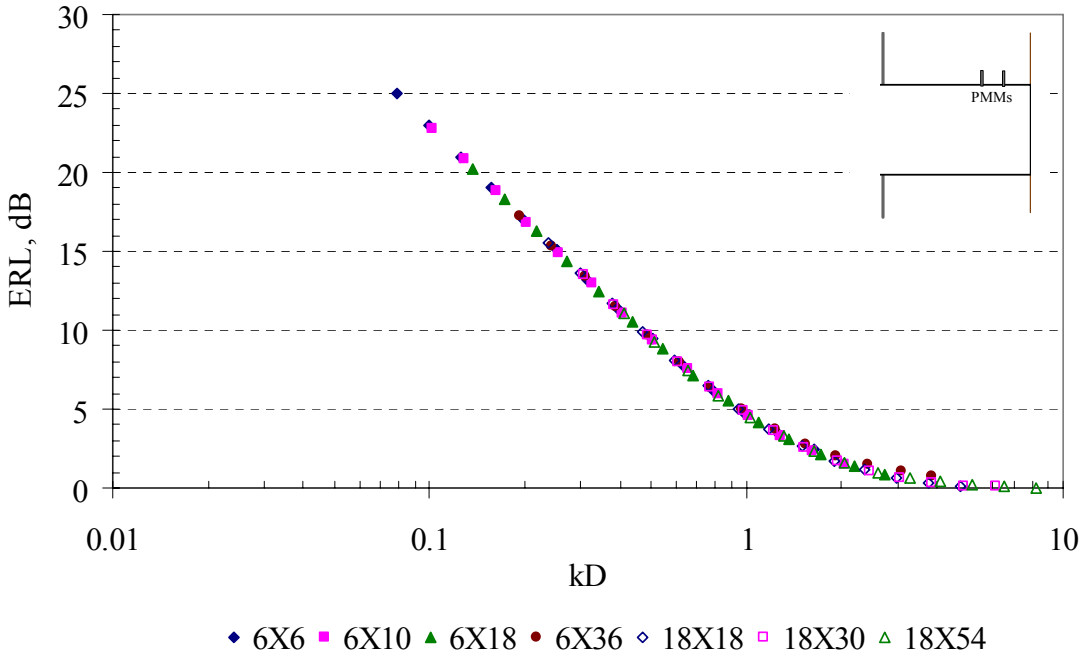

Figure 34. Analytic Hard-Flush-Open ERL for Duct Sizes from Figure 33 in One-Third Octave Bands vs. *kD*

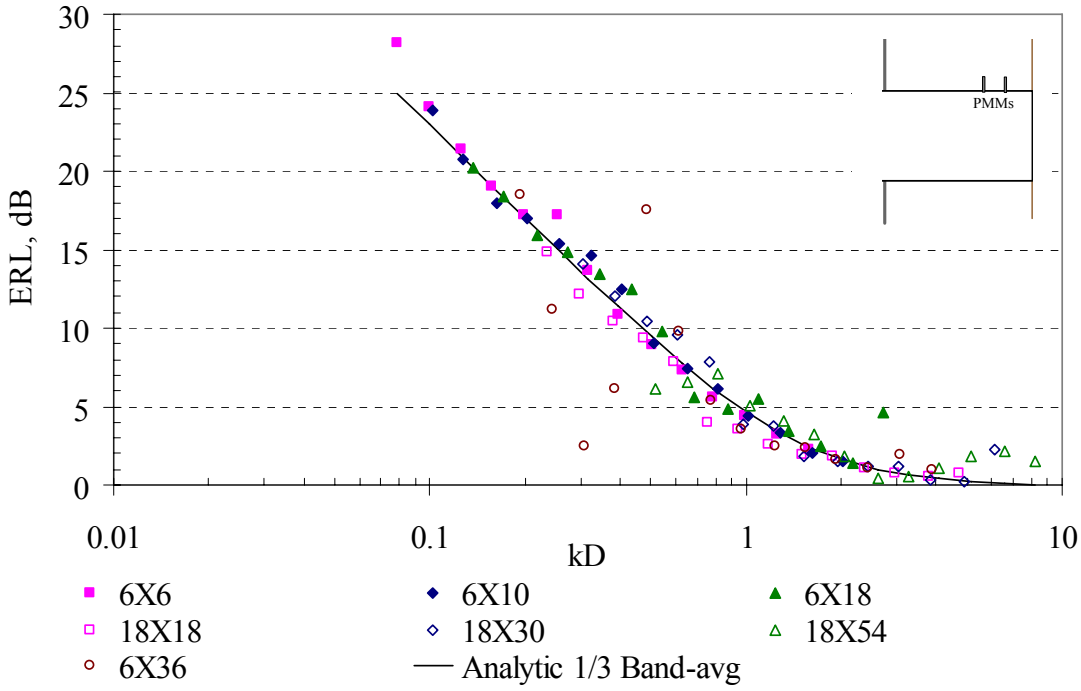

Figure 35. Experimental Hard-Flush-Open ERL Results for Duct Sizes from Figure 33 in One-Third Octave Bands

Overall experimental Hard-Flush-Open rectangular duct results depicted in Figure 35 agree with the corresponding Hard-Flush-Open analytic prediction for ERL. The experimental 6X6 rectangular duct results from the Hard-Flush-Open duct configuration agree well with corresponding analytic predictions. Deviation from the analytical ERL is observed in the 25 and 31.5 Hz one-third octave bands. As previously mentioned, the termination baffle was not large compared to a wavelength below 160 Hz, therefore the radiation impedance is likely to progress from flush to free space, which would be the case if the baffle does not appear to be infinite. 6X10 Hard-Flush-Open duct results agree well with analytic predictions. 6X18 Hard-Flush-Open duct results agree with

analytic predictions, with the 500 Hz one-third octave band ERL deviation likely caused by cross modes and evanescent wave effects. 6X36 duct ERL results indicate overall agreement with analytic predictions, but the extreme aspect ratio is not recommended for testing purposes [17]. Duct resonance is a possible cause for the 6X36 duct lower frequency ERL outliers at the 31.5, 40, 50, and 63 Hz one-third octave bands. The 18X18 Hard-Flush-Open ERL results agree well with analytic predictions. The 18X30 Hard-Flush-Open results agree well with analytic predictions except for the 500 Hz one-third octave band outlier, likely caused by cross modes and evanescent wave effects. The 18X54 Hard-Flush-Open results agree with analytic predictions, but duct resonance likely caused a 25 Hz one-third octave band outlier. Cross modes and evanescent wave effects likely caused the outlier ERL values at 315, 400, and 500 Hz. Individual ERL results for all Hard-Flush-Open duct configurations are given in Appendix C.

4.2 Duct Termination Distance Above the Baffle Wall

The ERL values for five duct termination distances above the baffle wall are depicted in Figure 36. Experimental ERL clarity is improved in Figure 36 by not using error bars. ERL differences for Flush, 0.5*D*, and 1*D* termination distances above the baffle were minimal. The ERL values depicted in the plot suggest that there is minimal deviation from the analytic flush prediction for termination distances of 1*D* and less above the termination baffle. At the higher frequencies, ERL deviation becomes more apparent. The 2*D* and 5*D* cases show limited agreement with the free space ASHRAE Table 22 values and analytic prediction. Figure 37 depicts the differences between the

analytic Hard-Flush-Open ERL and the five experimental configuration ERL values depicted in Figure 36. Figure 37 suggests that a duct termination distance above the termination baffle greater than 1*D* results in ERL deviation from the flush termination prediction that begins to behave like the free space analytic prediction.

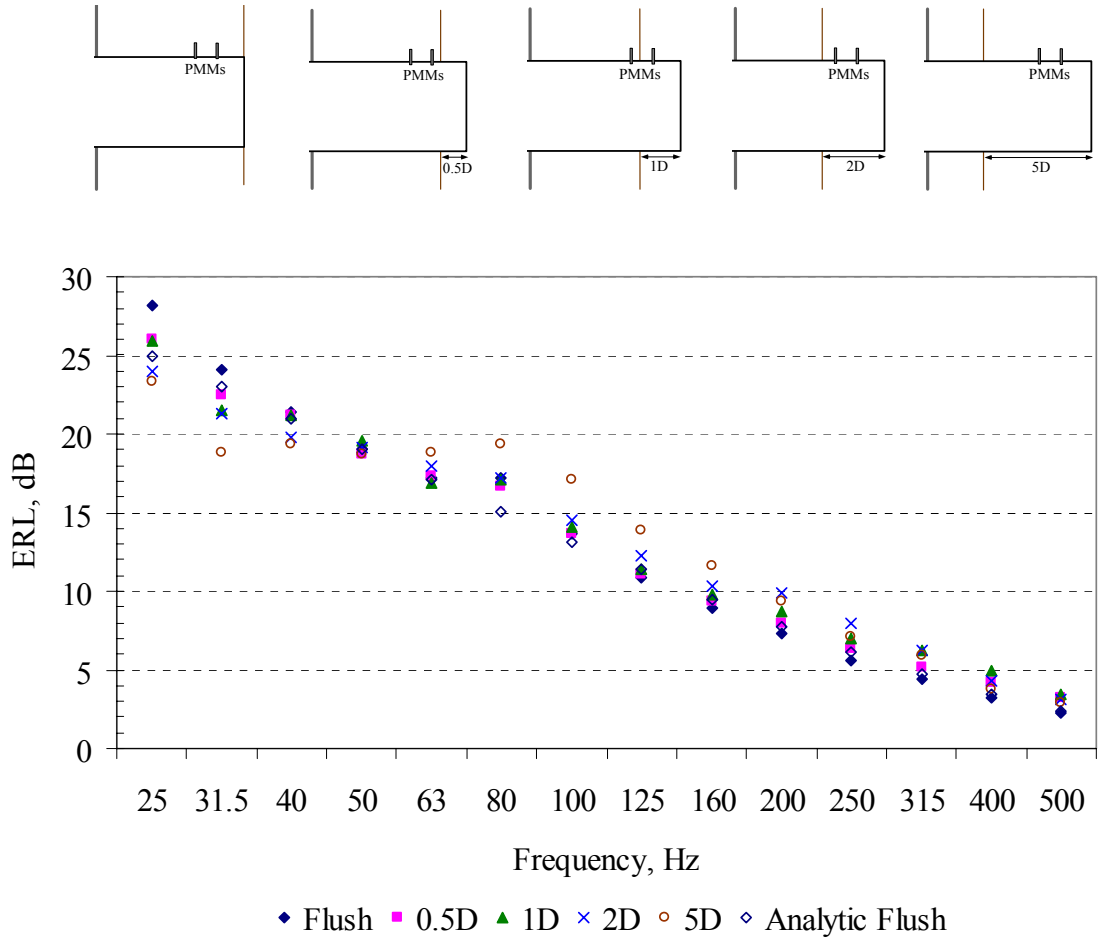

Figure 36. 6X6 Hard-VARIOUS-Open Duct Distance Variation ERL Results in One-Third Octave Bands

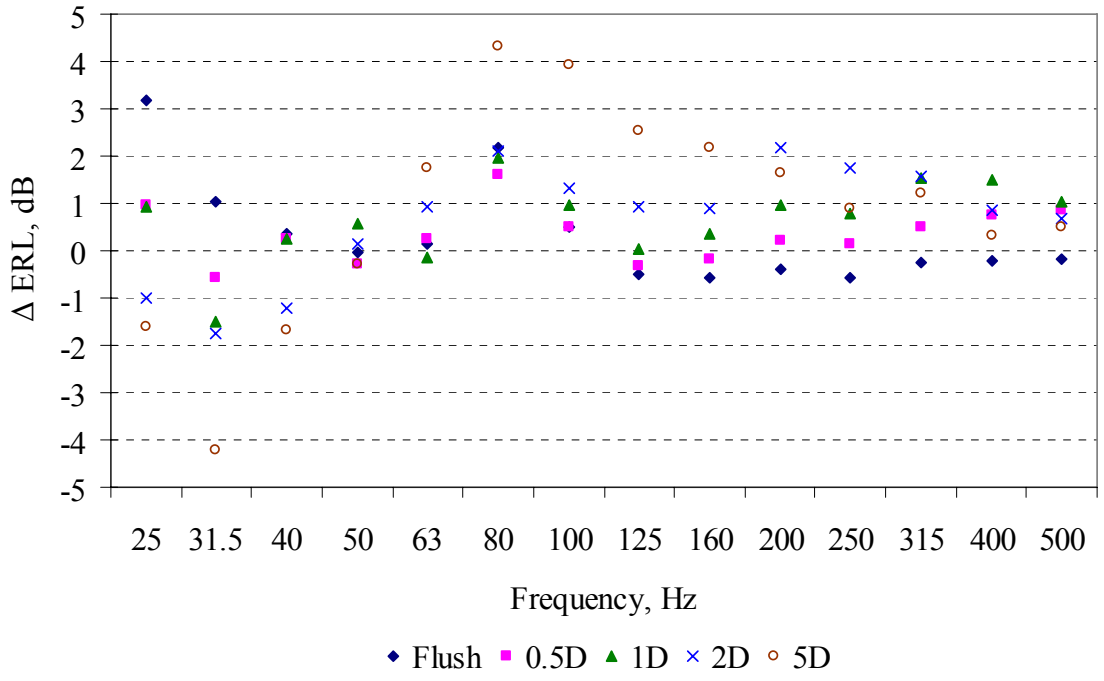

Figure 37. 6X6 Hard-VARIOUS-Open Duct ERL Difference from Hard-Flush-Open Analytic Prediction in One-Third Octave Bands

Experimental ERL for $D > 1$ showed limited agreement with analytic free space ERL and corresponding ASHRAE Table 22 values. Figure 38 compares experimental 2*D* and 5*D* ERL with analytic flush and free space predictions for the 6X6 rigid open duct. Experimental ERL clarity is improved in Figure 38 by not using error bars. The experimental 5*D* ERL results agree closely with the free space analytic prediction at the 80, 100, and 125 Hz one-third octave bands. The analytic free space prediction and experimental results from 2*D* and 5*D* ERL tests suggest that a limited free space condition was reached. Figure 39 depicts the differences between ERL for experimental 2*D*, 5*D*, and ASHRAE Table 22 values with respect to the analytic free space termination. Figure 39 indicates that the experimental 5*D* termination condition is closer

to analytic free space than the ASHRAE Table value at the 125 Hz one-third octave band. All termination distance variation ERL results are depicted in Appendix C.

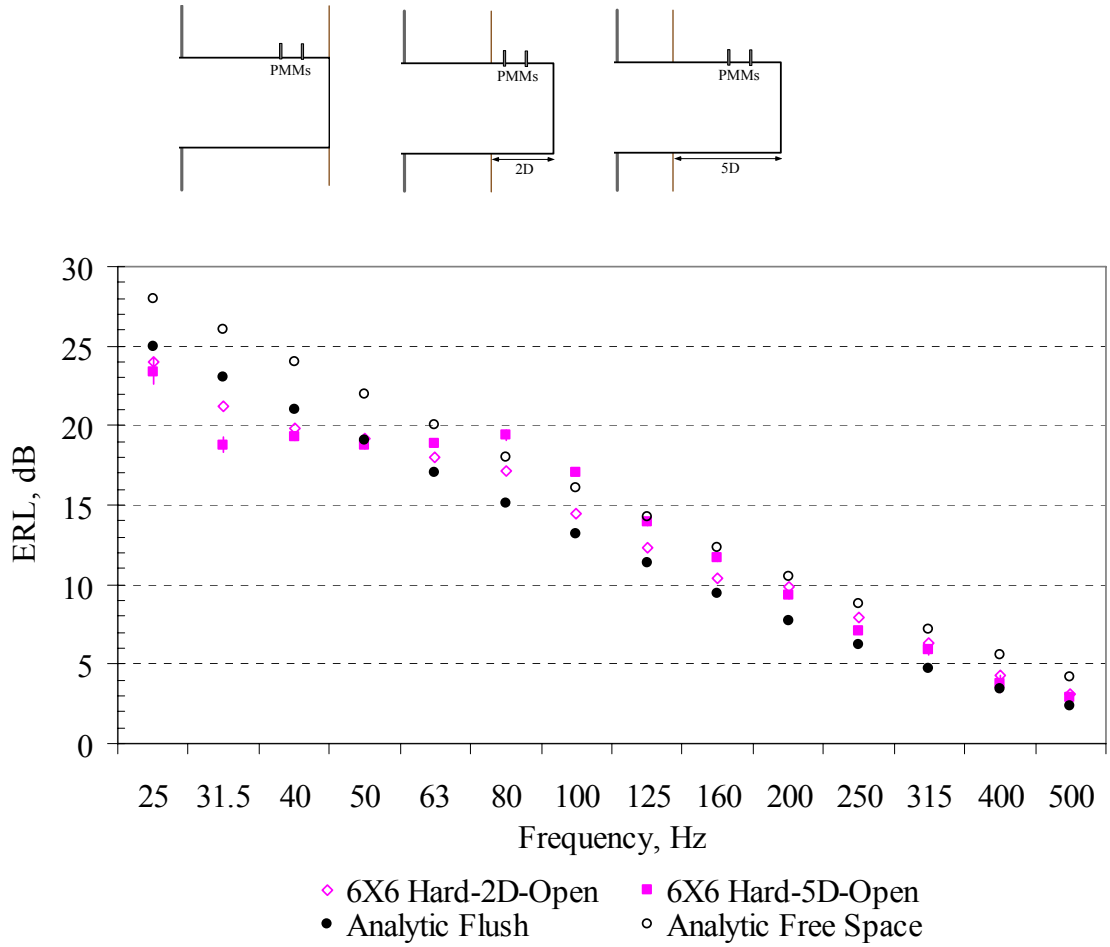

Figure 38. 6X6 Hard Open Duct Experimental 2*D* and 5*D*, Analytic, and Analytic Free Space ERL in One-Third Octave Bands

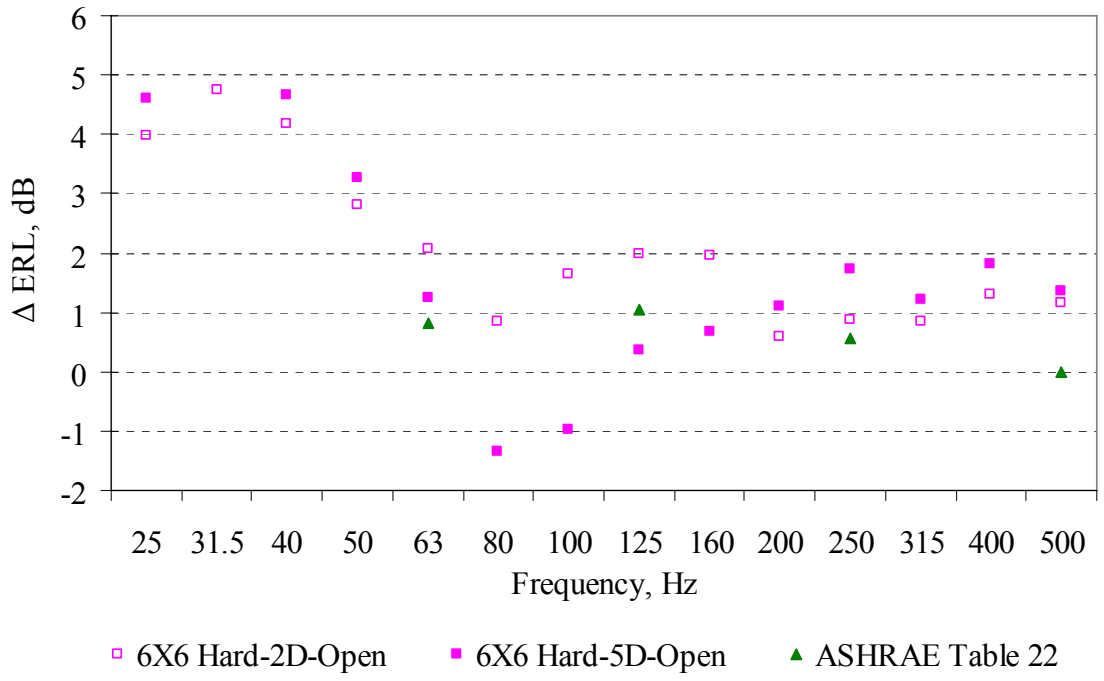

Figure 39. 6X6 Hard Open Duct Experimental 2*D* and 5*D*, ASHRAE Table 22, and Analytic Free Space ERL Differences in One-Third Octave Bands

4.3 Termination Baffle Wall Hardness

The ERL values from termination baffle wall hardness variation are depicted in Figure 40 for VARIOUS-Flush-Open duct configurations. Experimental ERL clarity is improved in Figure 40 by not using error bars. Negligible ERL variation from termination baffle hardness variation was observed. Specifically, the average ERL difference between hard and soft baffles for the small rectangular ducts was 0.6 dB. Baffle wall hardness variation for the large ducts was not tested. Appendix C shows the ERL results from termination baffle wall hardness variation testing.

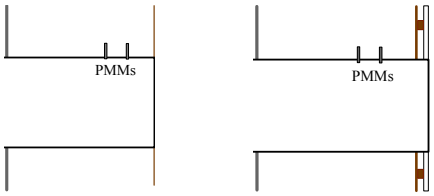

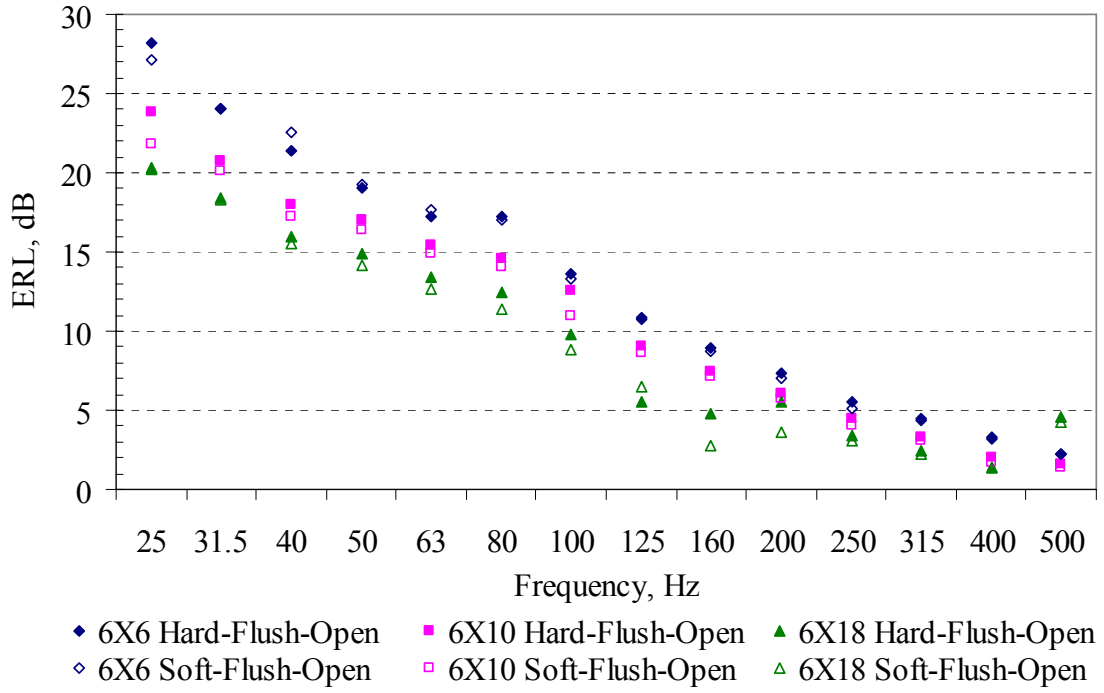

Figure 40. Small Duct Termination Baffle Hardness ERL Comparison in One-Third Octave Bands

4.4 Rigid Duct with Slot Diffuser Termination

Testing using a Titus ML-39 single-slot diffuser mounted directly to the rigid MDF test section was performed on the 6X10 duct. Figure 41 illustrates ERL values from distance and baffle hardness variation for a rigid duct with an ML-39 diffuser termination. Termination distance and termination baffle hardness had a negligible impact on ERL for this duct configuration. The slot diffuser results suggest a semi-rigid termination ERL independent of frequency, which occurs because of the small diffuser opening area with respect to the rigid duct area. In this setup, an area change occurs in the duct and is described by Kinsler and Frey [2]. In order to account for this area change, the reflection coefficient and transmission coefficients are estimated as

$$R_{\pi} = \frac{\left(S_1 - S_2\right)^2}{\left(S_1 + S_2\right)^2}, \tag{4.1}$$

$$T_{\pi} = \frac{4S_1S_2}{\left(S_1 + S_2\right)^2}, \tag{4.2}$$

where S_1 = area of the upstream duct and S_2 = area of the downstream duct.

The above size change approximations for the reflection coefficient agreed with experimental results. For the ML-39 diffuser configuration, the size change ERL approximation is 3 dB, which is close to the experimental ERL values shown in Figure 41. Experimental ERL clarity is improved in Figure 41 by not using error bars. The complex slot diffuser opening shown earlier in Figure 20 makes it difficult to obtain an accurate size change ERL. The ERL outlier at the 400 Hz one-third octave band is likely caused by duct resonance. Individual ERL results from these slot diffuser tests are shown in Appendix C.

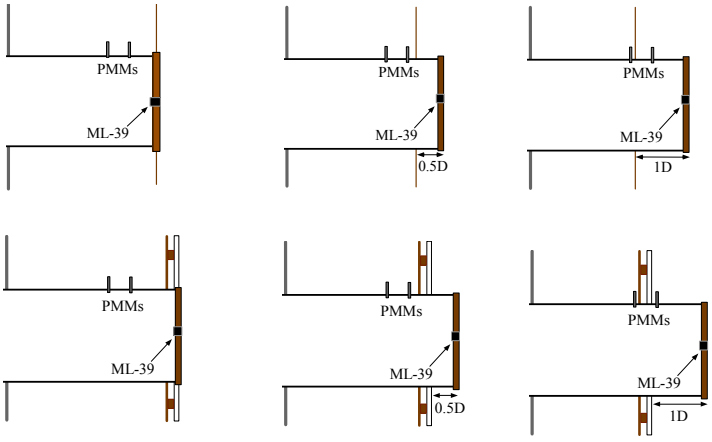

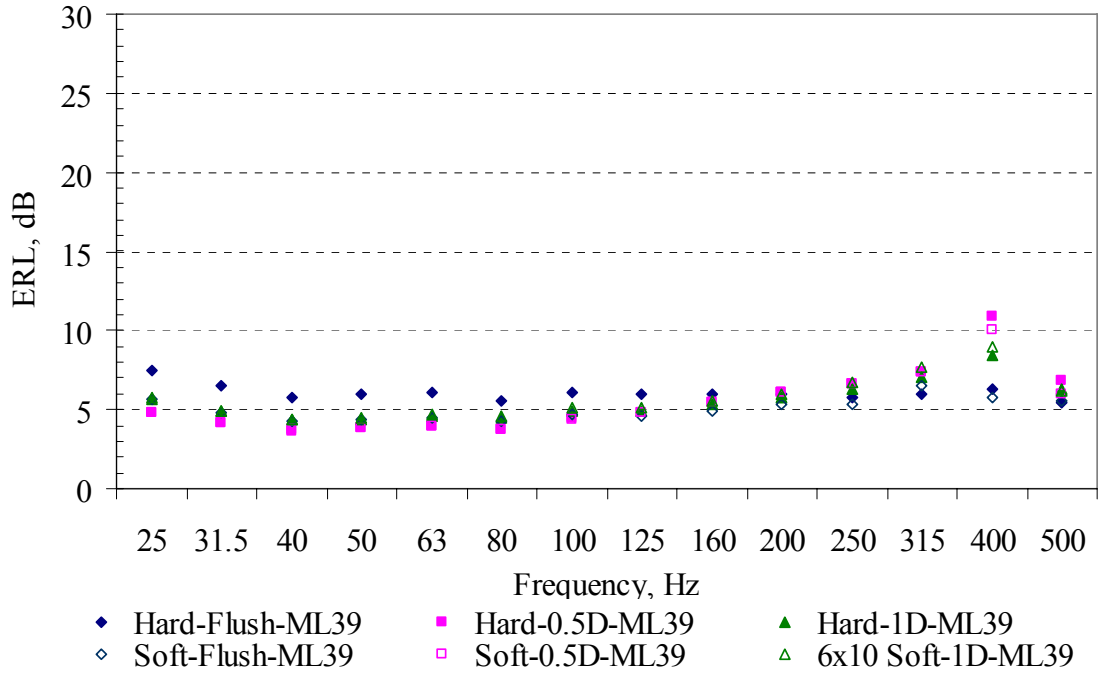

Figure 41. 6X10 VARIOUS-VARIOUS-ML39 ERL Results in One-Third Octave Bands

4.5 Flex duct Termination

Flex duct was used on the small ducts with open, rigid, and various diffuser termination conditions. Figure 42 illustrates the ERL results for five different flex duct configurations on a 6X6 duct terminating flush with a hard baffle. The results of flex testing are significant, in that they suggest that a large amount of sound exits through the flex duct that would normally be reflected back into the duct for the rigid open condition. It is also clear from the plot that termination variation has little effect on ERL when flex is present. This lack of termination variation effect on ERL is shown in Figure 43, which magnifies the flex results. Flex duct greatly reduces ERL and effectively acts as a semi-anechoic termination. The lower ERL values resulting from flex duct usage in Figure 43 are similar to ERL values for much larger duct sizes. Flex duct appears to have the effect

of increasing a duct's effective diameter, resulting in lower ERL values. Termination baffle wall hardness was varied with flex duct and had a negligible effect on ERL. All three small ducts used a six-inch diameter flex duct and a metal transition piece. A size transition occurred when going from the rigid duct to flex duct that could impact measured ERL as seen previously with the slot diffuser results. The area change ERL values using Equation (4.1) for the 6X10 and 6X18 ducts are 0.6 and 1.8 dB, respectively. Appendix C shows all the individual ERL plots from the flex duct testing.

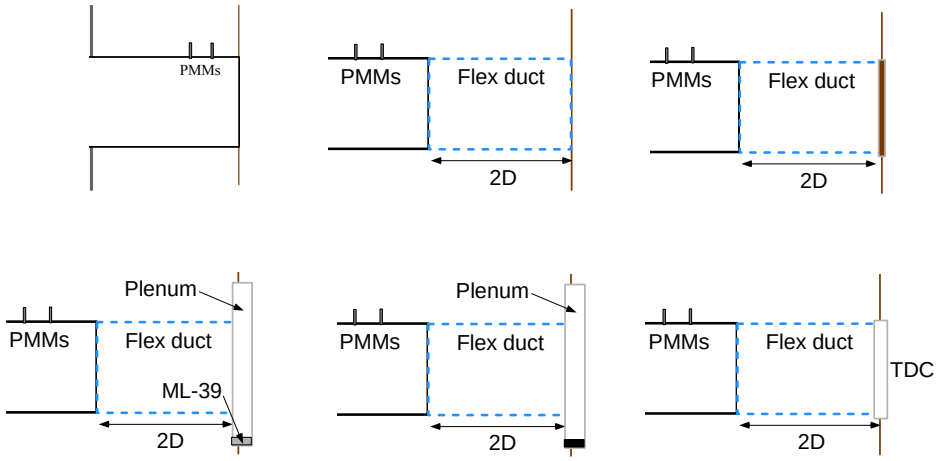

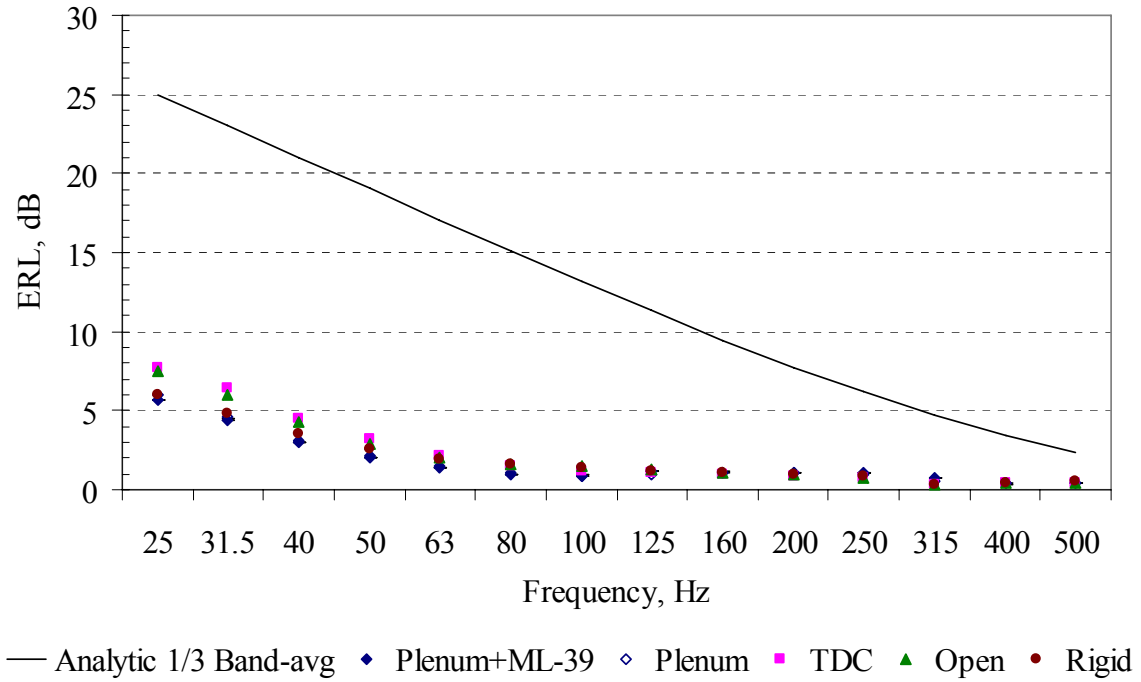

Figure 42. 6X6 Hard-Flex-VARIOUS and Hard-Flush-Open Analytic ERL Results in One-Third Octave bands

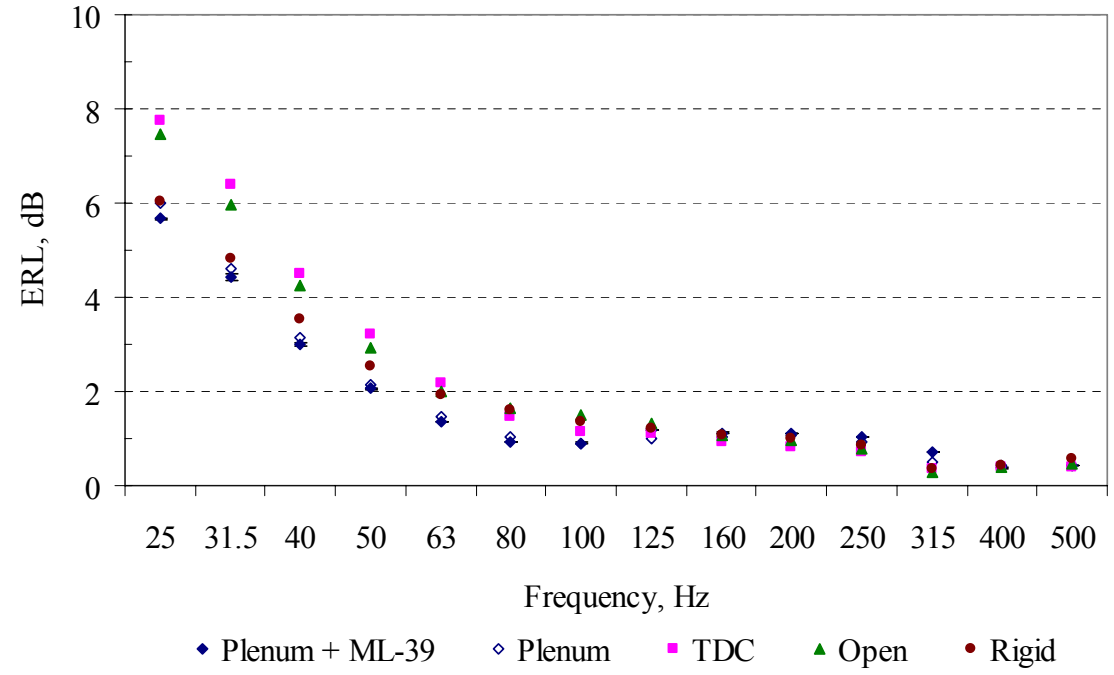

Figure 43. 6X6 Hard-Flex-VARIOUS ERL Results in One-Third Octave Bands

CHAPTER 5

CONCLUSIONS

An experimental method for determining the ERL for a variety of rectangular duct sizes and termination configurations was implemented. Hard-Flush-Open experimental ERL results agree with corresponding analytic predictions. Termination baffle hardness and small duct termination distances above the baffle (1*D* and less) were determined to have a minimal impact on ERL as compared to the Hard-Flush-Open configuration. At greater distances above the baffle (2*D* and 5*D*), experimental ERL values showed limited agreement with the corresponding analytic prediction between 80 and 160 Hz but not at higher frequencies. Introducing flex duct to the rigid open duct setup greatly reduces ERL. The use of flex duct also negates termination variation effects on ERL and leads to several questions for consideration in future research.

The experimentally determined ERL for Hard-Flush-Open ducts utilizing a variety of rectangular duct sizes agreed well with corresponding analytic predictions. The experimental ERL results presented are an improvement over the current ASHRAE Handbook values in several ways. Experimental ERL results extend the ASHRAE Table 23 values from 63 Hz down to 25 Hz. The experimental ERL results for a flush terminated rigid open duct have closer agreement with analytic predictions than corresponding ASHRAE ERL table values. ASHRAE ERL table values for a flush termination are consistently higher than corresponding analytic predictions. Also, it was shown that circular and rectangular ducts having equivalent diameters are equivalent with respect to ERL.

Termination baffle hardness and small termination distances above the baffle were determined to have a minimal impact on ERL for a variety of rectangular duct sizes and termination conditions. In the case of termination distance above the baffle (1*D* and less), ERL behavior is essentially that of a flush termination. When the termination distance above the baffle was increased, ERL deviation from the flush condition at higher frequencies was observed. With the 6X6 rectangular duct, varying the termination distance 2*D* and 5*D* above the baffle resulted in limited free space ERL values that agreed with corresponding analytic predictions between 80 and 160 Hz. Experimental 2*D* and 5*D* ERL values agreed with corresponding flush analytic predictions at larger frequencies. Experimental ERL results also agreed with ASHRAE Table 22 values at higher frequencies, though a substantiated distance above the baffle resulting in the free space condition is needed. This will improve the ability to experimentally determine free space ERL. ASHRAE Table 22 ERL values are consistently lower than the corresponding analytic prediction. The ASHRAE Handbook statement that "diffusers that terminate in a suspended lay-in acoustic ceiling can be treated as terminating in free space" [1] is not supported by the results. Baffle hardness has a negligible impact on low frequency ERL. Diffusers greatly reduce ERL, possibly resulting in more noise radiation at the duct termination.

Determining ERL for various termination conditions also included the use of diffusers and flex duct. Experimental results determined that flex duct greatly reduces Hard-Flush-Open duct ERL, acting as a semi-anechoic termination. Flex duct's definite impact on ERL should be taken into consideration when determining noise effects from the duct termination. Because almost all the sound energy exits a duct when flex duct is

used, low frequency sound levels in a space containing duct terminations could be much higher than previously predicted. In the case of a drop ceiling, noise is likely introduced into the open plenum space above the ceiling tiles. Flex duct also negates termination variation impact, allowing the majority of duct noise to escape.

Future Directions

One area of future ERL research stems from the inability to fully describe sound loss when flex duct is used. The actual flex duct sound loss path is not completely known and is important for determining how to effectively reduce sound output into a space. The impact of return air grills is another area of concern, since noise propagates down a return duct into an occupied space in the same way as a supply duct.

Current ASHRAE Handbook values show deviation from the corresponding analytic predictions for ERL. ASHRAE Table 22 ERL values are consistently lower than free space analytic predictions and caution should be used in their application until further validation is performed. In order to experimentally determine free space ERL more accurately, the free space condition must be determined. Experimental results imply that for small ducts, the free space condition is an artifact best suited for analytic expression. The difference between flush and free space ERL may not be enough to warrant special consideration in the case of human annoyance, especially when the use of flex duct or a diffuser would negate any difference between the two conditions. Finally, the experimental determination of rectangular duct ERL for a variety of termination

conditions with flow has not been performed and would prove useful for HVAC applications.

APPENDIX A

Configuration Matrix

No.	Size (in)	Termin Material	Termination Type	Distance (inches)	ERL files:	Absrel files:
01	6 X 6	Plywood	open	flush	0109_02-09	0109_01a, 02l
02	6 X 6	Plywood	open	0.5 D	0111_01-09	0111_01a, 02l
03	6 X 6	Plywood	open	1 D	0116_01-12	0115_01a, 02l
04	6 X 6	Plywood	open	2D	0223_01-17	0223_01a, 02l
05	6 X 6	Plywood	open	5D	0226_01-13, 0228_01-08	0226_01a, 02l
06	6 X 6	Plywood	Opn Flx B4	flush	1106_01-08	1106_01a, 02l
07	6 X 6	Plywood	Rigid flxduct	flush	1122_05-08	1117_02a
08	6 X 6	Plywood	TDC flxduct	flush	1120_07-10	1120_01a, 02l
09	6 X 6	Plywood	plenum flex	flush	1120_03-06	1120_01a, 02l
10	6 X 6	Plywood	ML-39 + plen	flush	1117_01-02, 18_01-02, 19_01-04	1117_02a, 03l, 20_01, 02
11	6 X 6	Acoustic	open	flush	1219_02-05	1219_01a
12	6 X 6	Acoustic	open	0.5 D	0112_01-04,07-09, 0115_01-04	0111_01a, 02l
13	6 X 6	Acoustic	open	1 D	0115_07-18	0115_01a, 02l
14	6 X 6	Acoustic	open flxduct	flush	1208_01-04, 05-08	1208_01a, 02l
15	6 X 10	Plywood	open	flush	0927_02-11, 0928_01-07	0927_01a, 0927_02l
16	6 X 10	Plywood	open	0.5 D	1002_01-08	1002_01a, 1002_02l
17	6 X 10	Plywood	open	1 D	1012_01-07, 1013_01-04	1012_01a, 1013_01a, 02l
18	6 X 10	Plywood	diffuser	flush	0928_08-09, 0929_01-14	0928_01a, 0929_02l
19	6 X 10	Plywood	diffuser	0.5 D	1003_01-11	1003_01a, 1003_02l
20	6 X 10	Plywood	diffuser	1 D	1011_01-08	1011_01-02
21	6 X 10	Plywood	opn w/ fxduct	flush	1106_01-08	1106_01a, 02l
22	6 X 10	Acoustic	open	flush	1023_01-02, 1024_01-05	1023_04a, 05l
23	6 X 10	Acoustic	open	0.5 D	1005_05-09, 1006_01-07	1005_01a, 1005_02l
24	6 X 10	Acoustic	open	1 D	1009_01-07, 1010_01-07	1009_01a, 1009_02l
25	6 X 10	Acoustic	diffuser	flush	1024_06-10, 1025_01-04	1023_04-05, 1025_02-03
26	6 X 10	Acoustic	diffuser	0.5 D	1004_01-08	1004_01a, 1004_02l
27	6 X 10	Acoustic	diffuser	1 D	1010_06-13	1010_01a, 02l
28	6 X 10	Acoustic	Open flxduct	flush	1030_01-08	1030_01a, 1030_02l
29	6 X 10	Acoustic	Rigid Flxduct	flush	1101_03-06	1101_01a
30	6 X 10	Acoustic	ML-39 flex	flush	1031_01-02, 1101_01-02	1031_01a, 1101_a
31	6 X 18	Plywood	open	flush	0122_04-09, 0123_01-14	0122_01a, 03l
32	6 X 18	Plywood	open	1 D	0131_05-15	0131_01a, 02l
33	6 X 18	Plywood	Opn flx B4	flush	0126_03-07, 18-21	0124_01a, 02l
34	6 X 18	Plywood	Rigid Flex	flush	0126_10-17	0124_01a, 02l
35	6 X 18	Acoustic	open	flush	0125_01-16	0124_01a, 02l
36	6 X 18	Acoustic	open	1 D	0201_01-05, 0202_01-05	0131_01a, 02l
37	6 X 36	Plywood	open	flush	0318_01-40	0318_01a, 02l
38	18 X 18	Plywood	open	flush	0312_02-05	0302_01a, 0312_01a, 02l
39	18 X 30	Plywood	open	flush	0316_02-05	0312_01a, 02l
40	18 X 54	Plywood	open	flush	0321_01-31	0318_01a, 02l

APPENDIX B

Hardware Specifications

Description	Company	Serial Number
½-inch phase matched microphone	Brüel & Kjær 2670	02484386
¼ inch microphone preamplifiers	Brüel & Kjær	2520406 2520407
Conditioning amplifier	Brüel & Kjær	02556743

APPENDIX C

Individual ERL Plots

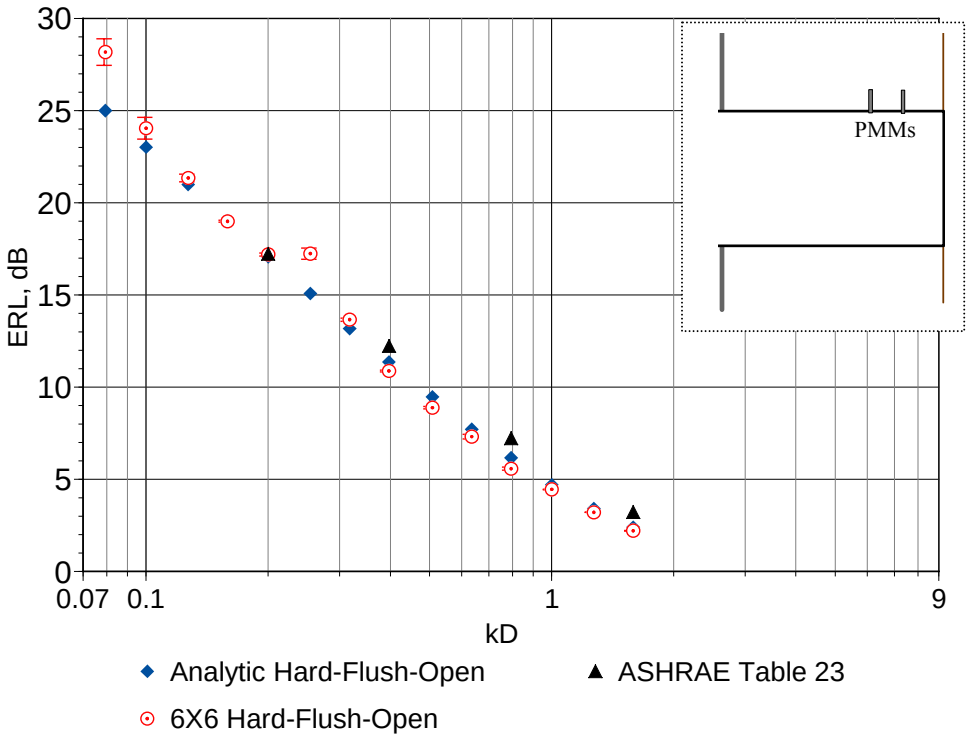

Figure C1. 6X6 Hard-Flush-Open ERL Results

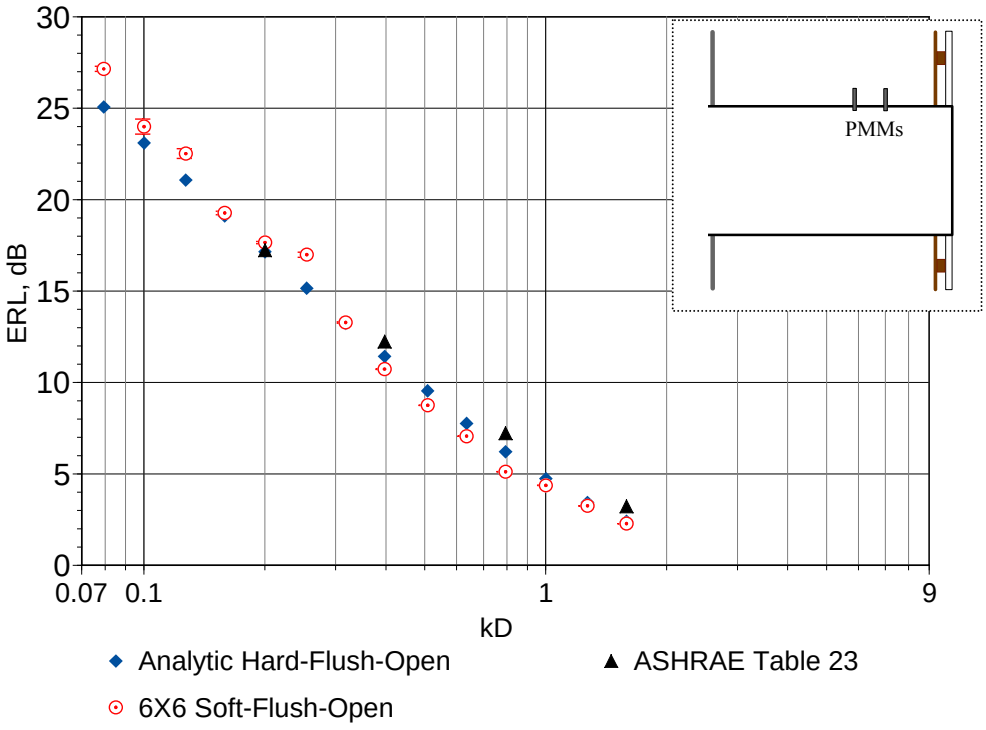

Figure C2. 6X6 Soft-Flush-Open ERL Results

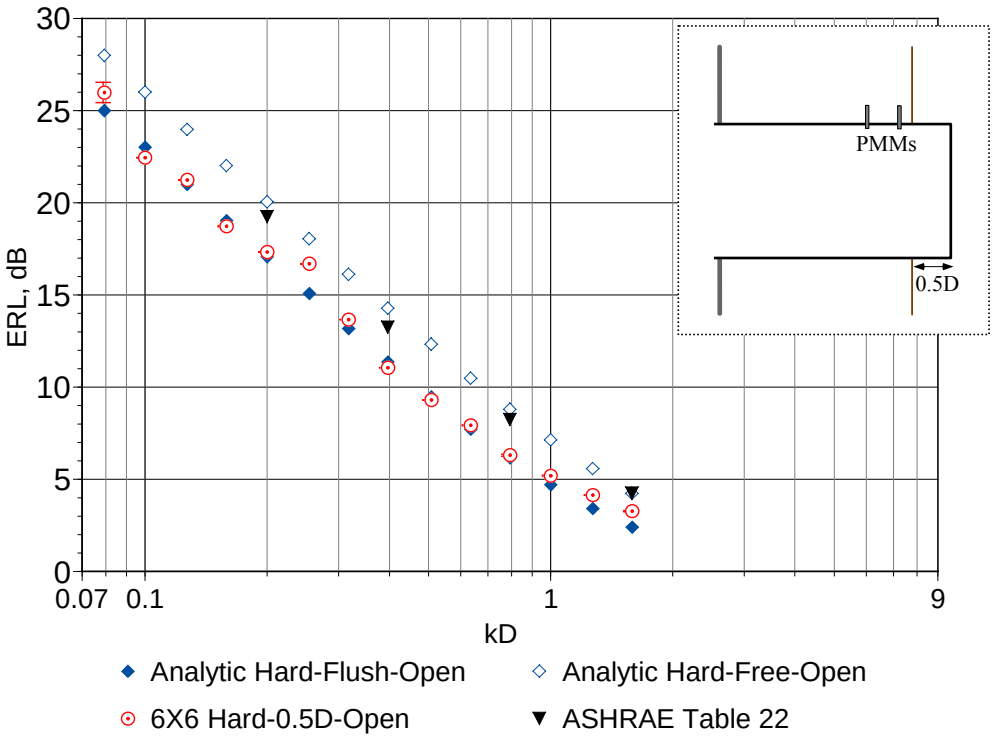

Figure C3. 6X6 Hard-0.5D-Open ERL Results

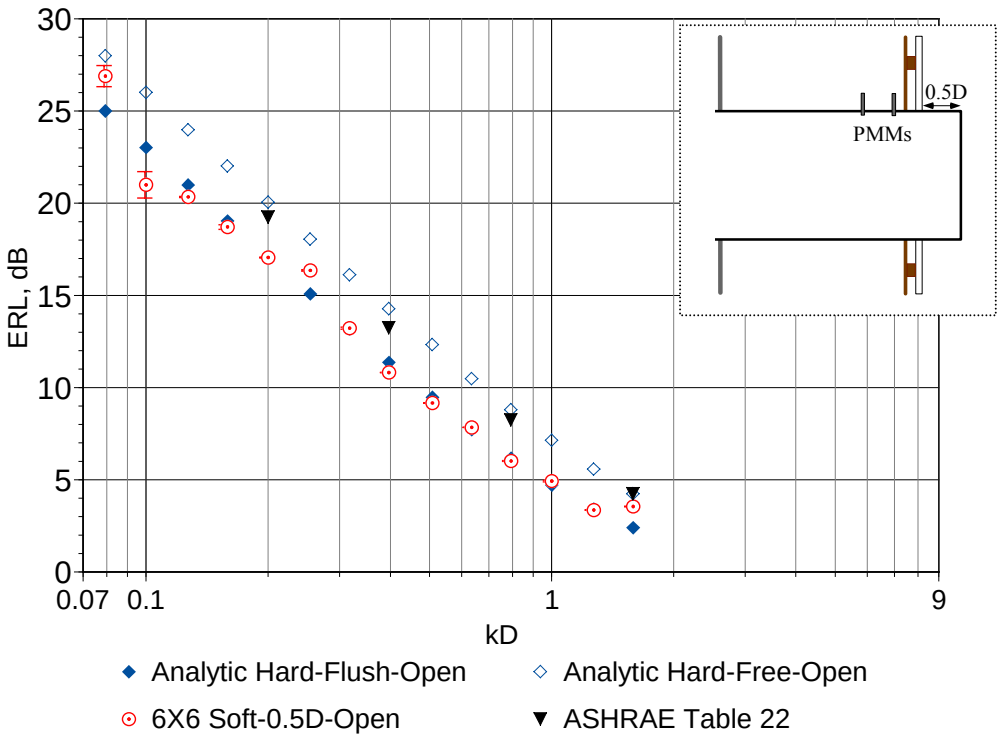

Figure C4. 6X6 Soft-0.5D-Open ERL Results

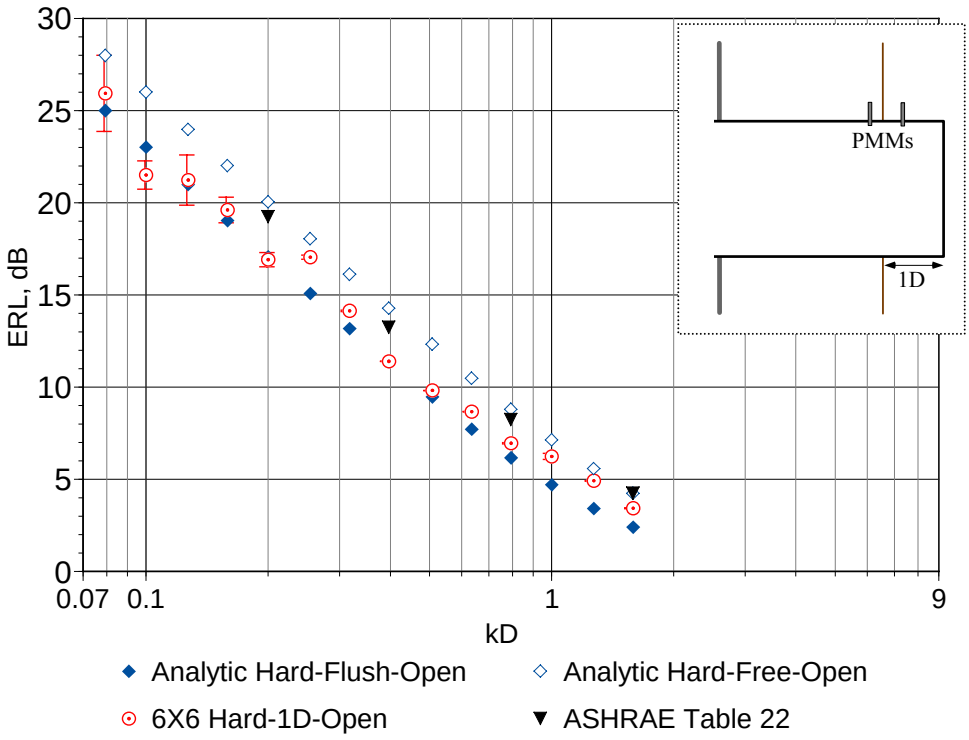

Figure C5. 6X6 Hard-1D-Open ERL Results

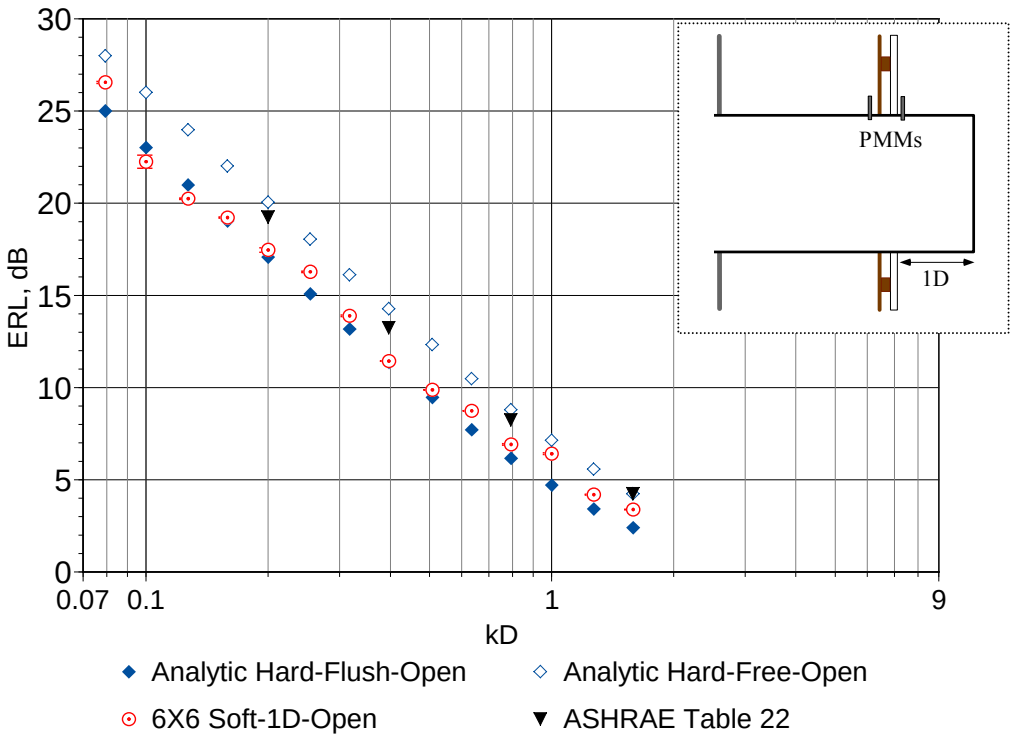

Figure C6. 6X6 Soft-1D-Open ERL Results

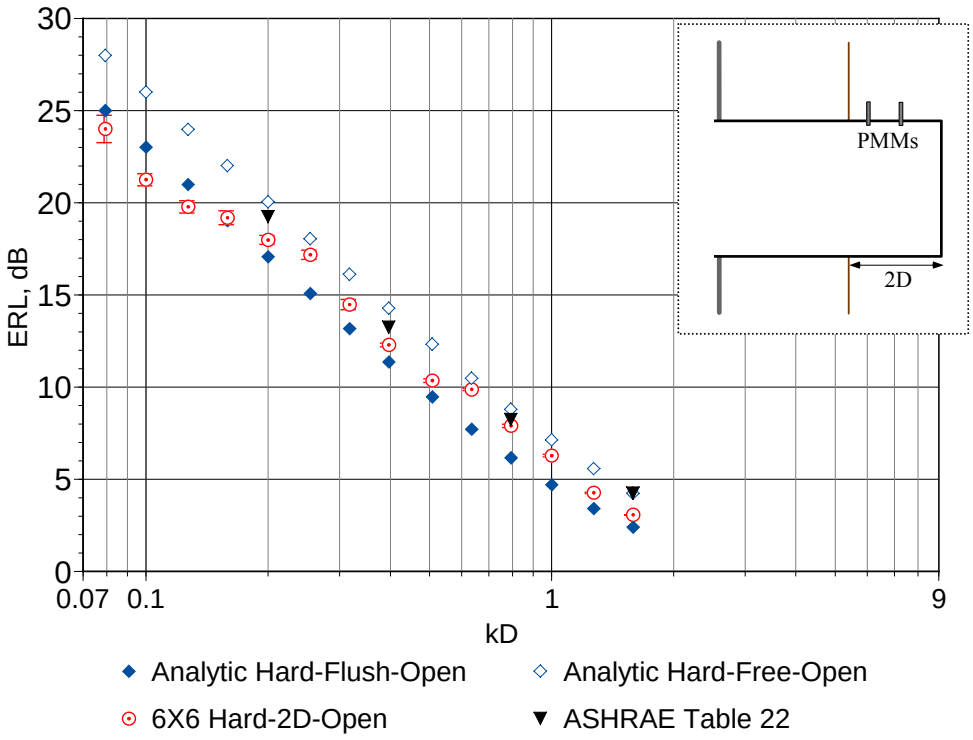

Figure C7. 6X6 Hard-2D-Open ERL Results

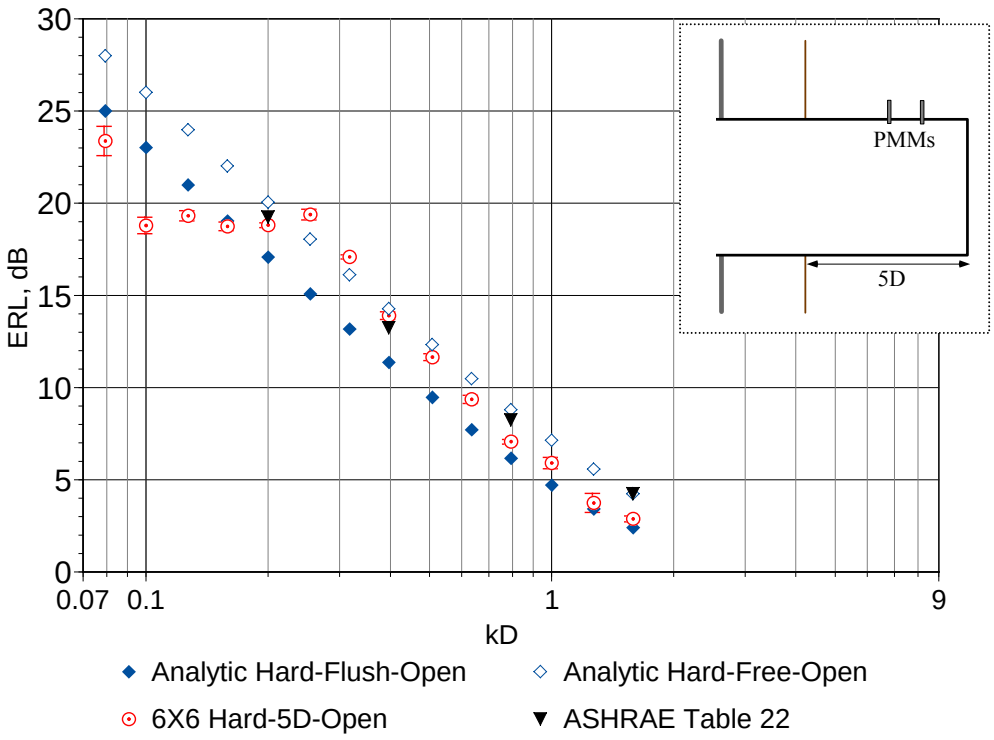

Figure C8. 6X6 Hard-5D-Open ERL Results

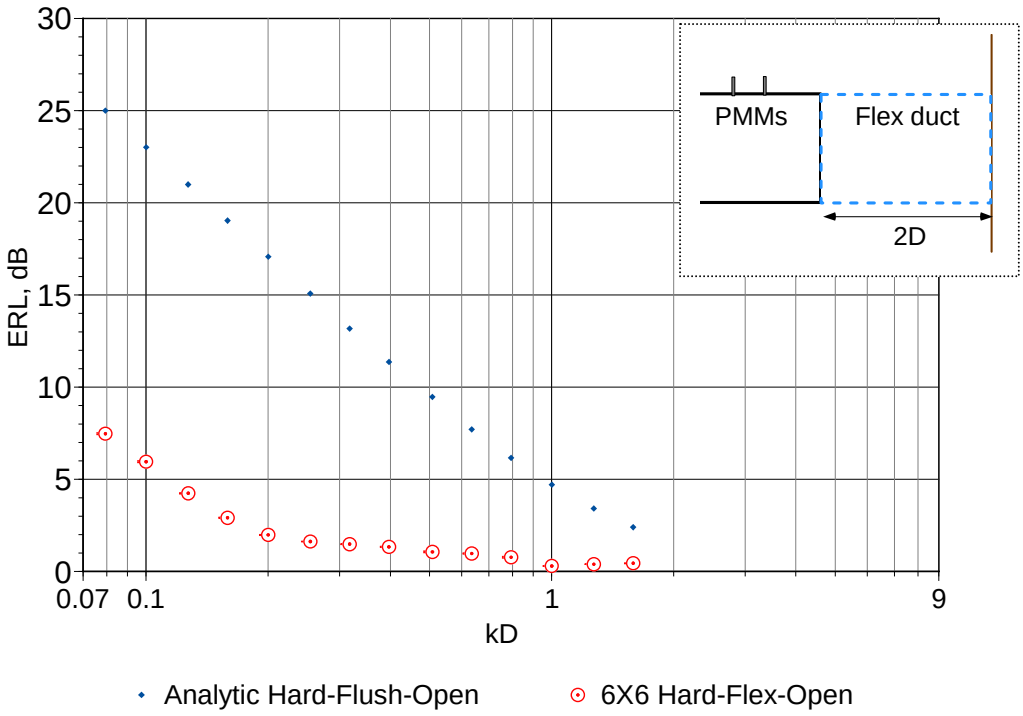

Figure C9. 6X6 Hard-Flex-Open ERL Results

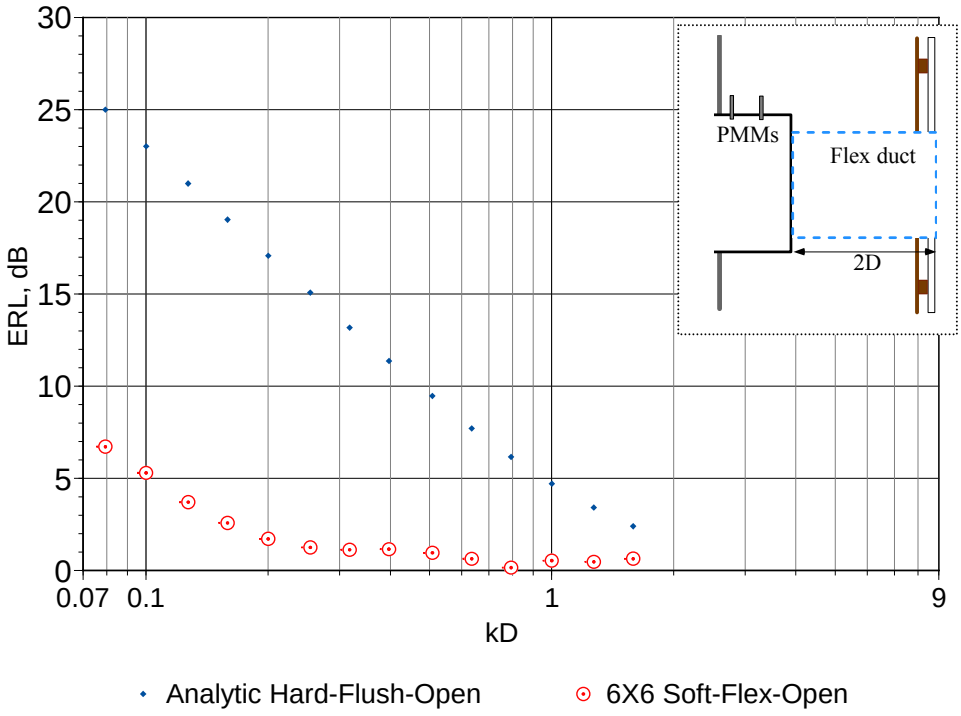

Figure C10. 6X6 Soft-Flex-Open ERL Results

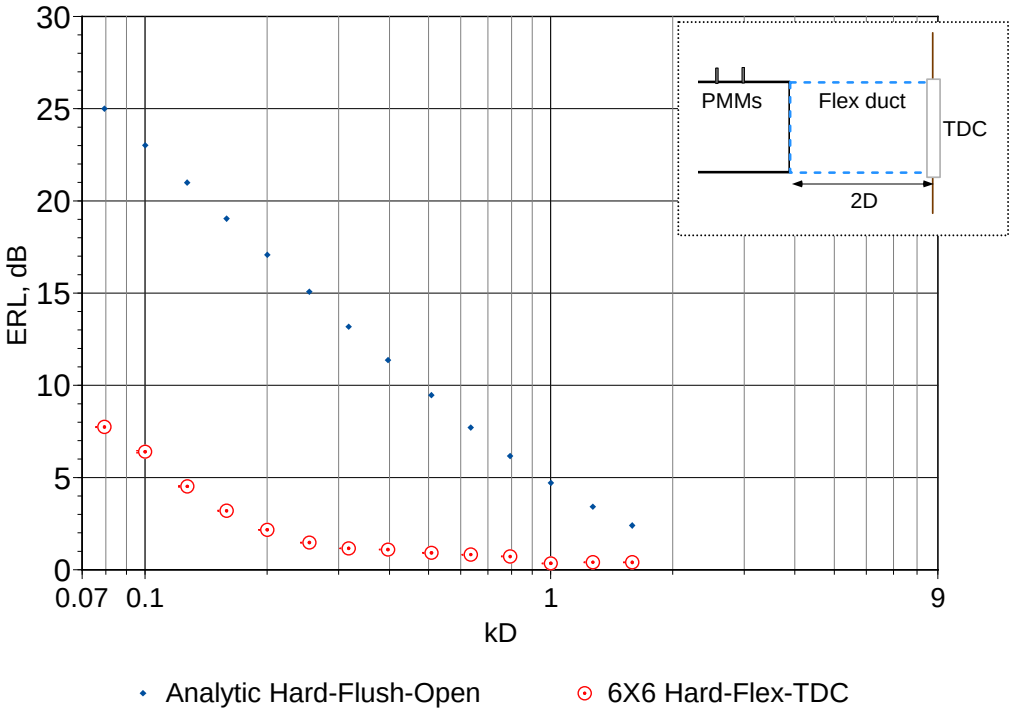

Figure C11. 6X6 Hard-Flex-TDC ERL Results

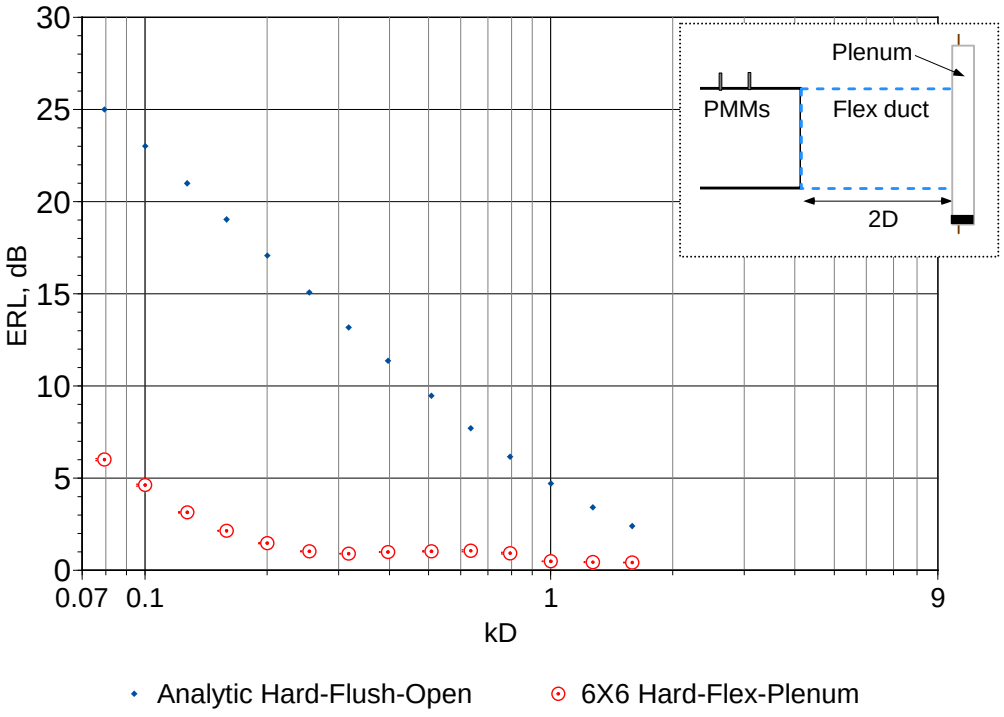

Figure C12. 6X6 Hard-Flex-Plenum ERL Results

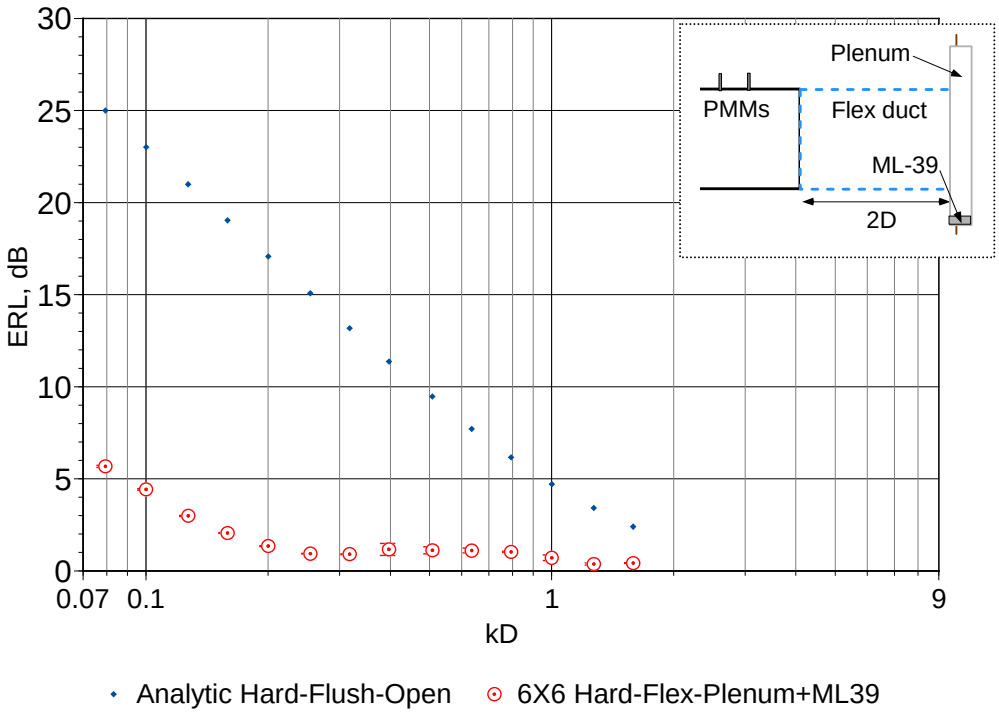

Figure C13. 6X6 Hard-Flex-Plenum+ML39 ERL Results

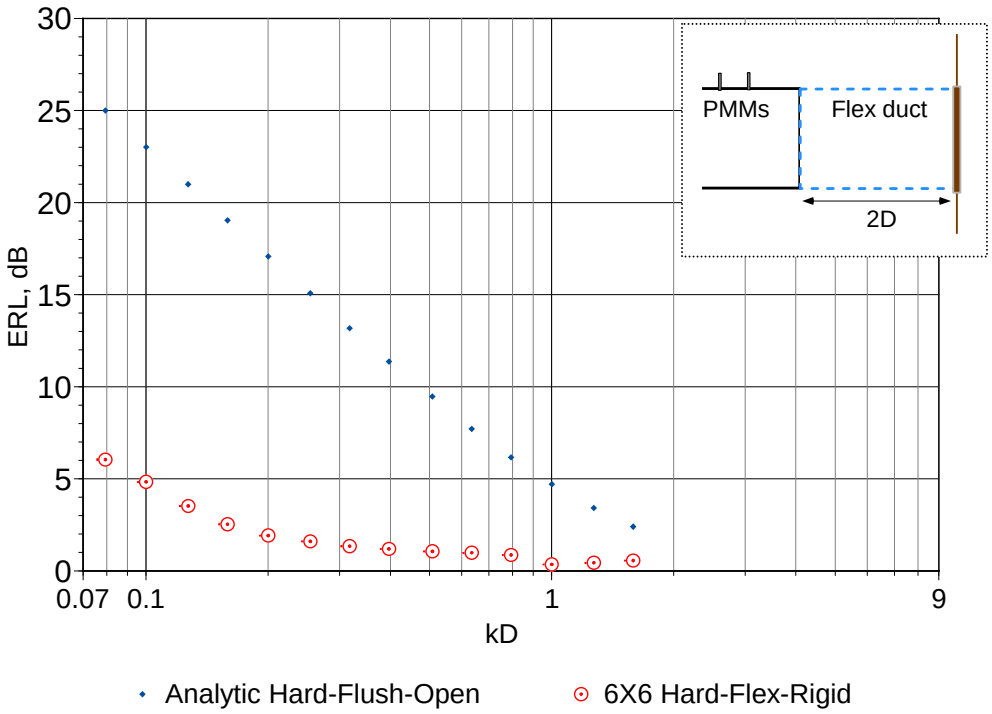

Figure C14. 6X6 Hard-Flex-Rigid ERL Results

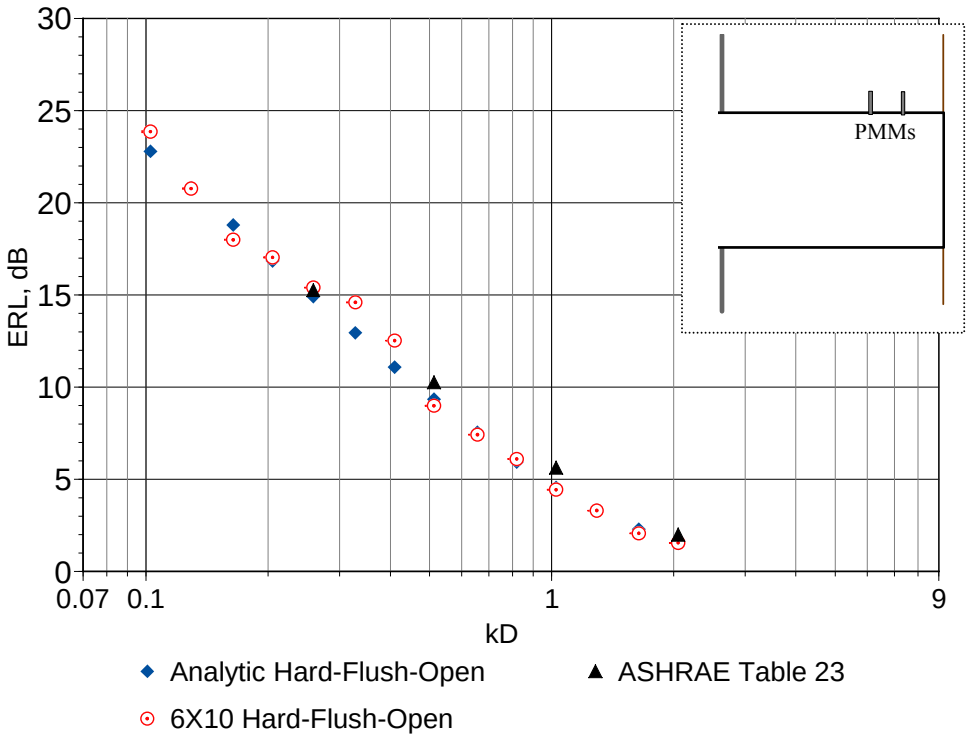

Figure C15. 6X10 Hard-Flush-Open ERL Results

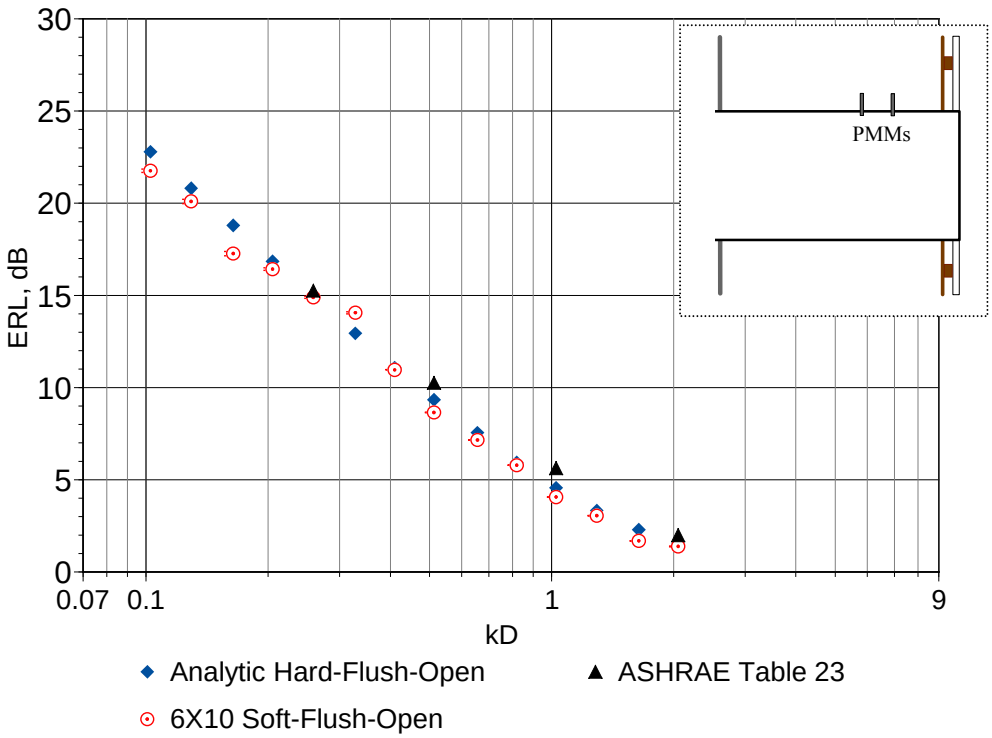

Figure C16. 6X10 Soft-Flush-Open ERL Results

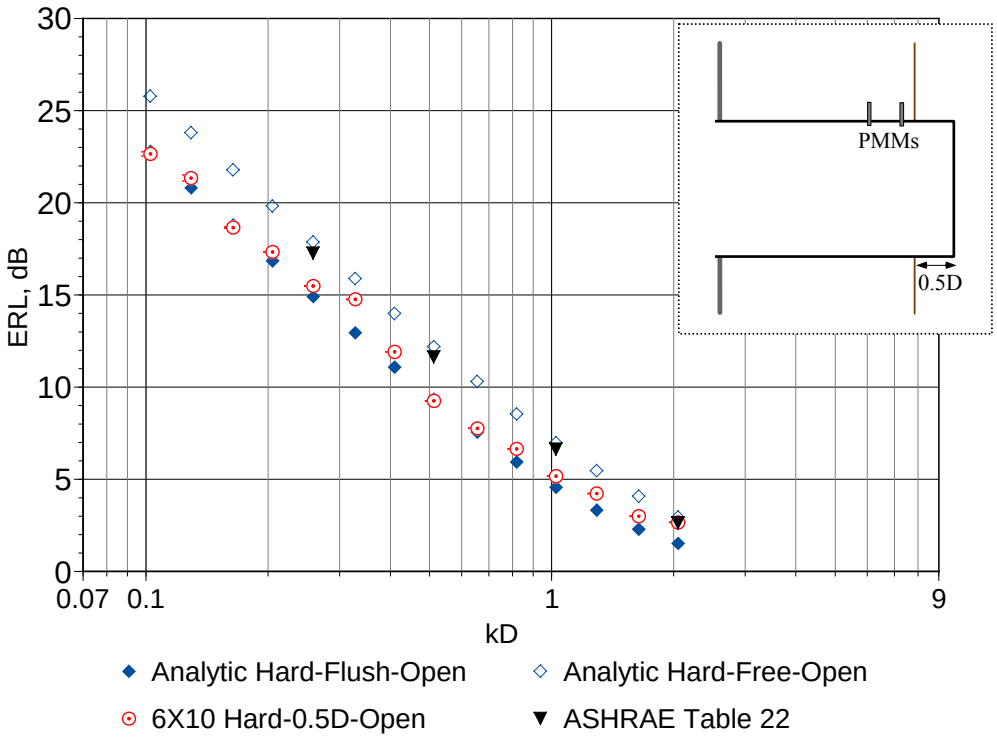

Figure C17. 6X10 Hard-0.5D-Open ERL Results

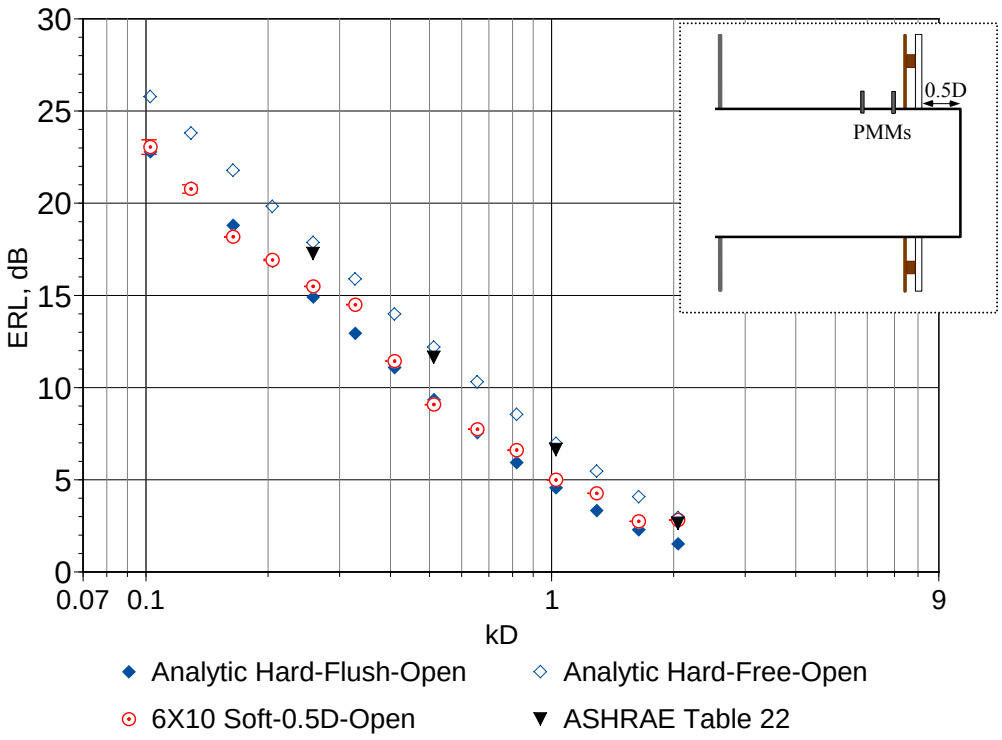

Figure C18. 6X10 Soft-0.5D-Open ERL Results

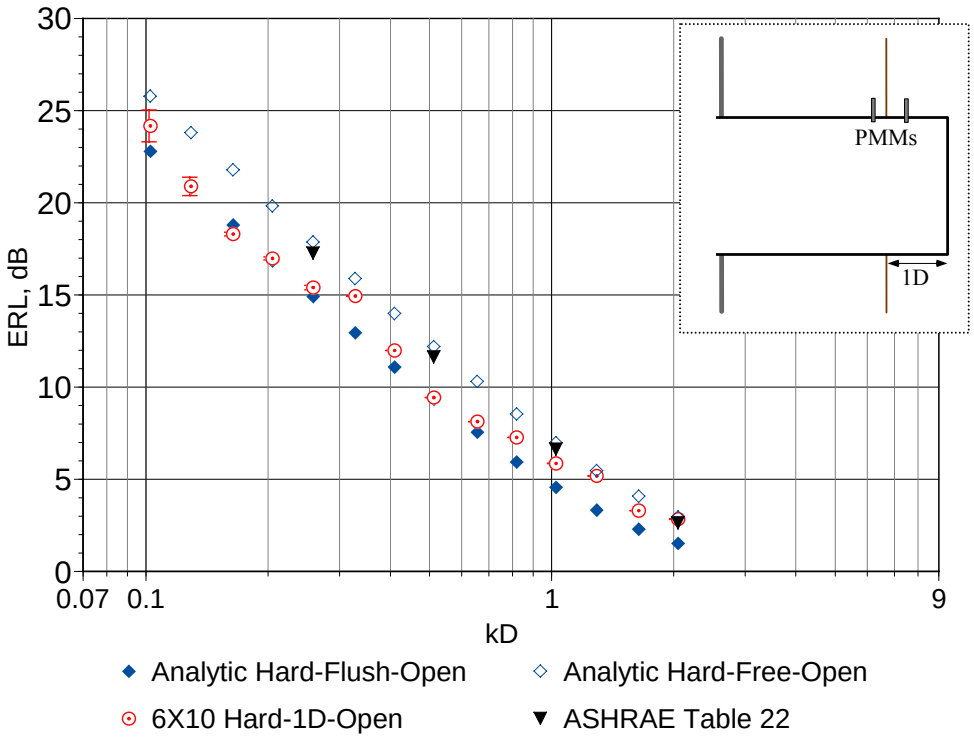

Figure C19. 6X10 Hard-1D-Open ERL Results

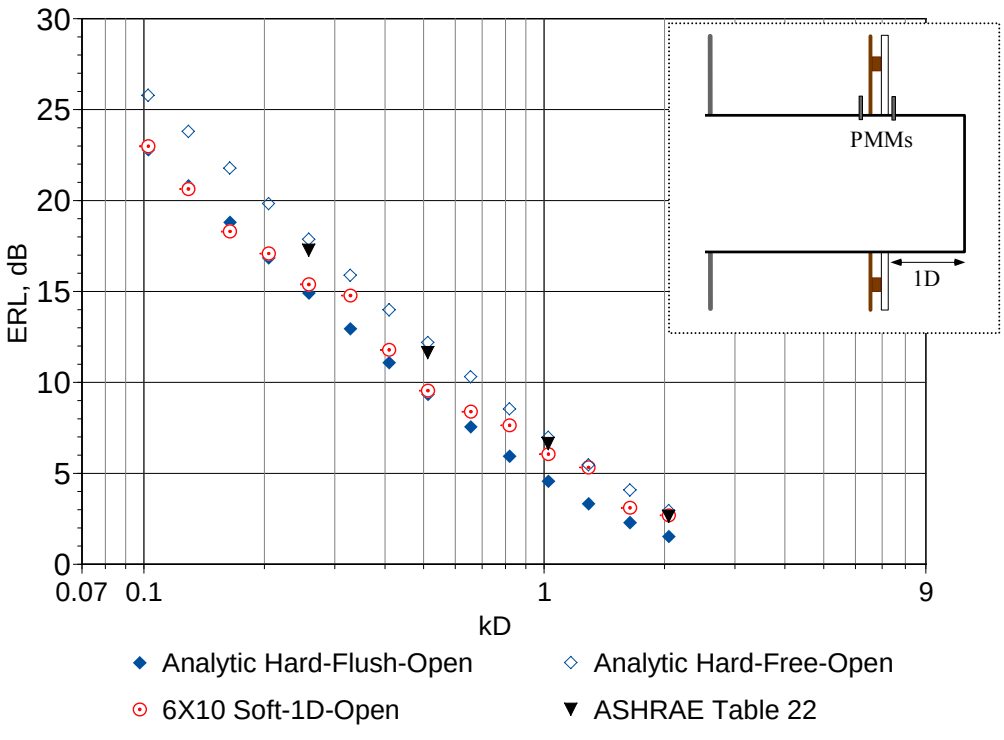

Figure C20. 6X10 Soft-1D-Open ERL Results

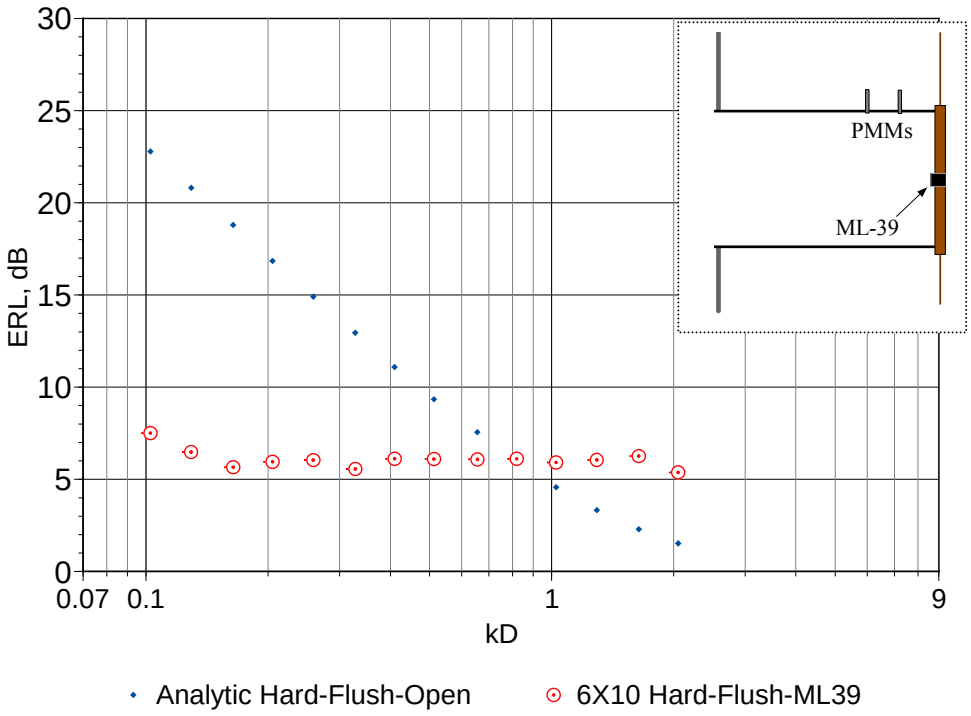

Figure C21. 6X10 Hard-Flush-ML39 ERL Results

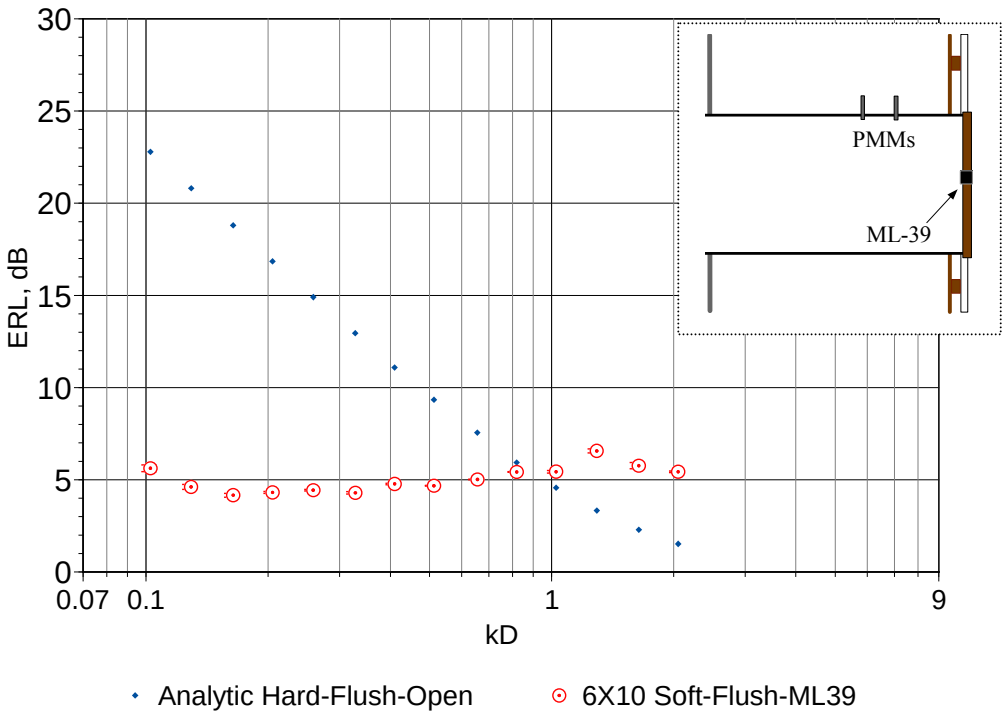

Figure C22. 6X10 Soft-Flush-ML39 ERL Results

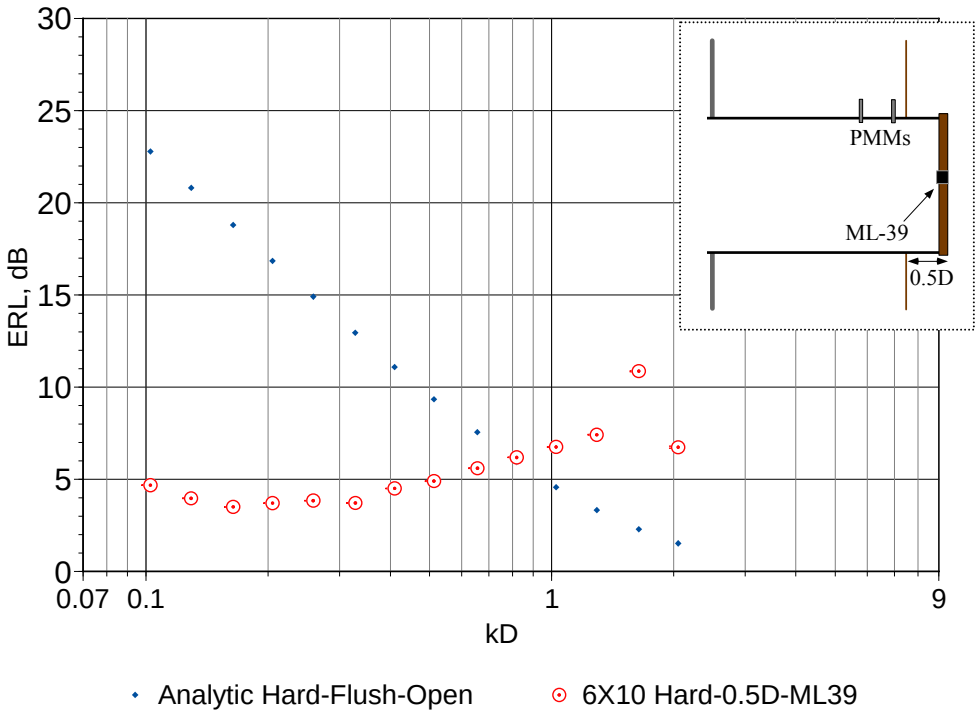

Figure C23. 6X10 Hard-0.5D-ML39 ERL Results

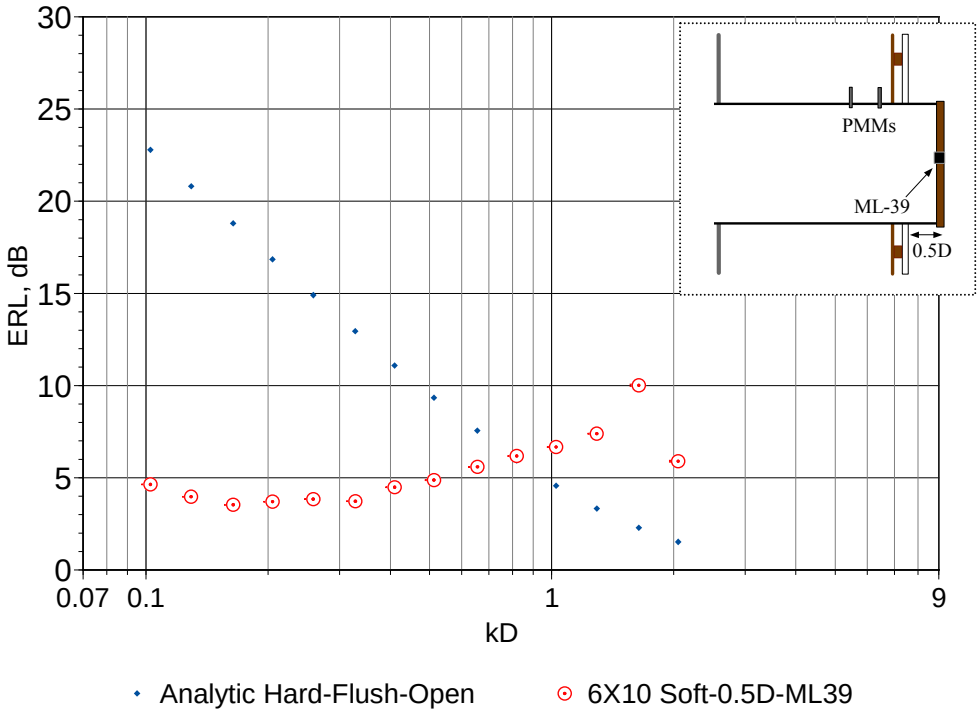

Figure C24. 6X10 Soft-0.5D-ML39 ERL Results

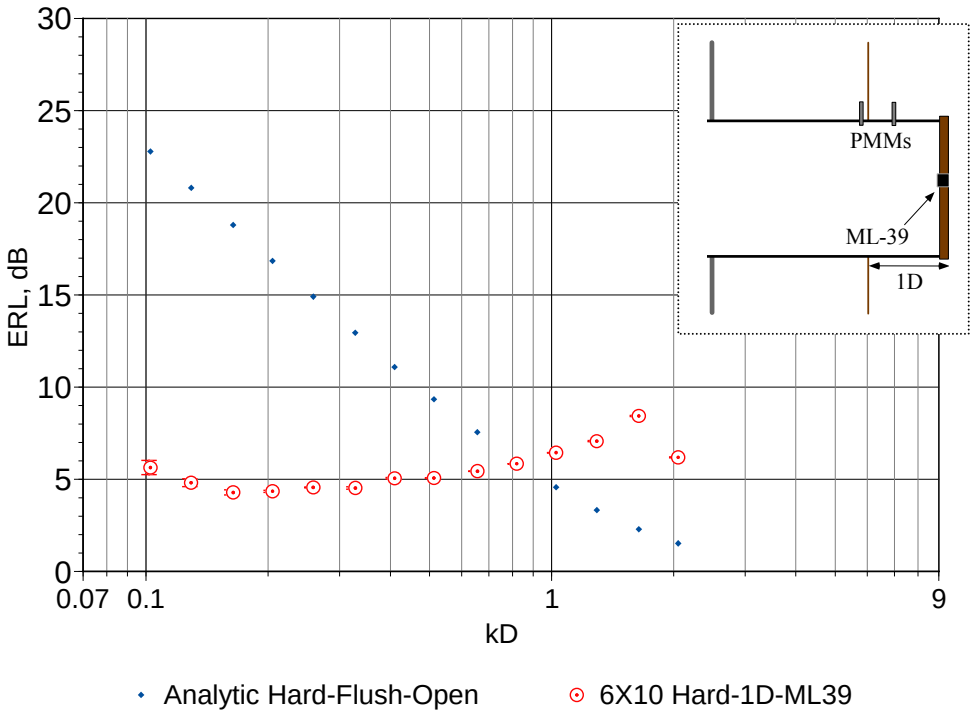

Figure C25. 6X10 Hard-1D-ML39 ERL Results

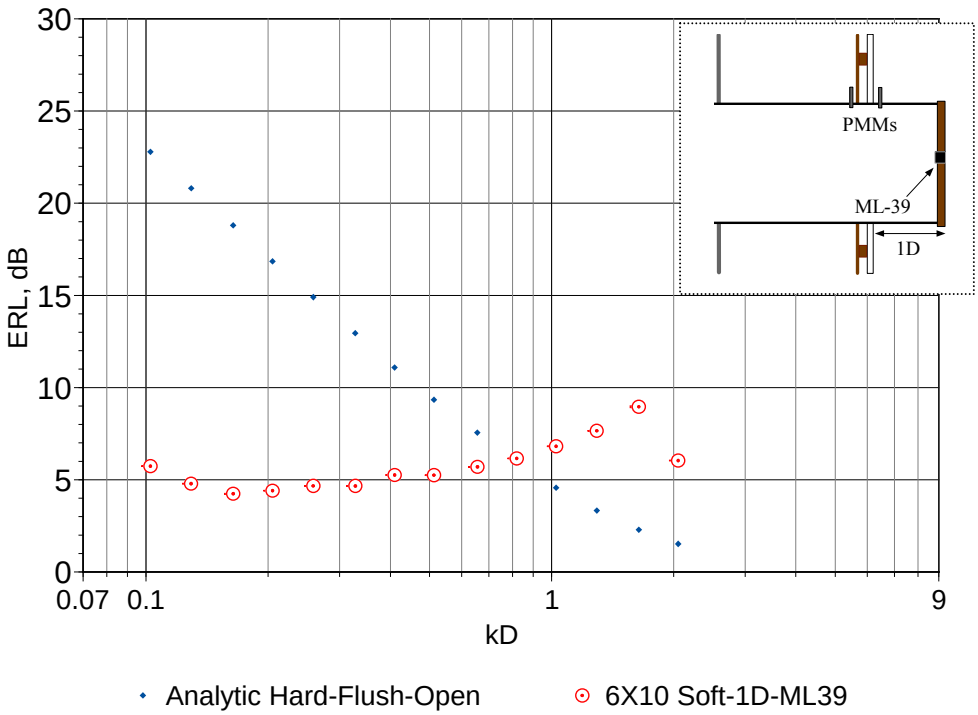

Figure C26. 6X10 Soft-1D-ML39 ERL Results

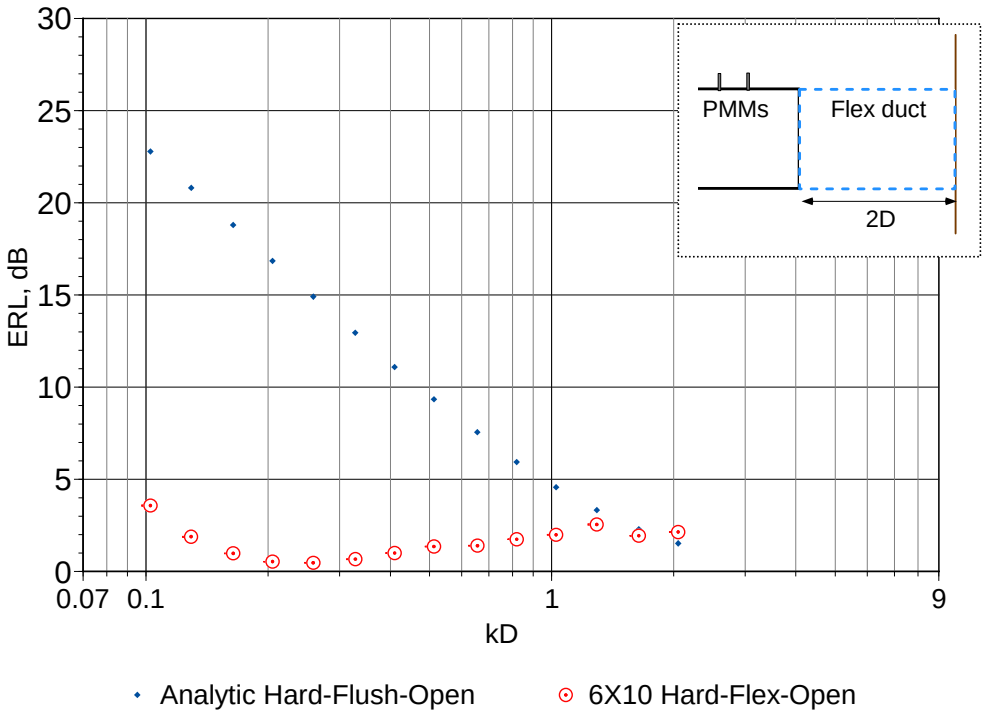

Figure C27. 6X10 Hard-Flex-Open ERL Results

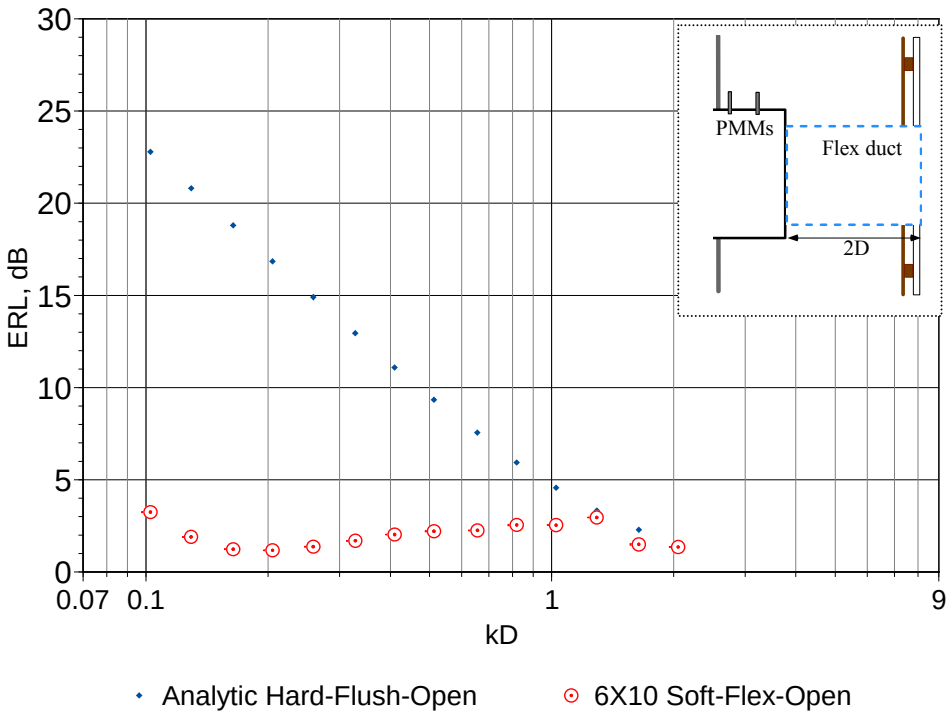

Figure C28. 6X10 Soft-Flex-Open ERL Results

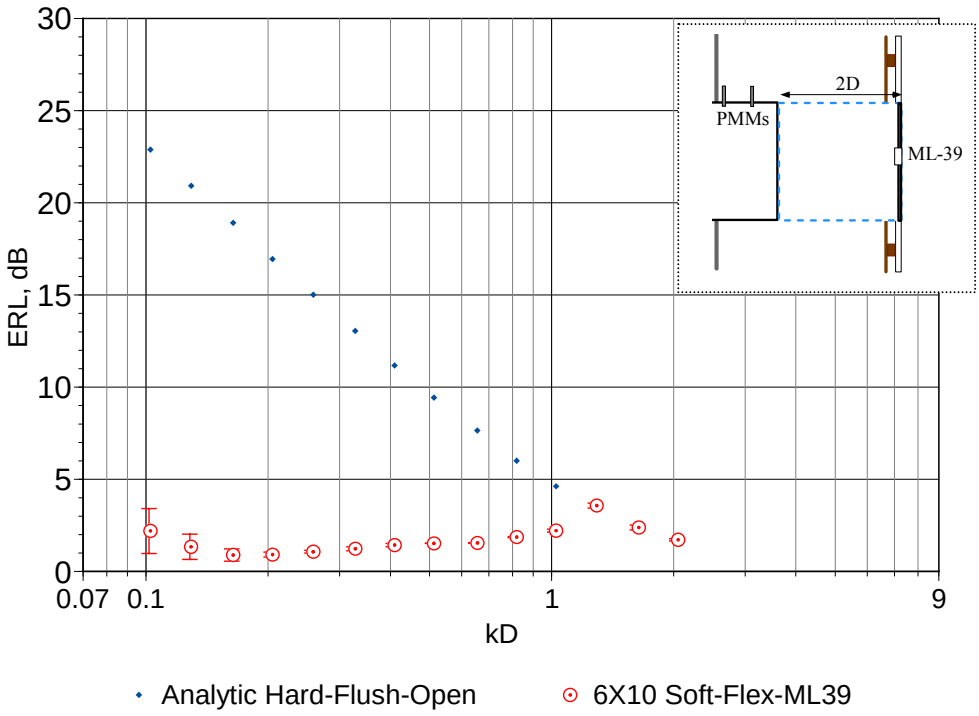

Figure C29. 6X10 Soft-Flex-ML39 ERL Results

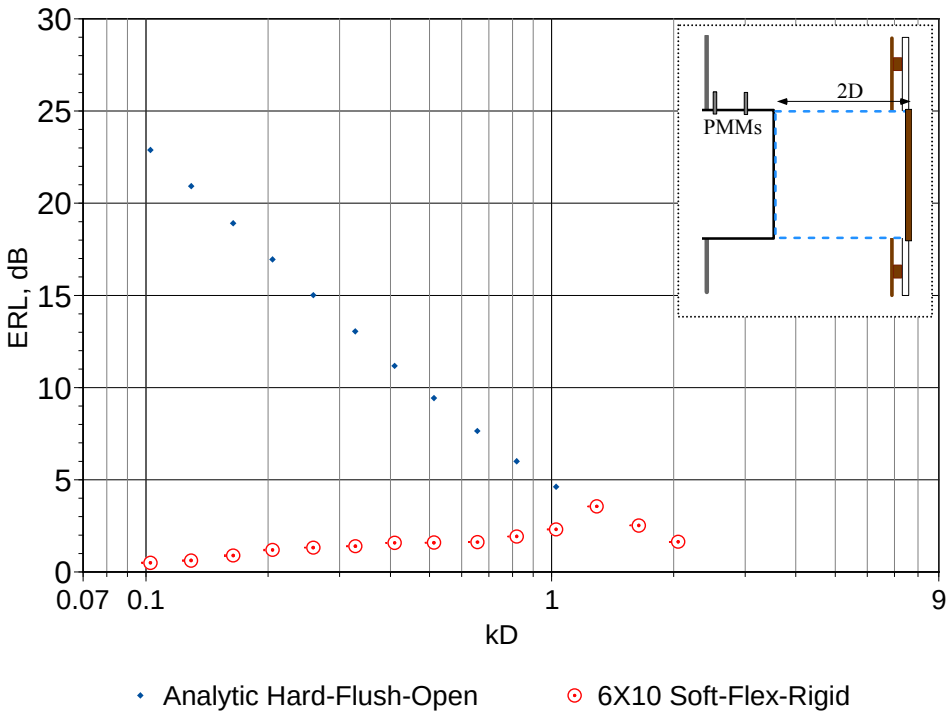

Figure C30. 6X10 Soft-Flex-Rigid ERL Results

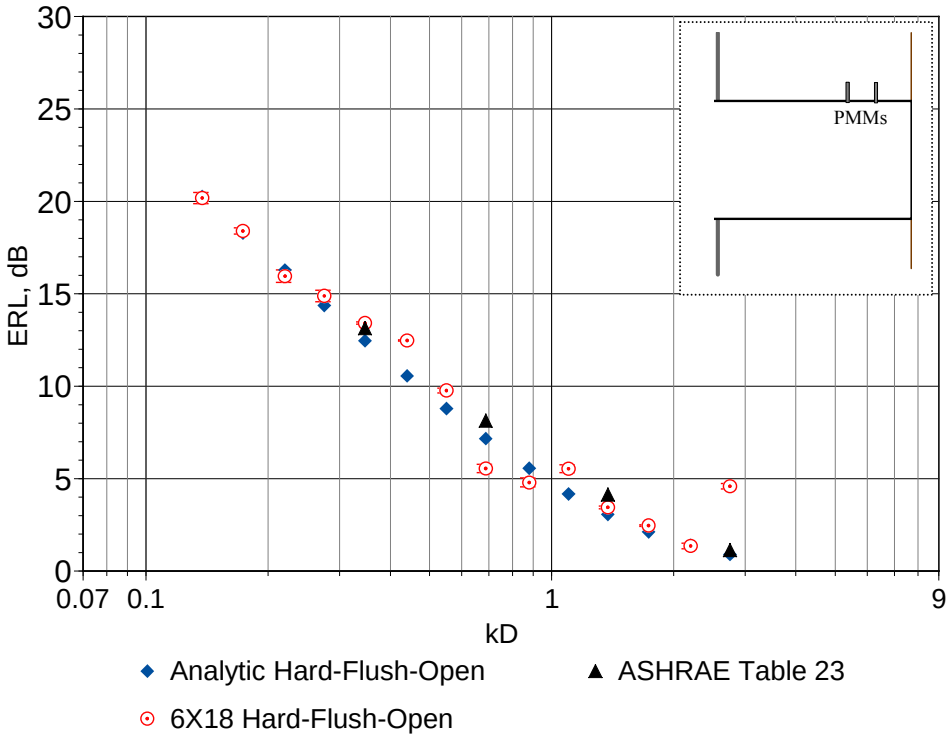

Figure C31. 6X18 Hard-Flush-Open ERL Results

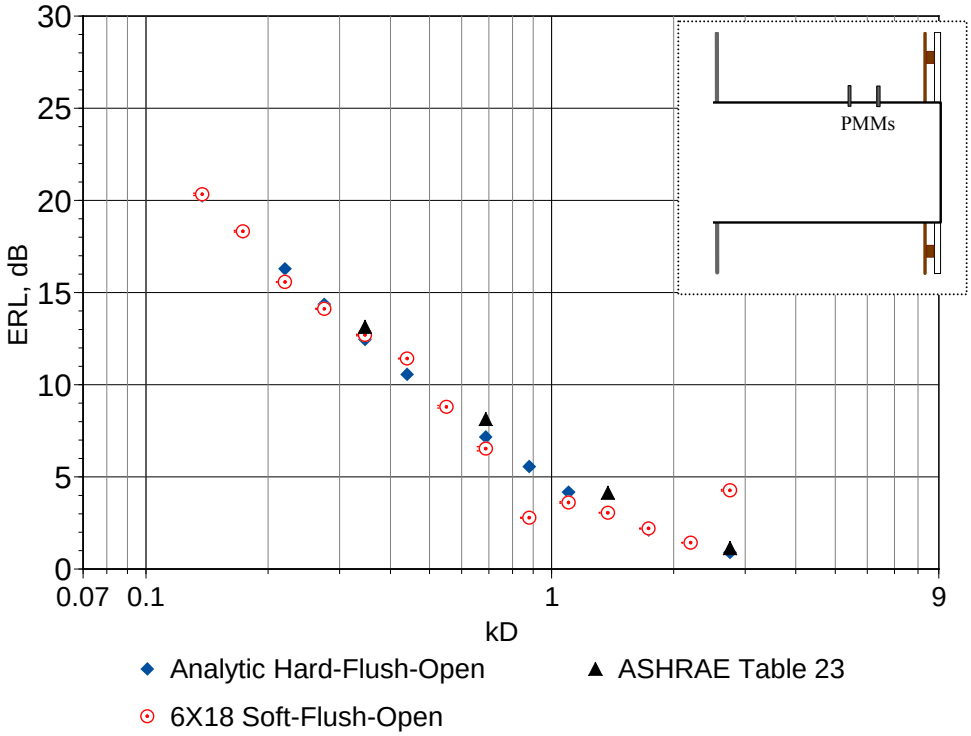

Figure C32. 6X18 Soft-Flush-Open ERL Results

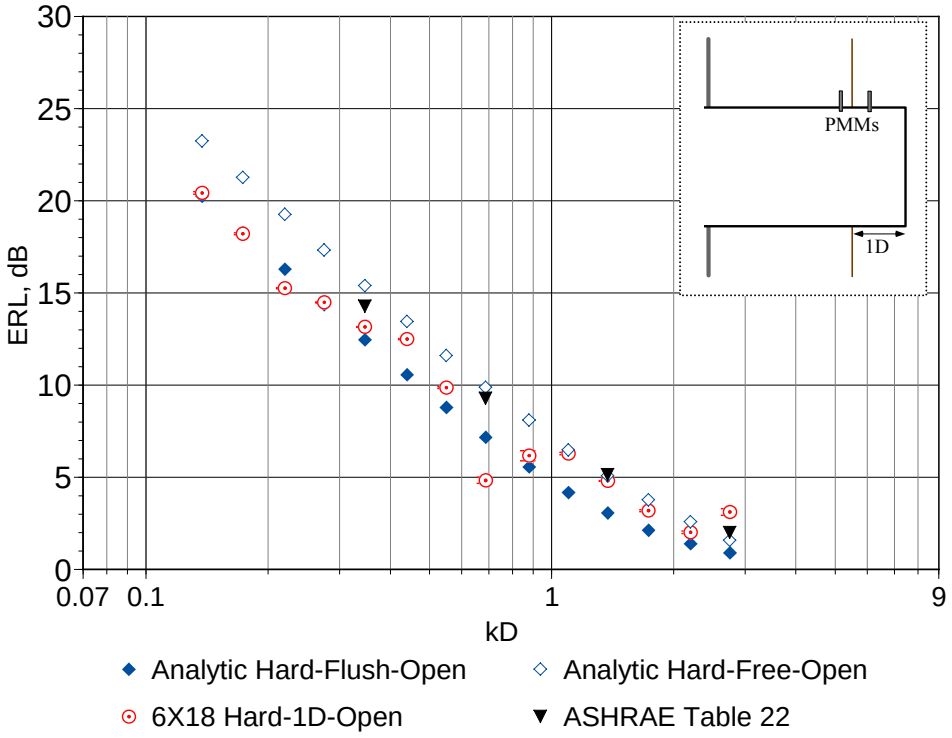

Figure C33. 6X18 Hard-1D-Open ERL Results

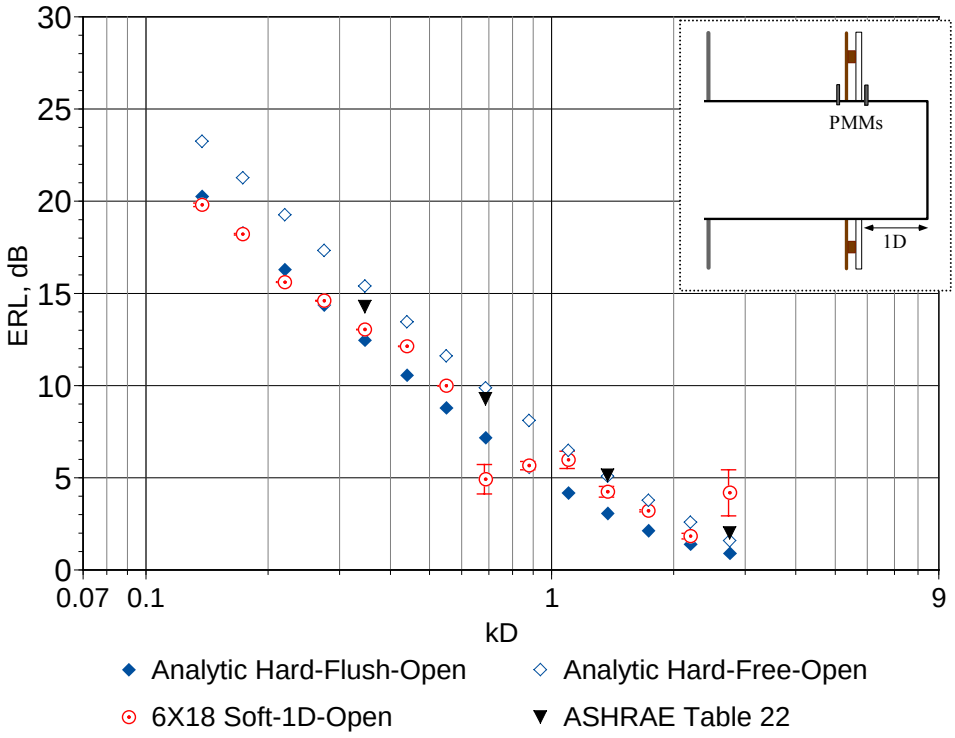

Figure C34. 6X18 Soft-1D-Open ERL Results

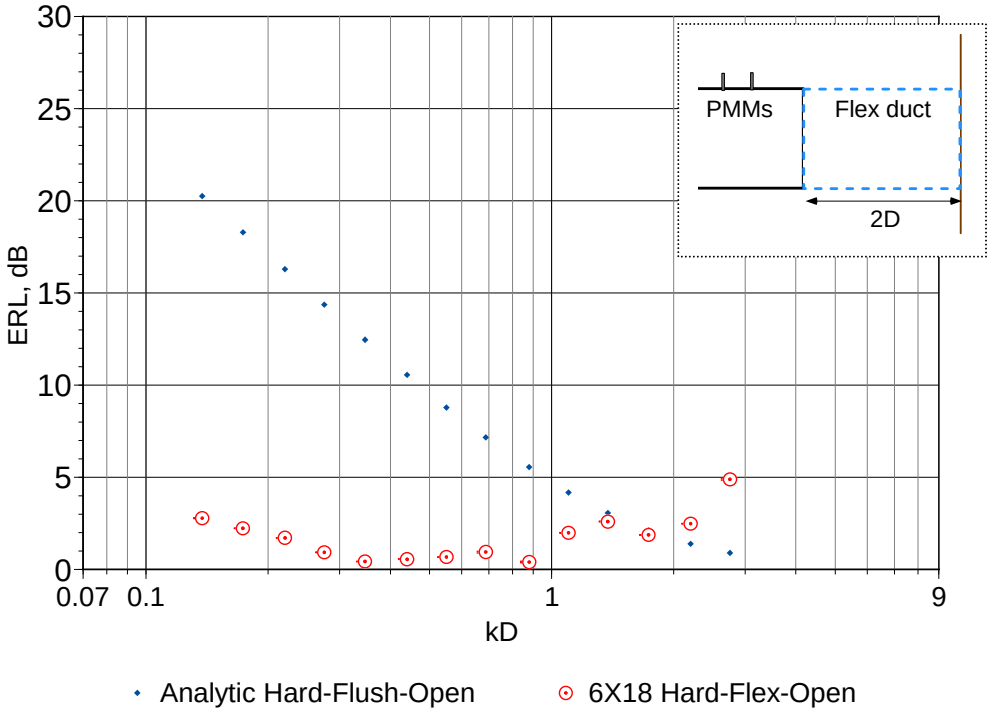

Figure C35. 6X18 Hard-Flex-Open ERL Results

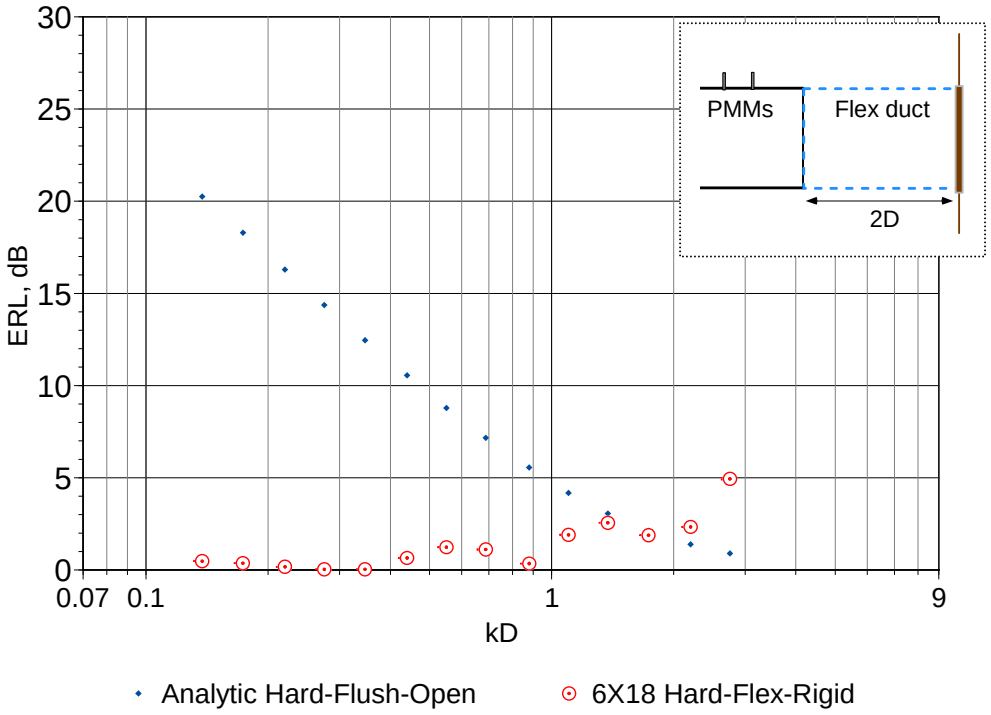

Figure C36. 6X18 Hard-Flex-Rigid ERL Results

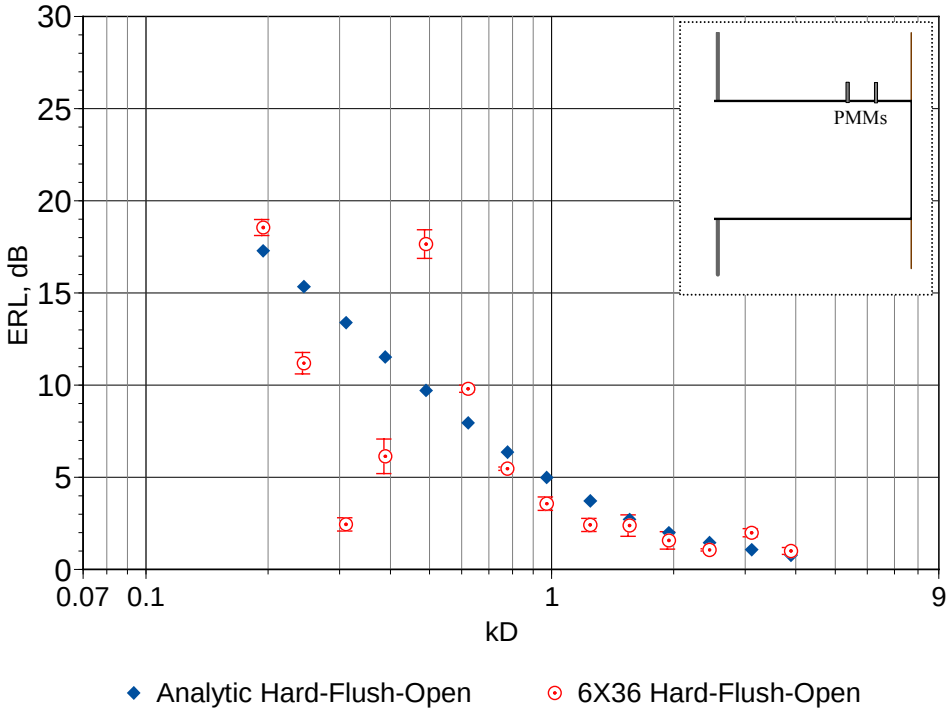

Figure C37. 6X36 Hard-Flush-Open ERL Results

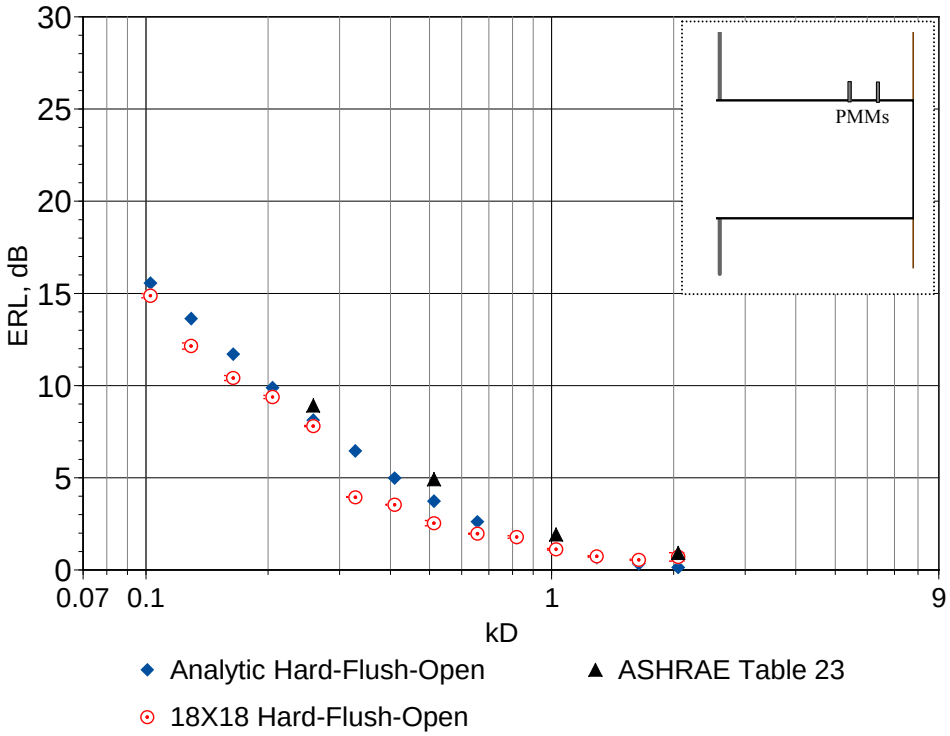

Figure C38. 18X18 Hard-Flush-Open ERL Results

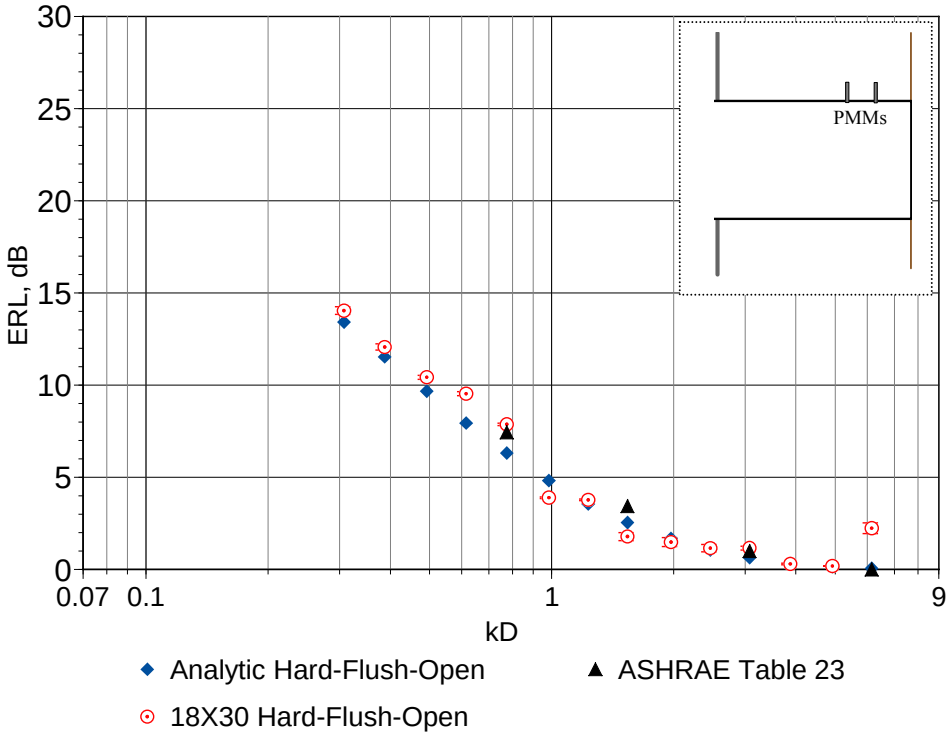

Figure C39. 18X30 Hard-Flush-Open ERL Results

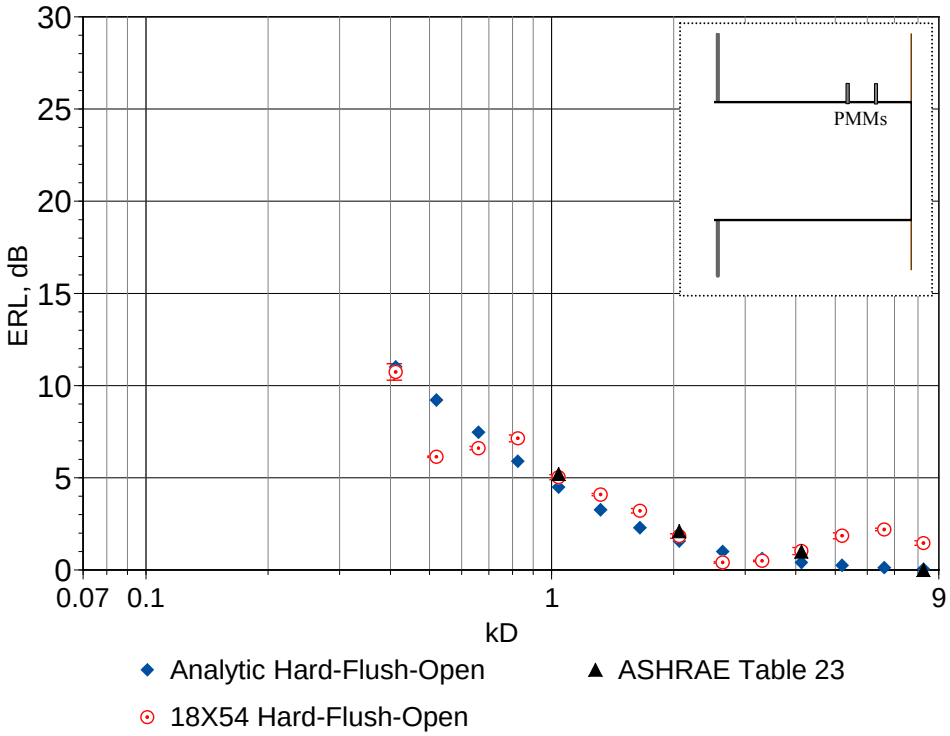

Figure C40. 18X54 Hard-Flush-Open ERL Results

BIBLIOGRAPHY

1. ASHRAE, *ASHRAE Handbook -- HVAC Applications*. 1995-2003.

2. Kinsler, L.E., et al., *Fundamentals of Acoustics*. 1982, New York: John Wiley & Sons.

3. Blackstock, D.T., *Fundamentals of physical acoustics*. 2000, John Wiley and Sons, Inc.: New York.

4. Pierce, A.D., *Acoustics - An Introduction to Its Physical Principles and Applications*. Second ed. 1989, Melville, NY: Acoustical Society of America.

5. Nomura, Y., I. Yamamura, and S. Inawashiro, *On the acoustic radiation from a flanged circular pipe.* Journal of the Physical Society of Japan, 1960. **15**: p. 510-517.

6. Levine, H. and J. Schwinger, *On the Radiation of Sound from an Unflanged Circular Pipe.* Physical Review, 1948. **73**(4): p. 383-406.

7. Pierce, A.D., R.O. Cleveland, and M. Zampolli, *Radiation impedance matrices for rectangular interfaces within rigid baffles: Calculation methodology and applications.* Journal of Acoustical Society of America, 2002. **111**(2): p. 672-684.

8. Davies, P.O.A., J.L.B. Coelho, and M. Bhattacharya, *Reflection coefficients for an unflanged pipe with flow.* Journal of Sound and Vibration, 1980. **72**: p. 543-546.

9. Norris, A.N. and I. Sheng, *Acoustic radiation from a circular pipe with an infinite flange.* Journal of Sound and Vibration, 1989. **135**: p. 85-93.

10. Selamet, A., Z.L. Ji, and R.A. Kach, *Wave reflections from duct terminations.* The Journal of the Acoustical Society of America, 2001. **109**(4): p. 1304-1311.

11. Chung, J.Y. and D.A. Blaser, *Transfer function method of measuring in-duct acoustic properties. I. Theory.* The Journal of the Acoustical Society of America, 1980. **68**(3): p. 907-913.

12. Chung, J.Y. and D.A. Blaser, *Transfer function method of measuring in-duct acoustic properties. II. Experiment.* The Journal of the Acoustical Society of America, 1980. **68**(3): p. 914-921.

13. Seybert, A.F. and D.F. Ross, *Experimental determination of acoustic properties using a two-microphone random-excitation technique.* The Journal of the Acoustical Society of America, 1977. **61**(5): p. 1362-1370.

14. Boden, H. and M. Abom, *Influence of errors on the two-microphone method for measuring acoustic properties in ducts.* The Journal of the Acoustical Society of America, 1986. **79**(2): p. 541-549.

15. Katz, B.F.G., *Method to resolve microphone and sample location errors in the two-microphone duct measurement method.* Journal of Acoustical Society of America, 2000. **108**(5): p. 2231-2237.

16. Jones, M.G. and P.E. Stiede, *Comparison of methods for determining specific acoustic impedance.* Journal of Acoustical Society of America, 1997. **101**(5): p. 2694-2704.

17. ASTM, *E1050-98 - Standard Test Method for Impedance and Absorption of Acoustical Materials Using A Tube, Two Microphones and A Digital Frequency Analysis System.* American Society for Testing and Materials, 1998.

18. Sandbakken, M., L. Pande, and M.J. Crocker, *Investigation of End Reflection Coefficient Accuracy Problems with AMCA Standard 300-67*. 1981, Purdue University: West Lafayette, IN. p. 1-50.

19. Titus, *E-Catalog*. 2007, Titus.

20. dspT, *dspTechnology SigLab Version 3.0 User Guide*. 1998: Fremont, CA.

21. NIST. *1.3.5.2. Confidence Limits for the Mean*. 2006 [cited 2006].